ELECTROCHEMICAL ASPECTS OF THE DEPOSITION OF REFRACTORY METAL CARBIDES FROM MOLTEN CHLORIDES

A Thesis submitted for the Degree of
DOCTOR of PHILOSOPHY
in the
UNIVERSITY of LONDON

by

RUTH WHEELDON, B.Sc.(Eng).,A.R.S.M.

Department of Materials
Royal School of Mines
Imperial College of Science, Technology and Medicine

September 1989

There is a music wherever there is a harmony, order or proportion; and thus far we may maintain the music of the spheres; for those well ordered motions, and regular paces, though they give no sound unto the ear, yet to the understanding a note most full of harmony. . . . .

Sir Thomas Browne

ABSTRACT

The chemistry and electrochemistry of molybdenum species in dilute solution in $CaCl_2$ at 850°C have been investigated. Anodically dissolved Mo gave rise to the formation of three Mo species, which were charcterised by cyclic voltammetry. Three waves were observed. At the first, Mo(III) is reduced to Mo metal. Another more anodic wave corresponds to the oxidation to Mo(V). The other peak may be attributed to the reduction of a dimer formed by: - $2MoCl_6^{3-} \rightleftharpoons Mo_2Cl_9^{3-} + 3Cl^-$

The electrochemistry of these species is dependent upon the temperature and concentration of $MoCl_6^{3-}$. As the concentration is increased the equilibrium is pushed to the right, but as the temperature is increased it is pushed to the left. Disproportionation of $MoCl_6^{3-}$ occurs in the melt :-

$$2MoCl_6^{3-} \longrightarrow 6/5\ MoCl_5 + 4/5\ Mo + 6Cl^-$$

The cyclic voltammetric behaviour of carbonate ions revealed an ill defined reduction peak indicating a complex reduction process:-

$$CO_3^{2-} + 4e \longrightarrow C + 3O^{2-}$$

At this temperature the chemical equilibrium lies well to the right:-

$$CO_3^{2-} \rightleftharpoons CO_2 + O^{2-}$$

Using a carbon dioxide atmosphere to suppress this dissociation resulted in its co-reduction to yield carbon monoxide. Examination of the electrochemistry of both $MoCl_6^{3-}$ and CO_3^{2-} in $CaCl_2$ revealed that the CO_3^{2-} pushes the dimer - monomer equilibrium in favour of the monomer.

The deposition of Mo,C and Mo_2C was analysed by chronoamperometry and deposits produced by constant potential electrolysis were examined by X-ray diffraction and scanning electron microscopy. Co-deposition of Mo and C yielded Mo_2C and Fe,Cr,Mo alloys. However these deposits are not coherent.

Investigations into the production of TiC by a similar method are noted.

CONTENTS

LIST OF FIGURES.

LIST OF TABLES.

MAJOR SYMBOLS.

a_M^{n+}	activity of species M.
C	solute concentration. ($moldm^{-3}$)
C_o^o	solute concentration at the electrode surface. ($moldm^{-3}$)
C_o^b	solute concentration of the bulk solution. ($moldm^{-3}$)
$C_o(0,t)$	concentration of species O at the electrode surface. ($moldm^{-3}$)
$C_o(R,t)$	concentration of species R at the electrode surface. ($moldm^{-3}$)
D	diffusion coefficient of depositing species. (cm^2sec^{-1})
D_O	diffusion coefficient of species O. (cm^2sec^{-1})
e	charge of the electron. (c)
E	potential applied to the electrode. (V)
E^o	standard electrode potential. (V)
E_p	peak potential in cyclic voltammetry. ^{a} anodic ^{c} cathodic (V)
$E_{p/2}$	half peak potential in cyclic voltammetry. ^{a} anodic, ^{c} cathodic (V)
F	Faradays constant. ($cmol^{-1}$)
i^o	exchange current. (mA)
i_p	peak current in cyclic voltammetry. ^{a} anodic ^{c} cathodic (mA)
i(t)	growth current at time t. (mA)
j	applied current density. (Acm^{2-},$mAcm^{2-}$)
j_L	limiting current density. (Acm^{2-},$mAcm^{2-}$)
j_p	peak current density. (Acm^{2-},$mAcm^{2-}$)
J^o	rate of nucleation. (sec^{-1})
K_f	charge coefficient for the reduction.
M	molecular weight of depositing material.
n	number of electrons involved in the reaction.
N	number of atoms forming the nucleus.
O	oxidised species.
R	reduced species or Universal gas constant. ($Jmol^{-1}K^{-1}$)

s	area of electrode surface. (cm^{2-})
t	time. (sec.)
T	absolute temperature. (K)
v	sweep rate. ($Vsec^{-1}$,$mVsec^{-1}$)
δ	thickness of the diffusion layer. (cm)
η	overpotential. (V,mV)
η_c	overpotential due to concentration polarisation. (V,mV)
ρ	density. (gcm^{3-})
σ	interfacial energy. (Jcm^{2-})

1. INTRODUCTION

1.1. REFRACTORY METAL CARBIDES

Refractory metals are usually considered to be the metals of groups IVa-VIa, titanium, zirconium, hafnium, vanadium, niobium, tantalum, chromium, molybdenum and tungsten. The carbides of these metals are characterised by extremely high melting points (2000-4000°C),but it is not particularly these refractory properties that are used commercially, but rather their great hardness. Hence carbides are used as cutting tool tips and wear resistant parts. Table 1.1.(1) shows some of the properties of these carbides.

phase	structure	micro-hardness kg/mm^2	m.p.t. (or decomp.temp.) °C	heat conductivity Cal/cm.sec.°C
TiC	β1	2900	3067	0.05
ZrC	β1	2600	3420	-
HfC	β1	2700	3928	-
VC	β1	2900	2648	-
NbC	β1	2400	3600	0.034
TaC	β1	2500	3983	0.053
Cr_2C_2	Ortho.	1300	1810	-
Mo_2C	Ortho.	1500	2687	-
WC	Hex.	2100(on basal plane)	2776	0.07

Table 1.1. SURVEY OF SELECTED PROPERTIES OF REFRACTORY METAL CARBIDES

Generally these carbides are chemically very stable, except at high temperatures, when oxidation occurs readily to form oxides (in oxygen containing atmospheres). At high temperatures carbides are very strong (E- 40-90 X10^6psi.) but at room temperatures, they are brittle, undergoing a brittle to ductile transition at approx. 1000^{o}C. Above this temperature slip deformation occurs, similar to that for fcc. metals. They have metallic like electrical, magnetic and optical properties, often very similar to those of the parent refractory metal.

An interesting property of these carbides is their wide composition range and thus the variation of properties available, due to the change in vacancy concentration and metal : carbon ratio. This wide composition range for titanium carbide is shown in Fig 1.1.(2).

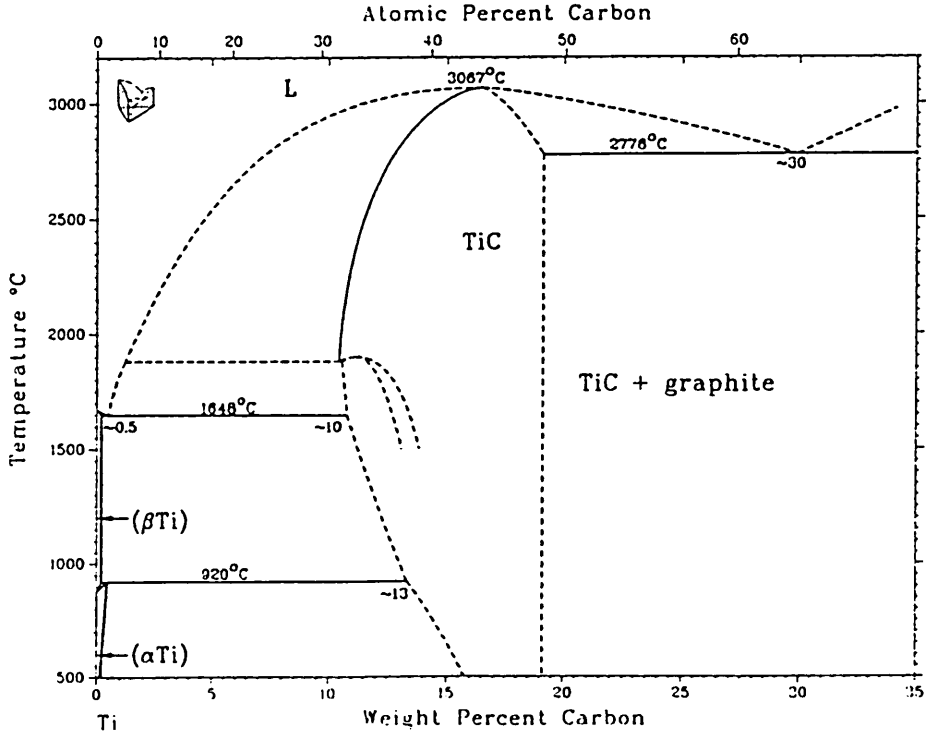

Fig.1.1.THE TITANIUM RICH PORTION OF THE TITANIUM-CARBON PHASE DIAGRAM.

1.2 ELECTRODEPOSITION FROM MOLTEN SALTS

Conventional production methods for refractory metal carbide, boride and silicide coatings are plasma arc, flame spraying, pack cementation and vacuum evaporation. These techniques frequently give coatings which have serious deficiencies, such as poor adherence, porosity or inclusions and often require great heat imput, which results in low efficiencies. Electrodeposition from molten salts has a number of advantages in the nature of the electrolytic techique and the deposits produced.

Molten salts are liquid compounds which exist over a temperature range of about 100^{o}C to over 2000^{o}C. There are three main types, distinguished by their structure :

i> simple ionic melts (alkali halides), ii> simple oxyanionic melts (carbonates), iii> complex polymeric melts (silicates).

Ionic melts are the most concentrated electrolytes. The particular advantages of these electrolytes for electrodeposition are as follows:

a> their high stability(3),in terms of large decomposition voltage and low gas solubility, allowing electrolysis at high current efficiency to take place, as the number of side reactions available are reduced.

b> the electrodeposition reactions in molten salts have high current densities (4), due to the number of available charge carriers . This also allows better throwing power.(5)

c> They are powerful solvents for inorganic materials(6),allowing high solute concentrations, making high deposition rates possible.

d> Electroplates are free from stress(7), due to undisturbed crystal growth, giving good ductility.

e> Substrate oxide films and surface moisture are dissolved in molten salts and thus adherence is improved. Diffusion layers are formed between the substrate and coating, (if the deposition rate is similar to that of the deposited species in the substrate), giving much greater adherence than is otherwise possible.

f> Good ionic conductivity typically 2-9 $\Omega^{-1}cm^{-1}$(8), allows good energy efficiency and reduces the cathodic overpotentials. (9)

g> The rate of metal deposition may be controlled by changing the cathode current density or the deposition potential, and the rate of diffusion into the substrate, by changing the temperature. Thus the desired deposit structure and morphology can be obtained.

However electrodeposition in molten salts often requires the use of inert atmospheres, to stop hydrolysis of any hygroscopic salts used.(10) Purification of the melt is thus necessary to give long term stability (11) and more resistant cell materials are required.

Electrodeposition in molten salts is usually mass transfer controlled and dendritic deposits are formed.(12) These are undesirable as they occlude solidified melt, requiring leaching out. Another problem with dendritic deposits is that they make the cathode dimensionally unstable, leading to lower current efficiencies. Conditions of mass transfer control can be avoided by introducing a slow irreversible step in the cathodic reaction, as used by Mellors and Senderoff in fluorides.(5)

They postulated that the polarising power of the solvent cations,for the anions, contributes to the stability of solute complexes, and thus the kinetics of the electrodeposition process. They assumed that if a sufficiently stable complex is formed, then the desolvation of the metal ions gives rise to the irreversible step required to stop dendritic growth. This analysis is based on the effect of anion additions forming less stable complexes. (i.e. Cl^- for F^-) However it is probable that these additions do not give rise to bulk substitution in complexes, but affect the electrode/electrolyte interface and thus the charge transfer step itself, so changing the kinetics as indicated.(13)

Powdery electrodeposits can also originate from secondary electrode processes, either by disproportionation reactions near the electrode surface or by chemical reactions between alkali metals and metal ions in the bulk electrolyte.(5)

Practically a series of other properties are required for molten baths, such as, low vapour pressure, low melting point, low corrosivity, ease of purification, non-polluting and low cost. This has led to the concentration of electrochemical and electroplating research in chloride and fluoride melts.

1.3 ELECTRODEPOSITION

Electrodeposition can be considered to be a two stage process. The first stage being the nucleation of the new phase on a substrate and the growth of nuclei to form a monolayer. The second stage being the growth of this layer. The second stage occurs for almost all of the total deposition time, but the nucleation stage is of particular importance, as the structure of the intial layer influences the final structure of the electroplate and thus its properties. Often the thermodynamics and kinetics of the whole process can be generalised to that of the second stage.

During the second stage the electrode is completely covered by depositing metal ,so that it behaves as an electrode of the type M/M^{n+} and thus the electrodeposition reaction can be written as:

$$M^{n+}(bulk) + ne \longrightarrow M^{o}(electrode)$$

giving a Nernst equation for this reaction as:

$$E = E^{o} + RT/nF . \ln a_{M}^{n+}$$

Where E is the potential of the electrode surface, R the gas constant, T the absolute temperature and n is the valency of the metal ion (M^{n+}) being deposited. The standard electrode potential of the M/M^{n+} couple (E^{o}) is given when the activity of the depositing ions is unity ($a_{M}^{n+}=1$).

The Nernst equation however does not account for the non-equilibrium behaviour encountered for electrode reactions, in practise nearly all electrode reactions are irreversible to some extent. This leads to the polarisation of electrodes and results in the overpotential required for the reaction to proceed. Under dynamic conditions the electrode potential is given by:

$$E = E_{ieq} + \eta$$

E_{ieq} is the Nernst potential and η is the overpotential. The overpotential is made up of

contributions from any source of increase in resistance to the reaction proceeding,e.g. a concentration barrier. The effect of this polarisation on the kinetics of cathodic deposition can be evaluated by considering the process rate determining step. The steps involved in the process are usually considered to be :

i) *migration*: The depositing ion in the bulk of the electrolyte migrates towards the cathode (or anode) under the influence of impressed current as well as by diffusion and convection.

ii) *Electron transfer*: In the electrical double layer alignment of electrolyte and complex ions occurs, allowing charge neutralisation and adsorption of depositing ion onto the electrode.
(The electron transfer process for complex ions is complicated and not clearly understood. Discharge itself is thought to proceed from simple ions after a previous dissociation reaction. This dissociation is believed to be so fast that it does not effect the overall kinetics.)

iii) *Incoporation*: The adsorbed atom then migrates or diffuses to a suitable growth site.

Fig.1.3. shows these steps schematically.
The slowest of the above steps is rate determining. In most cases diffusion of species to the electrode is rate determining and thus concentration polarisation is the major source of overpotential. This potential is quantitively given by the Heyrovsky-Ilkovic equation(14):

$$\eta_c = \frac{2.3\ R\ T}{n\ F} \log \frac{j_L}{j_L - j}$$

where j_L is the limiting current density and j the applied current density. At the limiting current density,

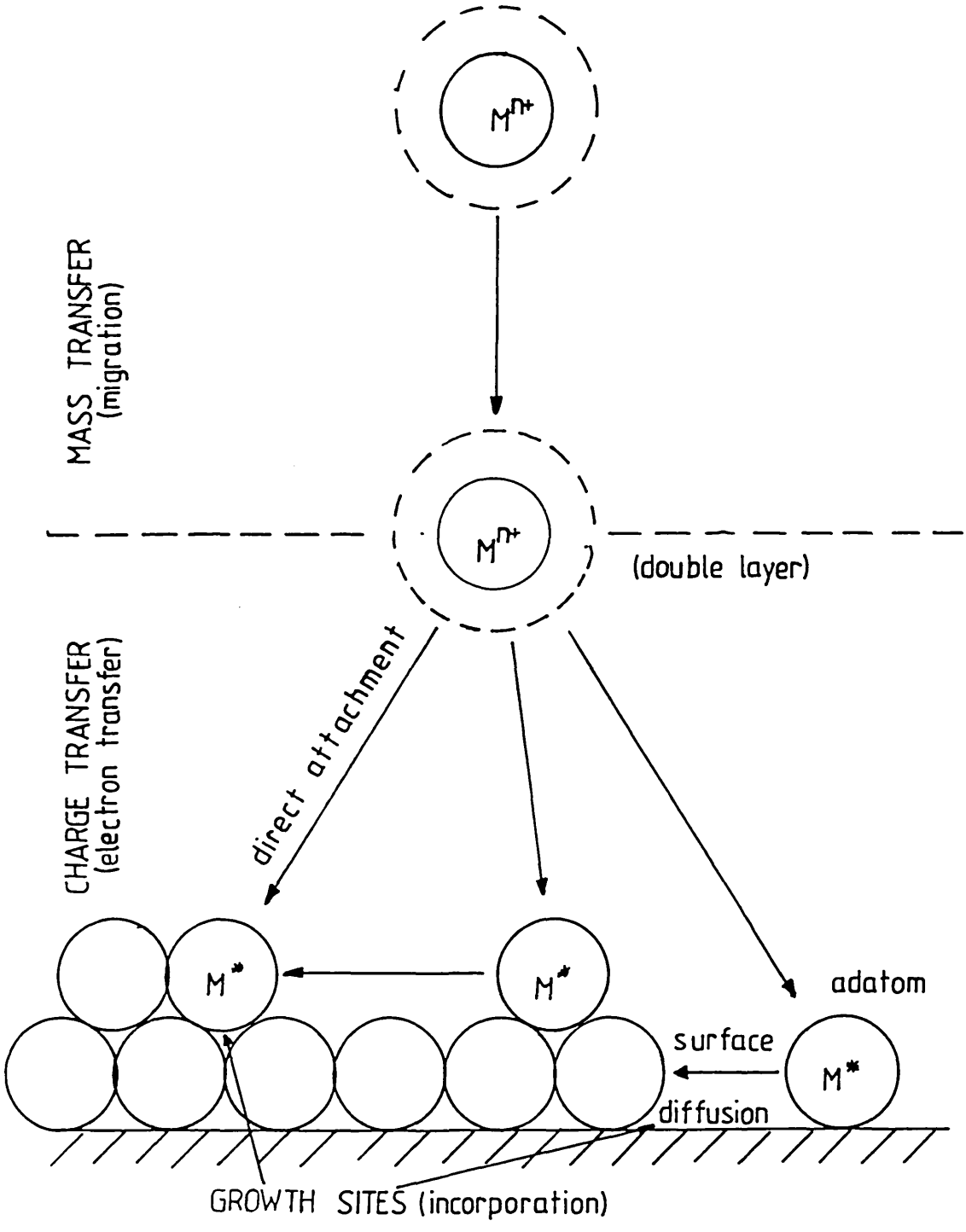

Fig.1.3. SCHEMATIC OF DEPOSITION

the concentration of the ionic species at the electrode surface reaches zero so that no further reaction can occur by a further increase in current density.

j_L can be determined from:

$$j_L = \frac{D\ n\ F\ a}{(1 - t)\delta}$$

Where D is the diffusion coefficient, n the valency, a the activity, t the transport number of the reacting ion and δ is the thickness of the diffusion layer.

The first stage is the nucleation of an adsorbed atom on to a substrate. When a constant potential is applied to a substrate, after an initial induction period, the number of nuclei increase linearly with time. The rate is dependent upon the overpotential. After sufficient time the surface becomes saturated and no more nuclei are formed. This initial layer involves the simultaneous growth and formation of nuclei, and the structure will depend on the relative rates of these two competitive processes. A continuous layer may be formed by complete coverage of the substrate by newly created nuclei, or by coalescence of growing nuclei already formed. This nucleation process is dependent upon the surface activity of the substrate. Heterogeneous nucleation occurs and is controlled by the interfacial energy (σ) of the two phases, and the super saturation, which is controlled by the overpotential (η) so that the rate of nucleation (J^o) can be given by (15-18):

$$J^o = K.\exp(\beta\sigma^3/\eta^2)$$

where K and β are constants.

These nuclei may present different morphologies and allow various degrees of epitaxy to develop with the substrate. These factors determine the characteristics of the initial layer and so to some extent, the properties of the whole deposit, such as adherence and the degree of coverage.

1.4.ELECTROCHEMICAL METHODS

1.4.1. Cyclic voltammetry

Several techniques can be used for investigation of electrochemical processes in molten salts. Chronopotentiometry, chronoamperometry and cyclic sweep voltammetry are most commonly used. Cyclic voltammetry and chronoamperometry were used to investigate electrochemical reactions and the processes in this work.

In cyclic voltammetry, the potential of a working electrode in an unstirred solution containing electroactive species is varied linearly with time. If the solution contains only the oxidized form, the potential sweep is started at a more positive potential than that of standard redox potential of the couple.(anodically). As the potential tends towards the standard potential, the oxidised species will begin to be reduced. Diffusion of oxidised species towards the electrode occurs due to a concentration gradient being established between the bulk solution and the electrode surface. As the potential is swept past the standard potential, the current rises rapidly, as the driving force for the reaction increases, reaching a maximum. This maximum is produced by the depletion of the electroactive species at the electrode. The net current begins to decay,when the rate of diffusion through the double layer, becomes slower than the rate of the electrode reaction, as a result of the increasing thickness of the diffusion layer. On reversal reoxidation occurs similarly, resulting in an anodic peak. A cyclic voltammogram for a simple reversible reduction process is shown in Fig.1.4.1.

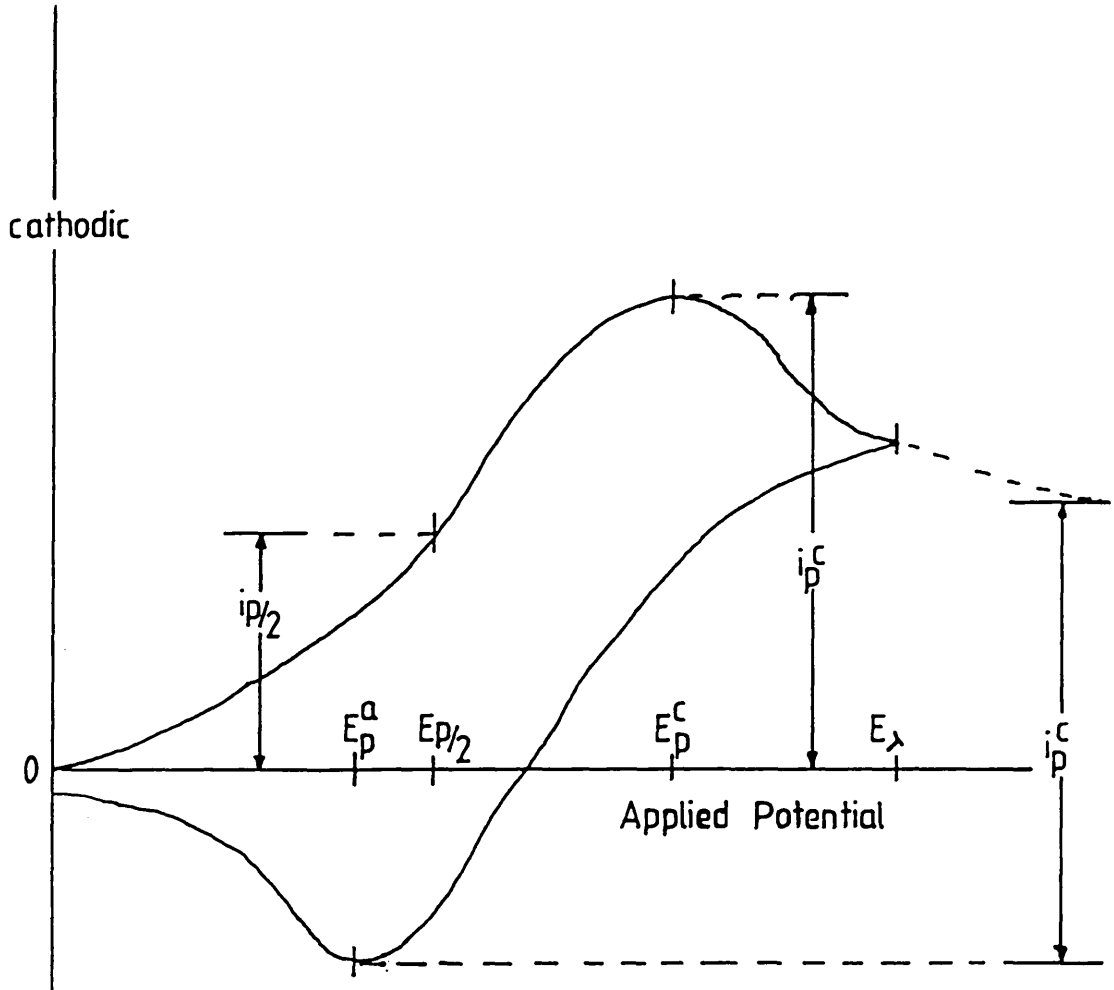

E_p^c peak cathodic potential

E_p^a peak anodic potential

i_p^c peak cathodic current

i_p^a peak anodic current

$i_{p/2}$ half peak cathodic current

$E_{p/2}$ potential corresponding to $i_{p/2}$

E_λ switching potential

Fig.1.4.1. CYCLIC VOLTAMMETRIC PARAMETERS

Electrochemical relationships between cyclic voltammetric parameters have been established:

The peak current (i_p) for a simple reversible diffusion controlled process is given by the Randles - Sevcik equation(19):

$$i_p = \frac{0.452(nF)^{3/2}}{(RT)^{1/2}} . n . D^{1/2} . C . v^{1/2}$$

where i = the faradaic current(mA), n = number of electrons involved in the process, C = bulk concentration of reactant(mol/l) and v the voltage scan rate(V/sec). Other parameters as before.

The peak potential (E_p) for this process can be related to the polarographic half wave potential ($E_{p/2}$) (20) which gives the following relation:

$$E_p = E_{p/2} - 2.2(RT/nF)$$

These equations are only valid for reversible reactions where the product is soluble, and it has been shown(21) for such systems, that a plot of log $(i_p - i)/i$ vs potential should be linear with a slope of 0.58(nF/RT), in the range 0.35-0.7i_p.

This theory has been extended to irreversible reactions of many mechanisms, so that the variation of i_p / $v^{1/2}$,E_p and $i_p{}^a/i_p{}^c$ with scan rate, allows both qualitative and quantitative characterisation of unknown systems.(22,23).

1.4.2.Chronoamperometry.

In chronoamperometry, a potential step is applied to the working electrode and the resulting current through the cell is monitored as a function of time. The observed current, time curves are dependent upon potential, concentration, mass transfer coefficients and kinetic parameters.

Generally the current, time characteristic has the form(24):-

$$i=\frac{n.F.D^{1/2}C_O^{o}}{(1-A\theta)^{1/2}t^{1/2}}$$

where $A=(D_O/D_R)^{1/2}$ and $\theta= C_O(0,t)/C_R(0,t)$.

For the reaction:- O + ne $\longrightarrow$ R and for the condition when the concentration of the reactant becomes zero at the electrode and the current is totally controlled by mass transfer, then this equation reduces to:- (for a planar staionary electrode)(25,26)

$$i= n.F.C_O^{b}(D_O/\pi t)^{1/2}$$

Thus plots of i vs $t^{-1/2}$ should be linear, with a gradient that is proportional to the bulk concentration at the electrode. When this condition is not satisfied, that is when the applied potential is not sufficiently negative, and if the potential is still sufficiently negative to cause electrolysis of O then the current is a function of the variation of this O concentration, according to the charge transfer process. For an irreversible charge transfer at short times the current form can be simplified to :-

$$i=n.FAK_fC_O(1-2K_ft^{1/2})(\pi D_O)^{1/2}$$

In order for these reactions to proceed, nucleation of the product at the electrode must occur. By relating the stable size of nuclei, to the transport of reactants to the nucleation site, the current form required to give nucleation can be determined. The current form for low overpotentials:-(simplification, not allowing for the change of nuclei radii)(27)

$$i(t) = n.F\pi M^{1/2}(2DC)^{3/2}(1-\exp(-nF\eta/RT))^{3/2}(t/\rho)^{1/2}$$

If both nucleation and growth occur at the same time, this equation becomes:-

$$i(t)=2/3i_OsnF\pi M^{1/2}(2DC)^{3/2}(1-\exp(-nF\eta/RT))^{3/2}(t^{3/2}/3\rho^{1/2})$$

The rising portion of i-t curves generated from chronoamperometry at low overpotentials, can give information about the type of nucleation process occurring.

1.5. AIMS

The successful electrodeposition of refractory metal carbides from molten fluorides and the production of Mo_2C from molten chlorides have been reported. However the electrochemical reactions that give rise to the formation of these carbides have not been investigated. In this study the chemistry and electrochemistry of Mo yielding species and carbonate ions in molten $CaCl_2$, and the chemistry and electrochemistry of both together, required to give Mo_2C coatings at stainless steel substrates, have been investigated. The investigation was approached by combining the electrochemical methods of cyclic voltammetry and chronoamperometry , with the characterisation of deposits by scanning electron microscopy and X-ray diffraction.

2.LITERATURE SURVEY

2.1.REFRACTORY METAL ELECTRODEPOSITION

Many processes for the production of refractory metal coatings by electrodeposition are reported in the literature. All have been successfully deposited from molten salts. Complex parameters control the deposit characteristics required to give good adherence and purity. Inorder to optimise these characteristics various electrolytes and reduction reactions have been used.

Chromium is the only refractory metal that can be obtained from aqueous electrolytes and thus this process has been developed and operated commercially over the last sixty years, using chromic acid-sulphate electrolytes (28). However the relatively poor quality of electroplates produced, due to the co-deposition of hydrogen giving rise to cracks and porosity (except in very thin plates)(29), has led to the development of molten salt plating processes for more demanding chromium plate applications. Vargas and Inman(30) using chromous chloride ,(LiCl-KCl) eutectic solutions, have developed a pulsed potential chromium plating technique, which gives rise to high initial nuclei coverage and avoids dendrite formation. Thus adherent, coherent and low porosity coatings are produced.

Mellors and Senderoff (31) developed a general process for electrodeposition of coherent zirconium, hafnium, vanadium, niobium, tantalum, chromium, molybdenum and tungsten. Using an electrolyte mixture of pure fluorides of alkali and refractory metals maintained under an inert argon atmosphere at 700-825^{o}C, they found that faradaic electrodeposition occurs provided the mean valence of the metal ion in solution is not too high. i.e.+5 - tantalum, +4.5 - tungsten, +4 - niobium, zirconium and hafnium and +3 - molybdemun, chromium and vanadium. However titanium deposits could only be produced to a thickness of <5 mils. before dendritic growth occured.

Coherent deposits of molybdenum and tungsten have been electrodeposited from other melts. Senderoff and Brenner (32) used the LiCl-KCl eutectic to electroplate molybdenum from K_3MoCl_6 at 600°C. Again the valence state of the molybdenum is important in the resultant quality of deposits and it is interesting to note that coherent deposits are not produced if a NaCl-KCl eutectic is used. Tungsten has been deposited from a LiB_2O_4,$NaLiWO_4$ and WO_3(6:2:1) mixture. This process (33,34) was operated at 900°C in a nitrogen atmosphere. Zuckerbrod and Bailey (35) note that tungsten coatings are produced from the LiCl-KCl eutectic with K_2WCl_6 by a disproportionation reaction during reduction, rather than by the "true" electroreduction of WCl_6^{2-}, as this potential probably lies beyond the melt limit.(36)

Probably the first attempt to electrodeposit titanium from molten salts was made by Cordner and Worner(37) who using a LiCl-KCl(60:40) and $TiCl_3$ electrolyte and they noted that at > 460°C two immiscible liquid layers formed, the upper being green ,the lower dark purple. Electrolysis of this upper layer gave fine powdered deposits of 99% Ti with a current efficiency of 40-60% ,the lower layer acting as a reservoir of Ti^{3+} for the upper. However from a $TiCl_3$-NaCl-KCl electrolyte at 900°C, Brenner and Senderoff(38) produced coherent deposits on tungsten substrates at current densities of 0.3 A/cm^2.

The electrolyte compositions which give coherent deposits for various halides were considered by Fortin et al., who found that KI-KF yielded coherent deposits but KI-NaI, dendritic titanium (39). In the LiCl-KCl eutectic the following titanium sources yielded high purity dendritic deposits a> K_2TiF_6 b> $TiCl_3$ and c> in situ anodic dissolution of Ti but using $TiCl_4$ produced spongy Ti.(40)

However cystalline deposits can be produced from $TiCl_4$ in LiCl-KCl-NaCl if the deposition cathode is only lowered into the melt after electrolysis has become established.(41)

An all fluoride process allowed production of coherent pure Ti deposits at a rate of 30(μmh^{-1}) which alloyed with the copper substrate at 700-800^{o}C. Low oxygen content was again indicated to be necessary for coherency.(42) As was noted with tungsten, titanium can be deposited by disproportionation reactions in chloride melts(43, 44).

2.2 REFRACTORY METAL CARBIDE, BORIDE AND SILICIDE ELECTRODEPOSITION.

Production of carbides by electrodeposition was first reported in the 1940's by Wiess and Andrieux(45.46), who used sodium carbonate, sodium metaborate and lithium fluoride or barium flouride and oxides of tungsten or molybdenum as electrolytes. They concluded that reduction of the carbonate accounted for the production of carbides. Similarly Mo_2C has been deposited from molybdenite in, KCl-KF-Na_2SiO_3 or NaF-NaB_4O_7-Na_2CO_3 using a graphite anode as a carbon source.(47) Attempts to co-deposit WC from WO_3 in these electrolytes, has resulted in powdery mixtures of WC, W_2C, W and C. More recently Mo_2C has been electrodeposited from NaF-KF containing $Na_2B_2O_7$, Na_2CO_3 and Na_2MoO_4 at 960^{o}C to give adherent silvery crystallites (48) and Shapoval (49) et. al. using Na_2WO_4, K_2WO_4, Li_2CO_3 and MoO_3 at 800-900^{o}C.

Gomes and Wong (50) using a NaOH-Na_2WO_4-$Na_2B_2O_4$ electrolye at 1000-1025°C with a consumable graphite anode, determined that the composition required for the optimum production of WC,was equimolar. Deposits were dendritic and contained W_2C and free C which were co-deposited.

These investigations have been adapted and extended to allow deposition of TaC and NbC at 750°C from $Na_2B_2O_7$, $NaCO_3$, NaF, KF and Ta_2O_5 or Nb_2O_5. Careful regulation of melt composition was required as too high a proportion of borates yields borides and also effects the morphology of the deposits.(51)

Stern and Godomski(52) used the commercially available K_2TaF_7 in LiF-NaF-KF (FLiNaK) eutectic and knowledge of carbonate reduction in fluorides to similarly produce TaC. This process was later extended to W_2C from Na_2WO_4 (53) and TaS from K_2SiF_6 (54). Charcterisation of W_2C (55) produced revealed that the coatings were made up of large crystallites and Stern et al. suggest that impurities control the morphology. Investigations into the effect of temperature, potential, current density and melt compositions in LiF-KF and LiCl-KCl on WC deposit morphology have revealed a complex effect but some trends can be noted.(56)

Topor and Selman (57) following Stern et al.'s work used addition of K_2CO_3 and $NaMoO_4$ to electroplate coherent dense Mo_2C coatings from FLiNaK at 850°C. Kushkhov extending Shapoval(49) work in tungstanate melts to chloride melts, has co-reduced MoO_4^- and CO_2 solutes to give Mo_2C.(58)

Borides have also been electrodeposited from fluorides.(59) Coherent deposits of ZrB_2 from KBF_4 in LiF-KF- K_2ZrF_6 at 800°C. and later work using a LiF-KF-K_2TiF_6-KBF_4 system (60) indicate that the reduction steps are :-

$$TiF_6^{2-} + e \rightleftharpoons TiF_6^{3-} \qquad (2.2.1)$$

$$BF_4^- + 3e \rightleftharpoons B + 4F^- \qquad (2.2.2)$$

$$TiF_6^{3-} + 3e \rightleftharpoons Ti + 6F^- \qquad (2.2.3)$$

$$Ti + 2B \rightleftharpoons TiB_2 \qquad (2.2.4)$$

Earlier powdery deposits of TiB_2 were produced from MgO, MgF_2, B_2O_3 and TiO_2 electolyte (61) and using $NaBO_2$-$LiBO_2$-$NaTiO_3$-$LiTiO_3$ and TiO_2 coherent deposits of TiB_2 were produced.(62)

2.3.MOLTEN SALTS AS SOLVENTS

In order to understand the interactions between titanium and carbide, molybdenum and carbonate and solvent ions, the structure and acid-base relationships in molten salts must be considered. The structure of molten salts is often considered to be one of interlocking quasi lattices (63,64), which allows the prediction of its physical properties. The separate nature of the anion and cation lattices does not allow grouping of ions from different lattices. The sterochemistry and co-ordination relationships noted from spectroscopic data (65) and the aqueous behaviour of transition metals indicate ion association (or formation of complex ions) occurs in molten salts. The 'life time' of such species is very debatable, due to the complex nature of IR, Raman and neutron scattering spectra.

This complex ion formation is reflected in the acid-base behaviour in molten salts. Lux and Flood developed an acid-base concept for molten oxide systems (66,67), such that:

$$\text{Acid} + O^{2-} \rightleftharpoons \text{Base} \qquad (2.3.1)$$

this can be extended to molten halides as:

$$\text{Acid(acceptor)} + X^{-} \rightleftharpoons \text{Base(donor)} \qquad (2.3.2)$$

Using a Lewis type definition of acidity so that a chloride ion acceptor can be considered an acid.(e.g. $TiCl_2$)

The nature of cations and anions present in the solvent can greatly influence reaction mechanisms for electrodeposition. This effect can be noted by considering the reduction steps of titanium in chloride compared with fluoride melts.

In chloride melts reduction proceeds :-

$$Ti^{4+} \longrightarrow Ti^{3+} \longrightarrow Ti^{2+} \longrightarrow Ti^{0}$$

whereas in fluorides :-

$$Ti^{4+} \longrightarrow Ti^{3+} \longrightarrow Ti^{0}$$

In fluorides the formation of complexes , TiF_6^{2-},$Ti_2F_7^{-}$ does not allow the formation of the lower oxidation state. The formation of such complexes in chlorides is not so clearly indicated and thus as such expected 'complexes' are probably ill-defined, short life time structures, resulting in the larger number of apparent oxidation states. Thus the more acidic nature of the titanium in fluorides is indicated by their complex stablity.

2.4. ELECTRODEPOSITION OF TITANIUM

The possibilities for titanium production by the direct electroreduction of chlorides is indicated by the properties of the three oxidation states available. $TiCl_4$ is a typical covalent compound, melting at -25°C and is virtually non conducting, $TiCl_3$ decomposes at 440°C and $TiCl_2$ has a strongly ionic character (68), but other

properties are, as yet, ill defined. It is reported that $TiCl_2$ sublimes in hydrogen and decomposes in vacuum at 475°C, but according to phase diagams of systems NaCl-$TiCl_2$ (69) and KCl-$TiCl_2$ (70), the melting temperature of this chloride is approx.1025°C. These unsuitable physio-chemical properties have led to the use of solutions of titanium halides, for titanium reduction. Practically (as noted before) the most suitable solvents are fluorides and chlorides of alkali and alkaline earth metals.

The different titanium plating processes can be considered in terms of the nature of the electroactive titanium species and thus three groups can be identified: using i> titanium chloro-complexes

ii> titanium fluoro-complexes

and iii> titanium dioxide (including mixed complexes e.g. $TiO(F,Cl)_4^{2-}$) as solutes.)

i> Titanium chloro-complexes

The electrochemistry and thus the electroplating of titanium from chloro-complexes in all chloride systems is complicated by the instability of the complexes formed, especially when several oxidation states are present together. The reduction sequence of:-

$$Ti(iv) \longrightarrow Ti(iii) \longrightarrow Ti(ii) \longrightarrow Ti(0)$$

has been established in a series of alkali and alkaline earth metal chlorides and mixtures, by Chassaing et al.(71)

They noted the following disproportionation reactions between the various oxidation states:-

$$3Ti(ii) \rightleftharpoons 2Ti(iii) + Ti \qquad (2.4.1)$$

$$2Ti(iii) \rightleftharpoons Ti(iv) + Ti(ii) \qquad (2.4.2)$$

$$4Ti(iii) \rightleftharpoons Ti + 3Ti(iv) \qquad (2.4.3)$$

$$2Ti(ii) \rightleftharpoons Ti + Ti(iv) \qquad (2.4.4)$$

These reactions are also noted by Baboian et al.(72). The formation of powdery titanium deposits noted in many papers(37,73,74,40) and low current efficiencies for

titanium deposition, can be accounted for by these disproportionation reactions.

Particular problems arise from the low solubility of $TiCl_4$ in the melt, such that the value of the redox potential Ti(iv)/Ti(iii) is tentatively valued. For example, in the LiCl-KCl eutectic at 450°C, it is ascribed the value -0.41 V w.r.t. Ag ref. electrode. This occurs due to the loss of volatile $TiCl_4$ from the melt. To allow the electrodepostion of titanium from $TiCl_4$, as a titanium source, reduction to lower oxidation states is required, especially as reoxidation of $TiCl_2$ and $TiCl_3$ can occur readily at the anode and be lost as $TiCl_4$.(75-77) The formation of powdery electrodeposits has also been accounted for via chemical reduction of Ti(iv) and Ti(iii) by alkali metals.(73,74,40) Reduction of alkali metal ions at the cathode, followed by dissolution into the melt locally, allows reduction of Ti ions in the proximity of the electrode. The activity of the alkali metal(s), convection of titanium and the temperature of the electrolyte, determine the 'availibility' of alkali metal ions for this reaction and thus whether the powdery titanium is formed. Due to the possible disproportionation reactions and alkali metal reduction processes available in these melts, the average valency of the titanium ions present, can be used as an indicator of this availability. Alpert et al.(75,77) have shown that coherent titanium deposits are produced most favourably with n values of approx. 2.2. Similarly Elyutin et al. (78) indicated that increases in current efficiency are possible if high $TiCl_2$ concentrations are achieved.

Numerous electrolytes containing Ti(ii) and Ti(iii) chlorides and mixtures of alkali and alkaline earth chlorides, have been considered by Tokumoto et al. (79-81), producing Ti coatings upto 0.5mm thick, with current efficiencies of 50-90% at 400-500°C.

ii> Titanium fluoro-complexes

Potassium hexafluorotitanate provides a readily available and easy to handle source of Ti^{4+} ions and as such, the electrochemistry of this complex has been considered most frequently. Brenner and Senderoff were probably the earliest workers to attempt to produce titanium coatings from K_2TiF_6 as a solute in LiCl-KCl and NaCl-KCl eutectics, but powdery rather than coherent deposits were produced.(82) Later workers (83,84) were more sucessful using K_2TiF_6 in various halides, between 750-950^oC and at current densities of 0.5-5.5 A/cm^2.

The electro-reduction of TiF_6^{2-} proceeds by two steps, as would be expected in an all-fluoride solvent (42):

$$TiF_6^{2-} + e \longrightarrow TiF_6^{3-} + 3e \longrightarrow Ti + 6F^- \quad (2.4.5)$$

Recent work (85) indicates that the fluoride concentration plays an important role in these reductions such that at < 3 wt% KF the reaction steps are:-

$$Ti^{4+} + e \longrightarrow Ti^{3+} + e \longrightarrow Ti^{2+} + 2e \longrightarrow Ti \quad (2.4.6)$$

rather than the two reaction steps at greater KF concentrations.

Use of a 5 mol% K_2TiF_6 and 95 mol% NaF electrolyte has allowed the production of coherent uniform titanium coatings at 1000^oC with current densities of 2-4 A/cm^2, on an iron substrate with an intermetallic Fe_2Ti layer providing good adherence. Dendritic titanium is often yielded from electrolysis of K_2TiF_6 containg halide melts and methods to control neucleation and growth have been considered to allow suitable deposits to be made. Pulsed current electrolysis using KF-LiF and 10 wt% K_2TiF_6 has yielded 50μ deposits on an iron substrate at 750^oC.(86)

iii> Titanium dioxide

Several attempts have been made to deposit titanium from electrolytes containing TiO. TiO dissolved in alkali and alkaline earth metal halides have yielded titanium contaminated with oxygen and carbon.(87) Rutile was produced using Na_3AlF_6-NaCl-TiO_2 as an analogue to aluminium production (88) and TiO, $MgTiO_3$ and $CaTiO_3$ titanium sources dissolved in fluorides at 1300-1850^oC, produced titanium contaminated with carbon and other impurities. (89,90)

The introduction of oxygen into chloride melts, gives rise to the rapid formation of grey oxide precipitates. Littlewood(91) produced E v pO^{2-} diagrams for Ti-LiCl and Ti-KCl at 800^oC and thus revealed the low concentration of oxide required to allow formation of oxide precipitates. Similarly E v pO^{2-} diagrams for TiO_2 using oxacidobasic couples based on FeO have been developed for LiCl-KCl eutectic mixtures.(92)

2.5. ELECTRODEPOSITION OF MOLYBDENUM

The electrochemistry of molybdenum in molten salts is controlled by the availability of oxidation states in the solvents.

In chlorides, species of Mo(VI) to Mo(0) have been observed, but the conditions giving rise to these states and their interactions is very dependent upon the solvent. For example : in NaCl-$AlCl_3$ melts(93), Mo(V) to Mo(0) species may be obtained, depending upon the basicity of the melt, favouring complexing and thus the stability of various species.

White and Twardoch(94) extensively reviewed the processes and routes for the reduction of molybdenum in molten salts and considered the conditions which allowed the deposition of coherent molybdenum, thus only the most relevant work in chloride melts will be considered here.

Coherent electrodeposits of Mo are most readily produced by the reduction of Mo(III) species in molten chlorides (95,96,40,41), although the disproportionation of complexes and dimer formation complicate the chemistry of this process. The reactions available are indicated below:

$$Mo_2Cl_9^{3-} + 3Cl^- \rightleftharpoons 2\ MoCl_6^{3-} \quad (2.5.1)$$

$$MoCl_6^{3-} + 3e \rightleftharpoons Mo + 6Cl^- \quad (2.5.2)$$

$$Mo_2Cl_9^{3-} + 6e \rightleftharpoons 2\ Mo + 9Cl^- \quad (2.5.3)$$

$$5\ Mo_2Cl_9^{3-} \rightleftharpoons 3\ MoCl_5 + 2\ Mo + 15Cl^- \quad (2.5.4)$$

Cyclic voltammetric studies using LiCl-KCl and CsCl-LiCl eutectic solvents allowed the stability of the dimer to be controlled and hence its involvement in electrochemical reactions. (45) These studies gave results showing:- Time dependency indicating the availabilty of chemical reactions, temperature dependency indicating the loss of volatile species and/or the change in controlling equilibrium reactions. Scan rate dependency also indicates coupled chemical reactions to those occuring at the electrode. The observation of two cathodic peaks and only one corresponding anodic peak in the presence of Cs^+ rather than K^+ indicates the presence of two species in the same oxidation state. Chronopotentriometric studies also indicate this.(97) Indicating the availab ility of all of the above reactions, in these melts.

Interestingly, the papers reviewed by White and Twardoch (94) indicated that reduction of molybdate solutes in chlorides do not produce metal, but Mo(VI) species and other valence states are generated by chemical dissociations.(98,99,50) However Shapoval and Makogan (100) found that in more acidic chloride melts (e.g.LiCl-KCl eutectic) MoO_3 could be reduced to the metal at platinum electrodes, provided the Pt had formed a Pt/Li alloy prior to reduction of MoO_3. They attributed this phenomenon to heterogeneous catalysis. Similarly Shapoval has reduced

MoO_3 to metal in a $NaWO_3$ melt at low MoO_3 concentrations according to the reaction:

$$4\ Mo_2O_7^{2-} + 6\ e \rightleftharpoons Mo + 7\ MoO_4^{2-} \qquad (2.5.4)$$

but at concentrations > 4-5 mol% MoO_3 reduction proceeds:-

$$Mo_2O_7^{2-} + 2\ e \rightleftharpoons MoO_2 + 3\ MoO_4^{2-} \qquad (2.5.5)$$

and

$$MoO_4^{2-} + 2\ e \rightleftharpoons MoO_2 + 2\ O^{2-} \qquad (2.5.6)$$

Smooth adherent deposits of Mo on Cu,Ni,Mo, stainless steel and graphite substrates have been electroreduced from a 70% KF, 10% $K_2B_4O_7$, 20% K_2MoO_4 mixture.(101)

2.6. ELECTRODEPOSITION OF CARBON

Carbon does not react with these melts and anodisation of carbon electrodes produces chlorine (thus the use of graphite auxillary electrodes in this melt). Cathodisation of carbon does not yield stable potentials prior to melt decomposition, but if oxide ions are present anodisation of carbon produces CO_2, consuming the electrode(102).

The cathodic reduction of carbonate melts to carbon is well established and Selman and Steunenberg(103) have shown that carbonate ions are reduced on gold in LiCl-KCl eutectic electrolytes. Similarly solutions of calcium carbide have been shown to yield carbon in these melts.(104)

2.6.1.Carbonate Reduction.

In molten carbonate melts, carbonate reduction occurs at the cathodic limit and elemental carbon is formed. Ingram and Janz(105) showed that this process may be considered as:

$$CO_3^{2-} + 4e \longrightarrow C + 3O^{2-} \qquad (2.6.1.1)$$

or

$$3CO_2 + 4e \longrightarrow C + 2CO_3^{2-} \qquad (2.6.1.2)$$

Both these reactions are available in carbonate melts, although (2.6.1.1) is usually the reaction responsible for carbon formation. These reactions can be defined in terms of the Lux-Flood acid-base equilibrium(66,67) and under normal conditions the production of carbon is thermodynamically preferred over the alkali metal. Barlett and Johnson(106) considered favourability of these reductions for various temperature and carbonates. They showed that as the temperature increases the reduction of CO_2 and/or CO_3^{2-} leads to carbon monoxide rather than carbon.

In halide melts both carbonate and carbon dioxide can be reduced to carbon. (depending upon the temperature) Deanhardt et al.(107) argued that the reaction (2.6.1.1) does not occur in FLiNaK carbonate reduction, but that the cathodic reduction of alkali metal leads to the chemical reduction of the carbonate and thus carbon deposition on the electrode. Similarly Stern and Gadmorski(108) could not observe carbonate reduction prior to the cathodic limit of FLiNaK, giving the reduction mechanism:

$$4\ Me + Me_2CO_3 \longrightarrow C + 3\ Me_2O \qquad (2.6.1.3)$$

Young(109) used cyclic voltammetry to investigate the reduction of sodium carbonate in LiCl-KCl-NaCl at 50°C with a tungsten working electrode. A pair of reduction and oxidation waves were obtained due to the presence of carbonate ions, suggesting that reaction (2.6.1.1) corresponds to the reduction wave at a potential of -1.8 V w.r.t. Ag(0)/Ag(I)(0.5M)reference electrode. As this potential is dependent upon the sweep rate, the reaction (2.6.1.1) can be concluded to be irreversible. Mo(110) continuing this work determined reduction potentials on tungsten, stainless steel and platinum.(Table 2.5.1)

Electrode	E^o (V) w.r.t.Ag(O)/Ag(I)(0.4M)
Pt	-1.745
W	-2.05
s/steel	-1.90

Table 2.5.1. DEPOSITION POTENTIALS FOR CARBON FROM CARBONATE IONS

She also tentatively suggested that the reduction proceeded via reaction (2.6.1.1) and that carbides were formed on oxidation on tungsten electrodes at potentials more anodic than - 0.60V w.r.t. Ag(O)/Ag(I). Delimarski et al.(111) were able to produce carbon by the reduction of both carbonate ions and carbon dioxide in NaCl-KCl eutectic at 680°C. They inferred a reduction sequence:

$$CO_2 + 2\,e \longrightarrow CO_2^{2-} \qquad (2.6.1.4)$$

$$CO_2^{2-} + 2\,e \longrightarrow C + 2O^{2-} \qquad (2.6.1.5)$$

and that in the presence of carbonate the chemical reaction:

$$CO_3^{2-} \rightleftharpoons CO_2 + O^{2-} \qquad (2.6.1.6)$$

preceeded the above reduction steps. Single reduction waves noted by other workers(112,109,110) indicate that direct reduction by (2.6.1.1) is more likely.

2.6.2. Carbide Oxidation

Barber and Sloan(113) have determined the solubility of CaC_2 in a number of pure alkali and alkaline earth halides and their mixtures up to temperatures of 1000°C. The highest solubilities were found to be in lithium salts and calcium chloride and its mixtures. Alkali halides other than Li showed much lower solubilities and free alkali metal is found in such melts indicating that displacement reactions of the following type are occuring :

$$2\,NaCl + CaC_2 \longrightarrow 2\,C + 2\,Na + CaCl_2 \qquad (2.6.2.1)$$

The chemical nature of the dissolved carbide and the chemical equilibrium:

$$CaC_2(soln.) \rightleftharpoons 2\ C(s) + Ca(soln.) \quad (2.6.2.2)$$

has been investigated in molten calcium chloride(114). The dissociation products of the above reaction are evident in significant amounts and as free calcium is formed in solution, this has a great effect on the chemistry and electrochemistry of the system. This work was confirmed by Maillot and Morris(115), who found CaC_2, CaO, free Ca and C all present in melt samples and determined phase diagrams for the binary system $CaCl_2$-CaC_2 and the psuedo-binary $CaCl_2$-(CaO+CaC_2). Technical grade CaC_2 is used in the above quasi binary rather than high purity CaC_2, as the removal of CaO (the significant impurity in techical CaC_2) results in the presence of free calcium, which even at low concentrations is a less desirable impurity for electrochemical analysis.

The presence of CaC_2 in the form:

$$CaC_2(soln.) \rightleftharpoons C_2^{2-}(soln.) + Ca^{2+}(soln.) \quad (2.6.2.3)$$

is also consistent with the liquidus line determined for this pseudo-binary.

The oxidation of carbides in molten salts especially in $CaCl_2$ from CaC_2 has been considered from a number of view points. The importance of CaC_2 as a slag component in many metal winning processes has led to its electrochemical examination.

Most workers (116) report the deposition of carbon from carbide solutions, although there are conflicting proposals as to whether this is a purely chemical decomposition or electrochemical oxidation of the acetylide ion, or some combination of these. There is little doubt however that thermodynamically the chemical equilibrium (2.6.2.2) at typical melt temperatures (400 -1000^{o}C) lies predominantly to the right and thus carbon deposition on all surfaces occurs to some extent.

White(117) invesigating these reactions concludes that the carbon deposition occurs both by an electrochemical / chemical route and by a pure electrochemical route:-

A priori anodic production of Ca^{2+} from calcium formed by reaction(2.6.2.2).:

$$Ca \rightleftharpoons Ca^{2+} + 2e \qquad (2.6.2.4)$$

allows the calcium content of the melt, to decrease locally at the electrode and pushes the chemical equilibrium further to the right (reaction 2.6.2.5):

$$CaC_2(soln.) \rightleftharpoons 2\,C(s) + Ca(soln.) \rightleftharpoons Ca^{2+} + 2e \qquad (2.6.2.5)$$

This accounts for carbon deposition occuring at cathodic limit potentials. Thus by controlling the oxidation of calcium, the deposition of carbon at the electrode may also be controlled.(104)

The direct oxidation of C_2^{2-} also occurs at potentials close to the cathodic limit, consistent with the free energy of formation of CaC_2.

The electrochemistry of Li_2C_2 in LiCl-KCl eutectic appears to reveal a quite different picture. Large decomposition potentials (2.0V) are required for the direct oxidation of carbide, although the free energy of formation of this salt is very small. According to Selman(103), a Li/Li^+ potential shift arising from the intercalation of graphite by Li, leading to a fall in activity of Li, may shift the carbide oxidation potential in the anodic direction.

Carbon deposits are similarly produced from Li_2C_2. The oxidation of aluminium carbides in cryolite to carbon at the anode has also been reported by Odegard et al.(118).

3. EXPERIMENTAL

3.1. APPARATUS

3.1.1. Furnace and Temperature Control.

A simple vertical Kanthal-wound (20 s.w.g.) alumina tube furnace was used. (Fig. 3.1.1) The temperature of the furnace was controlled by a PID/SCR/10A Eurotherm unit, with a monitoring Pt/Pt-13% Rh thermocouple located along side the furnace tube. This system provides a 10cm constant temperature zone. By locating a further Chromel-Alumel thermocouple inside the melt, the cell temperature can be controlled to ± 2K. An earthed nickel sheet lining the furnace provided a faraday shield for the electrodes, from inductive currents generated by the furnace windings.

3.1.2. Electrochemical Cell.

The cell assembly and arrangement are shown schematically in Fig.3.1.2a. The cell consisted of a lower round bottomed silica glass envelope, 55mm. in diameter and 200mm long in which an alumina crucible (40mm dia. 100mm high) contained the melt. This crucible rested on a bed of graphite impregnated asbestos sheet, which also lined the silica envelope, to protect it from "splashes". This cell was topped by a pyrex head. A vacuum tight seal between the head and lower envelope was achieved by squeezing silicone grease between the ground glass flanges, the pressure being applied by two bulldog clips. Quickfit SQ13 and SVL22 screw cap joints in the cell head allowed cell components to be introduced and removed. Also a side arm allowed the cell to be attached to a gas and vacuum line.

Ca_2CO_3, and CaC_2 could be added to the cell using the assembly shown in Fig.3.1.2b.

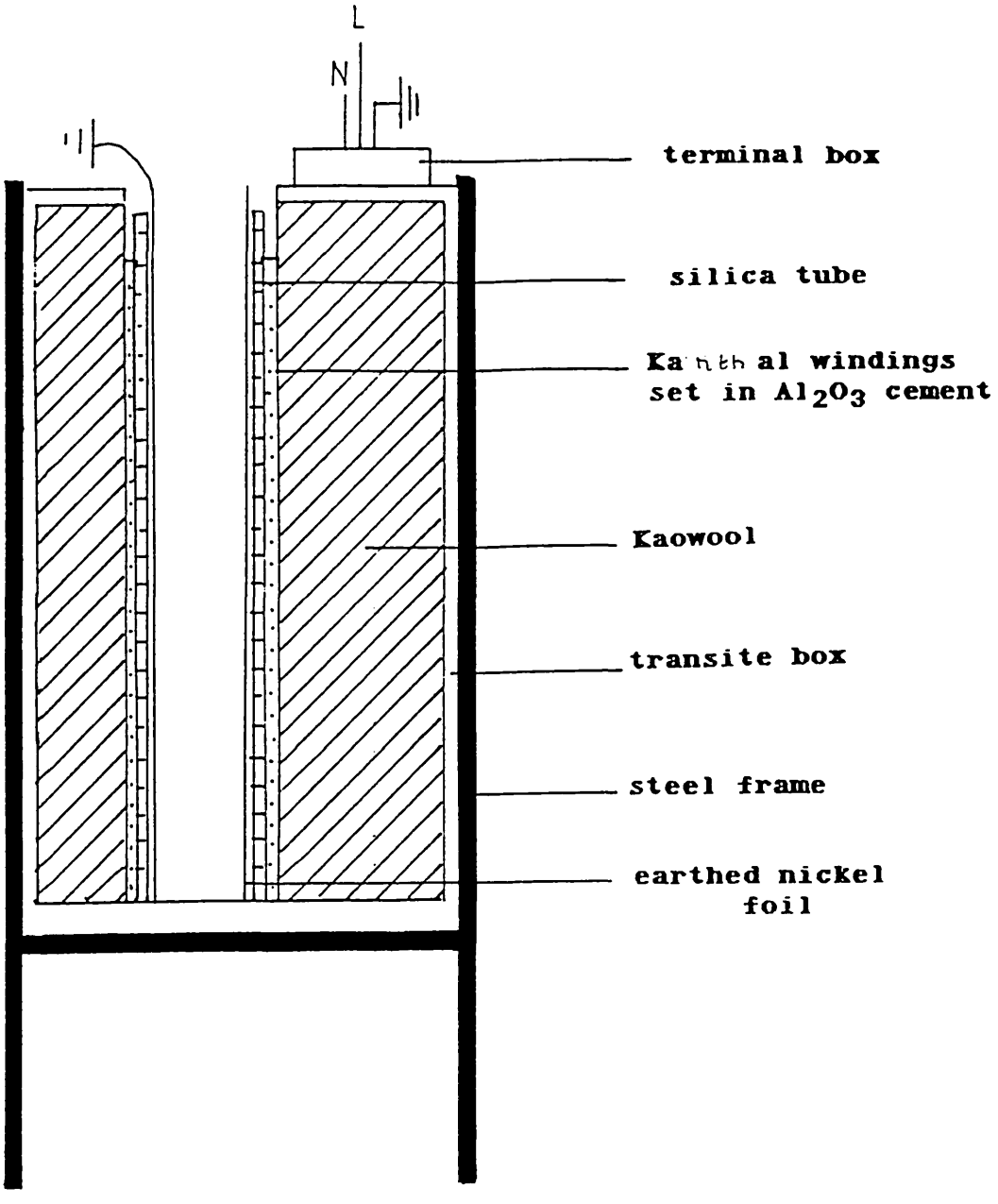

Fig. 3.1.1 SECTION THROUGH RESISTANCE FURNACE

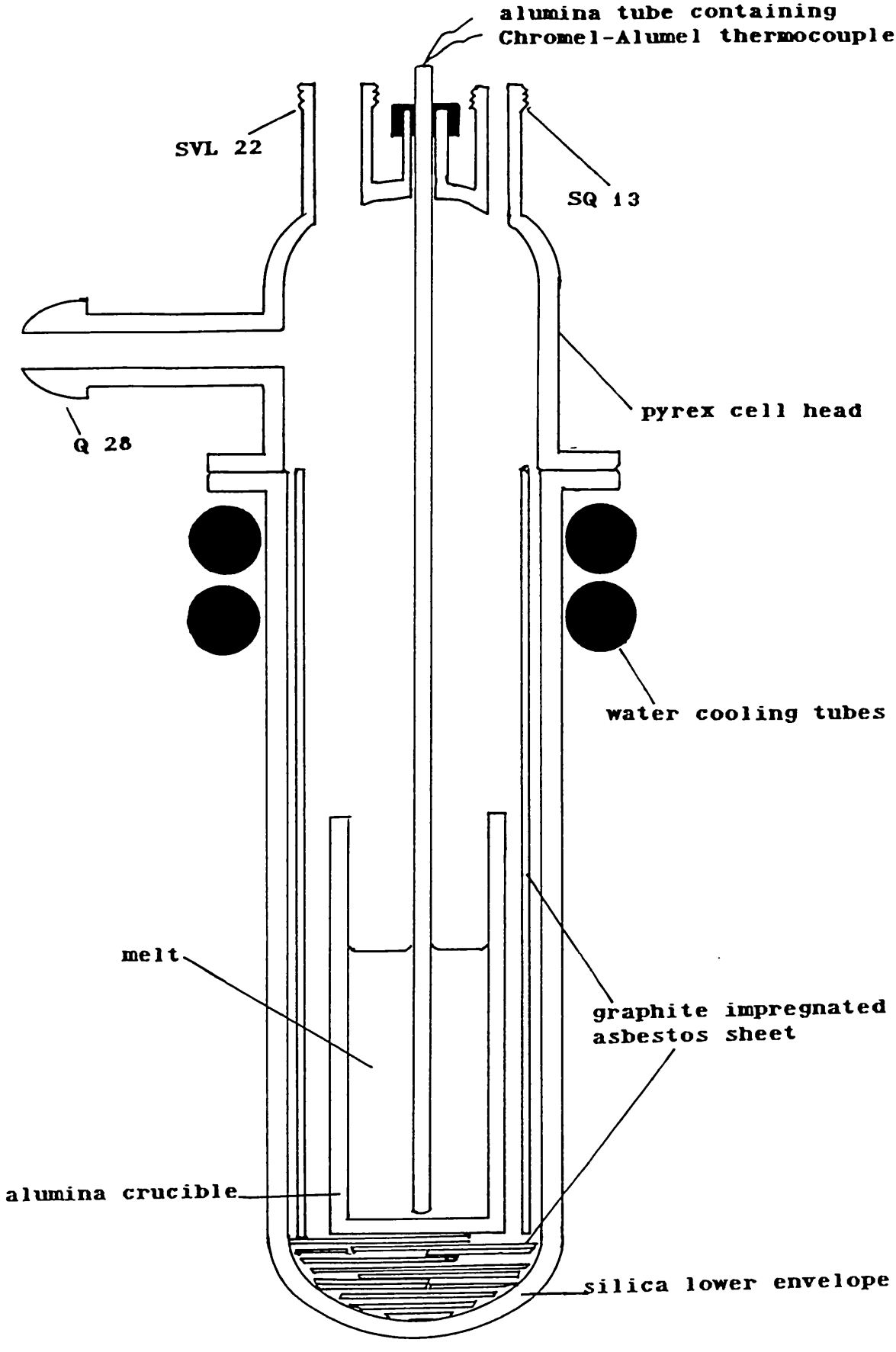

Fig. 3.1.2a SECTION THROUGH ELECTROCHEMICAL CELL

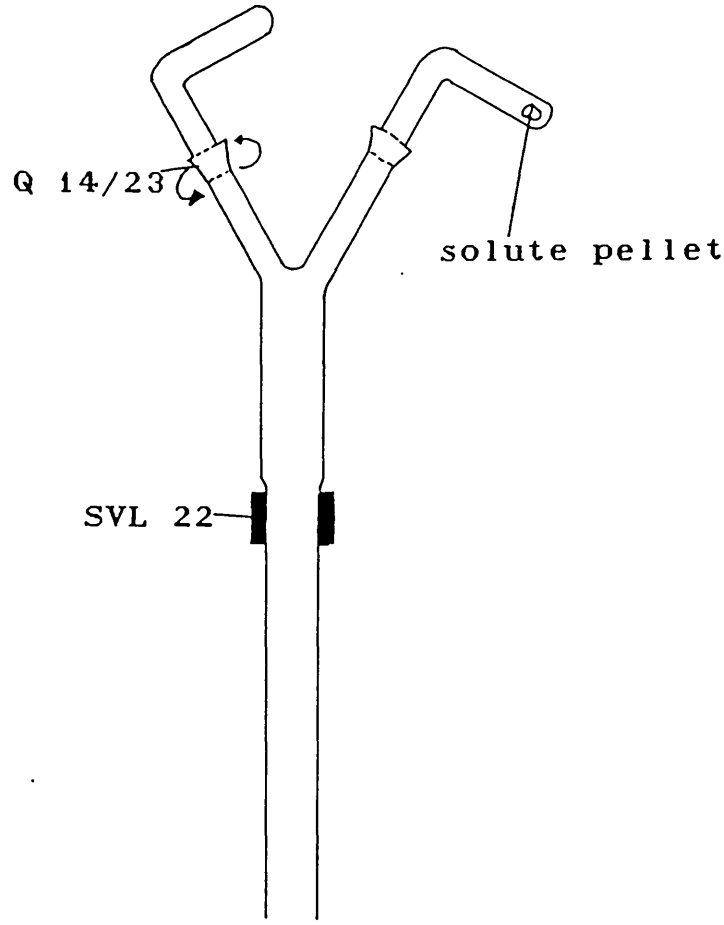

Fig. 3. 1. 2b SOLUTE ADDITION ASSEMBLY

3.1.3. Vacuum and Gas Supply.

An integrated gas and vacuum line was used to produce pressures down to 1 $X10^{-2}$ torr and argon/carbon dioxide environments. Two gas bags also allowed the maintainance of these environments by balancing the cell pressure against the external atmospheric pressure. The vacuum being generated by an Edwards ED 200 rotary pump and measured by an Edwards G5C-2 pirani gauge. Argon from a high purity cylinder (99.999%) was further purified by passing it through self indicating silica gel and '3A' molecular sieve to remove water and other gases. The gas was also passed through titanium beads heated to 700°C to remove oxygen. Hydrogen chloride gas was also purified prior to use for purification by passing it through molecular sieves and silica gel. The molecular sieves and silica gel were regenerated before each experiment, by heating to the necessary temperatures under vacuum. Similarly the titanium beads were replaced when oxidised.

3.1.4. Electronic Equipment.

All electrochemical measurements and electroplating processes were carried out using a three-electrode potentiostatic circuit (Fig.3.1.4) using a Thompson (259) IR compensating potentiostat and a Princeton Applied Research (+75) sweep generator. The current-voltage transients being recorded on a Bryans 29000 A4XY recorder.

3.1.5. Electrodes.

Working electrodes:

Tungsten and platinum working electrodes were used. (Fig.3.1.5). Tungsten electrodes were made from 0.87 mm. wire sheathed by a very close fitting alumina tube leaving the last millimetre exposed to the melt. This wire was sealed into 6mm alumina tubing. The exposed tip was then polished to give a mirror finish, washed with distilled water and dried with acetone before each use.

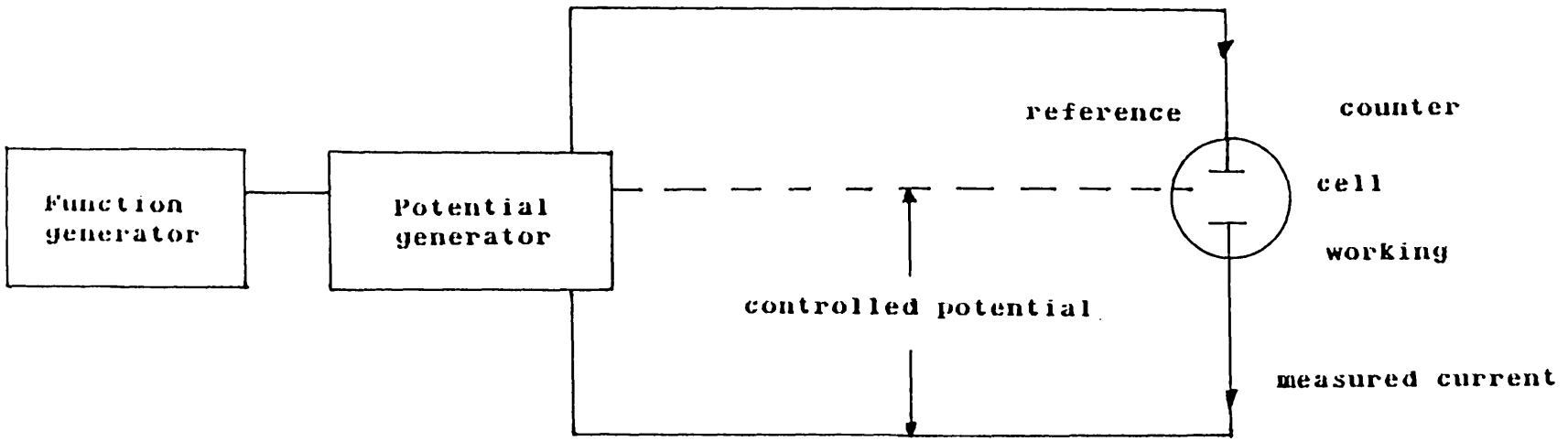

Fig. 3.1.4 CELL CIRCUIT DIAGRAM

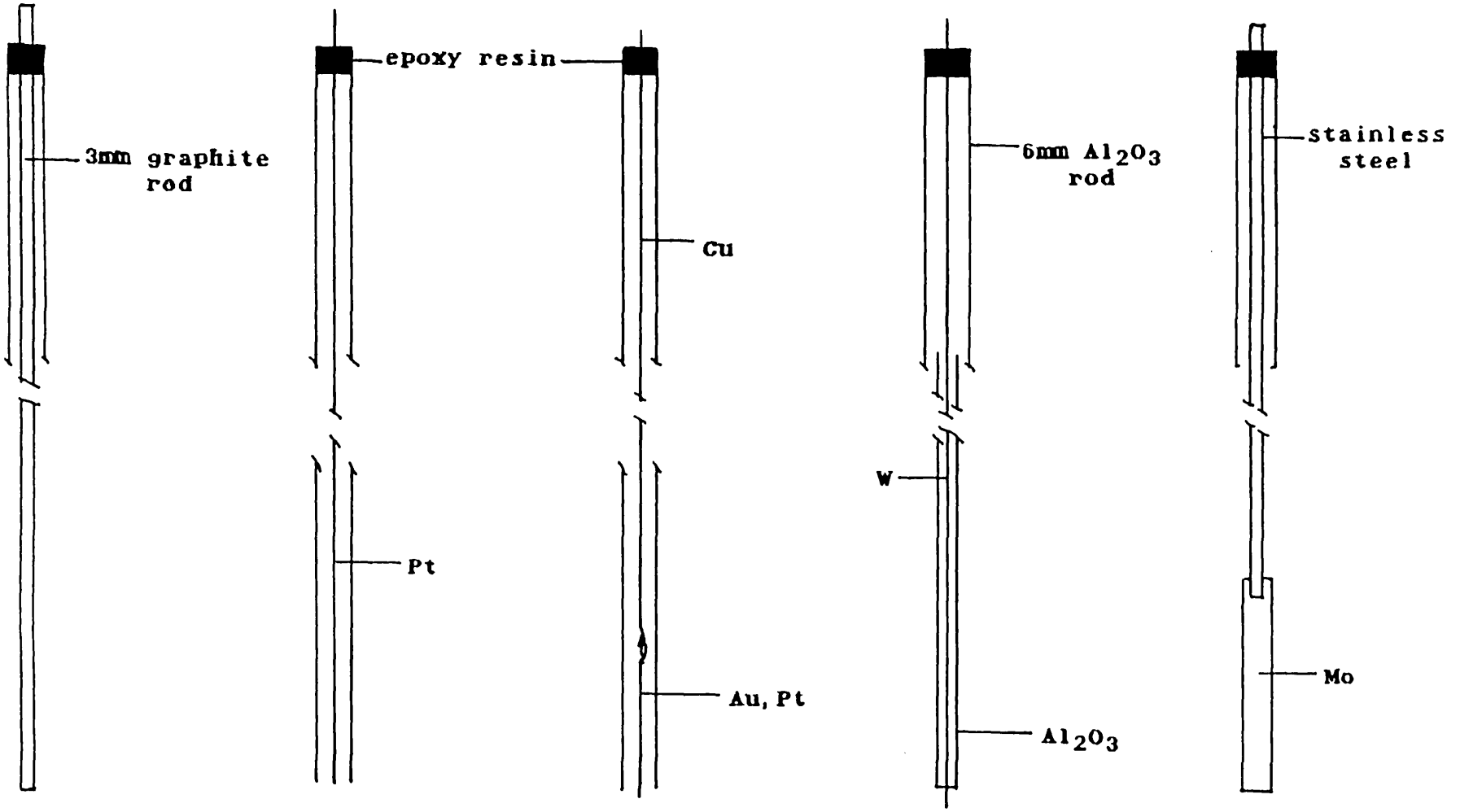

(a) graphite counter (b) Pt quasi reference (c) Au, Pt working (d) W working (e) Mo dissolution anode

Fig. 3.1.5 ELECTRODES

The platinum electrodes were simply made by looping a short length of wire through a longer nickel/chrome supporting wire and sealing this wire into alumina tubing leaving the bottom two millimeters exposed. These electrodes were also polished and washed as indicated above.

Plating Electrodes:

Stainless steel sheet cut into ~ 1.0cm x 3.0cm. coupons were electropolished using H_3PO_4(40%)-H_2SO_4(35%)-CrO_3(3%)-H_2O(22%) (119),and washed in distilled water, and dried with acetone. Copper wire looped through a hole in the coupons provided the electrical connection, and was also sealed into a silica tube. Titanium plating electrodes were made simliarly but polished in 2%v/v HF soln.

Counter Electrodes:

Graphite counter electrodes were used in both electrodeposition and electrochemical analysis. 3.0 mm. diameter rods (30cm. long) were sealed into 6mm. alumina tubing (Fig. 3.1.5)

Reference Electrodes:

Platinum quasi reference electrodes were used.(120) 30cm. lengths of wire were sealed into alumina tubing. The tube was then dipped into the full depth of the melt to allow maximum area to be in contact with the melt, whilst stopping contact with other electrodes. (Fig. 3.1.5)

Anodic Dissolution Electrodes:

Molybdenum rod and a titanium block, having large surface areas were supported by threaded stainless steel rods sealed into alumina tubing. The molybdenum rod was pre-electropolished in a sulphuric acid, methanol solution (119) and the titanium etched with 2%v/v HF.

3.2. CHEMICALS AND MATERIALS

The details of the chemicals and materials used in experimental work are given in Table 3.2.

Chemical or Material	Grade	Supplier
$CaCl_2.2H_2O$	analaR	BDH Chemicals Ltd.
$CaCO_3$	"	" " "
CaC_2	technical	Aldrich Chemical Co.
Graphite rod	ultra pure	Johnson-Matthey
Au,Pt wire	spec. pure	" "
Ti sheet	"	" "
Mo rod	"	" "
Ti block	"	" "
Argon	High purity	B.O.C Ltd.
CO_2	" "	" "
HCl	" "	B.O.C Special gases

Table 3.2. CHEMICALS AND MATERIALS

3.3. EXPERIMENTAL PROCE DURE

3.3.1. Preparation of the Cell.

Analytical grade $CaCl_2.2H_2O$ was initially dehydrated by vacuum drying at 250°C, raising the temperature slowly and maintaining this temperature for 3 days, whilst the vacuum stablised at > 10^{-3} torr. The $CaCl_2$ produced was transferred to a dry box to stop rehydration.

All glassware in contact with the melt was soaked in 1:1 sulphuric/nitric acid bath for at least 24 hrs, to remove any adsorbed ions, washed with distilled water and acetone and dried. Approx. 50g of $CaCl_2$ was placed in the alumina crucible and the whole cell assembled with a chromel-alumel thermocouple buried in the salt, with all other joints in the cell head sealed to allow good vacuum to be achieved, for purification. The cell was then placed in the furnace.

3.3.2. Melt purification.

The $CaCl_2$ was purified by vacuum drying and by bubbling hydrogen chloride gas through the melt. This melt requires purification due to the presence of hydrolysis products as a result of the hy groscopic nature of $CaCl_2$.

Various methods have been employed to reduce and remove these impurities , use of anhydrous hydrogen chloride (121,122),or chlorine (123) or vacuum pre-electrolysis (124) or by a combination of these. All of these treatments are usually completed by a filtration step, but this requires the melt to be transferred before electrochemical analysis. To avoid melt contamination during transfer, in situ purification in the electrochemical cell was used and any solid impurities allowed to settle out.

A critical review by White(125) suggests the effectiveness of each of these approaches.

Thus using the cell shown in Fig.3.1.2a. purification proceeded as follows:

The whole apparatus was slowly evacuated until a pressure of $< 10^{-2}$ torr was achieved, whilst heating to 600°C and then maintained there for at least one day. The cell was then filled with argon to atmospheric pressure and a bubbling tube lowered into the powder. HCl was then bubbled whilst heating through fusion and bubbled for a further four hours, the melt temperature rising to approx. 850°C. Residual HCl was removed from the melt by bubbling with argon for at least 8 hrs.

HCl bubbling allows the hydrolytic equilibrium to be pushed to the left (121):

$$H_2O + Cl^- \rightleftharpoons OH^- + HCl \qquad (3.3.2)$$

The water vapour produced is flushed out by the HCl gas. The bubbling tube was then removed and the cell atmosphere balanced with an argon bag to stop air leaking into the cell. The purity of the melt was then checked using cyclic voltammetry, before beginning electrochemical experimentation. A typical response for a purified $CaCl_2$ melt is shown in Fig.3.3.2 at a tungsten electrode. The melt range indicated by this voltammogram is > 2.7 V, but there is a gentle rise in residual current at -1.7 V wrt. Pt Quasi ref. electrode. Cycling to the cathodic limit and potentials near it, can result in significant dissolution of calcium, resulting in loss of melt range. This calcium may also allow chemical reductions to occur.In order to avoid this effect cycling past -2.3 V was avoided.

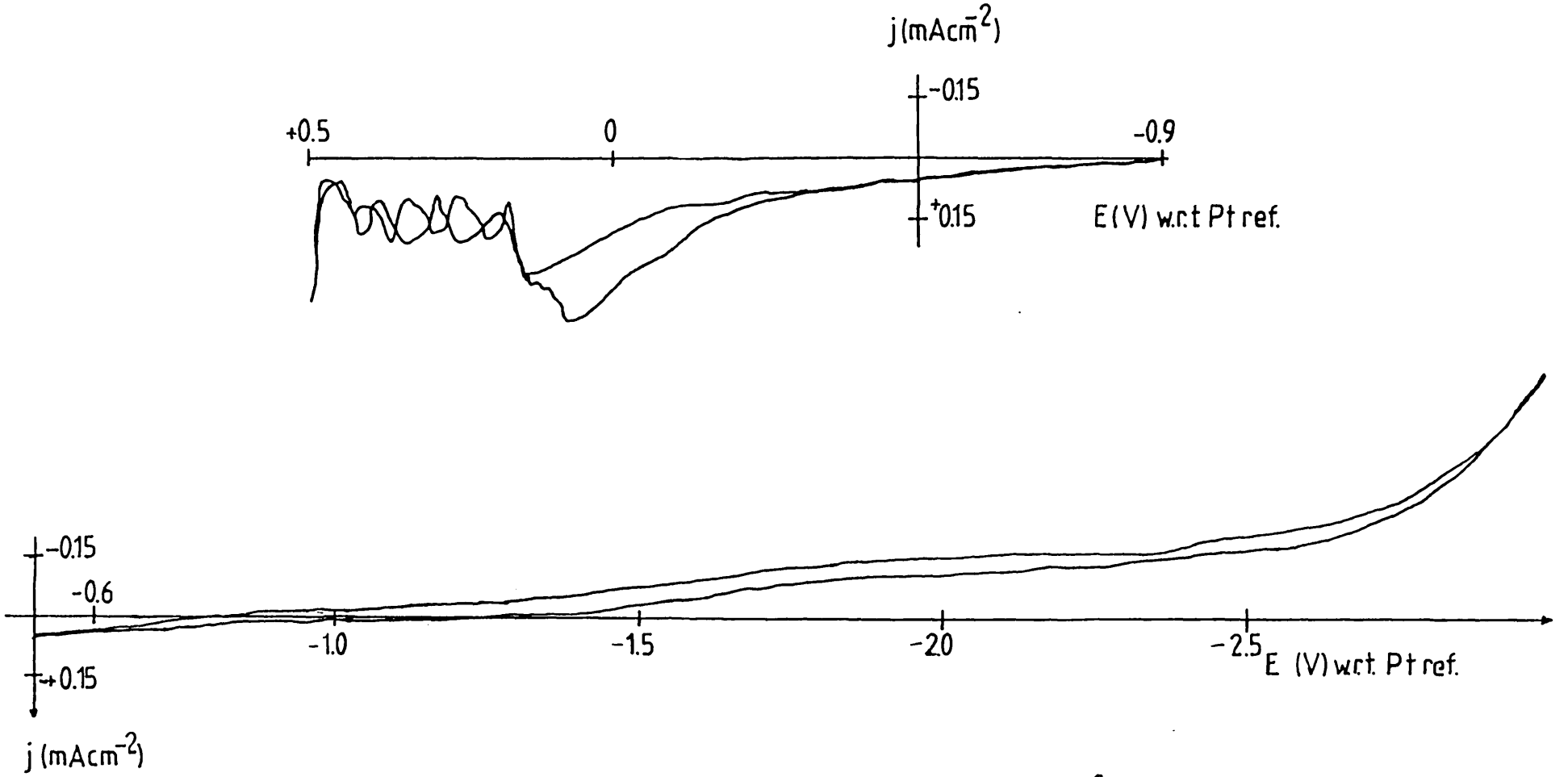

Fig.3.3.2. A typical voltammogram obtained in pure $CaCl_2$, at 840°C at a tungsten electrode, area 0.55 cm^2

3.3.3.Electrochemical experimentation.

Electrochemical studies of Mo, Ti, CO_3^{2-} and C_2^{2-} in $CaCl_2$ were carried out using cyclic voltammetry. The applied signal and idealised response for sweep voltammetry are shown in Fig.3.3.3. Potential scans were commenced at potentials where no current was seen to flow and the resultant i/E curve recorded at various scan rates.

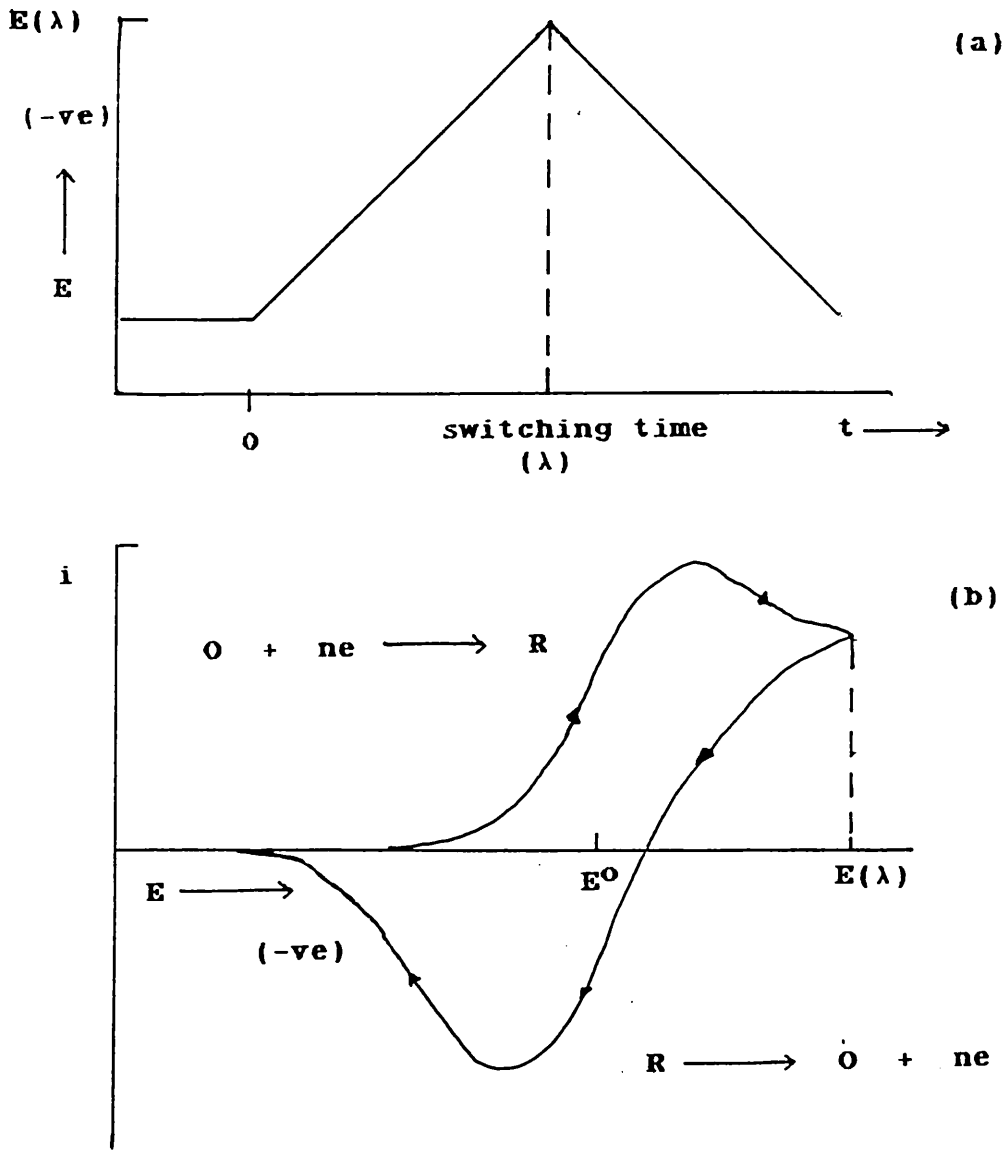

Fig. 3. 3. 3 APPLIED SIGNAL (a), RESPONSE (b) FOR CYCLIC VOLTAMMETRY

3.3.4. Electrodeposition.

The electrodeposition of molybdenum, carbon and titanium on to stainless steel or titanium was achieved by controlled potential electrolysis, either by holding the potential of the working electrode (substrate) at some suitable value, for various potentials and deposition times, or by cycling between two potentials, for varying potential ranges, sweep rates and deposition times.

3.3.5. Deposit Analysis.

After plating the electrodes were washed in running water to remove melt from the deposit and dried. The composition and morphology of these deposits were analysed by scanning electron microscopy (JEOL-T200) and x-ray diffraction using a Phillips X-ray generator with a copper target.

4.ELECTROCHEMICAL BEHAVIOUR OF ANODICALLY DISSOLVED MOLYBDENUM

4.1.INTRODUCTION

This chapter investigates the electrochemical behaviour of anodically dissolved molybdenum in $CaCl_2$ at temperatures from 812 to 864 ^oC, and for concentrations from 2.5 x 10^{-3} to 27 x 10^{-3} moldm^{-3}.

Observations during the course of experiments showed that a volatile species is produced and Mo metal is found at the melt/crucible interface indicating that a disproportionation reaction is occuring in this melt. Initial investigations gave rise to complex cyclic voltammetric responses with three peaks varying at different sweep rates, although it is generally agreed (126,94-96) that molybdenum anodically dissolves to form 3^+ species forming complex anions with chloride ions. The effect of 1) sweep rate, 2) concentration, 3) temperature and 4) time on these electrochemical and chemical reactions are considered here:-

4.2.CYCLIC VOLTAMMETRIC ANALYSIS OF Mo(III) IN $CaCl_2$

A Mo rod was anodically dissolved by constant potential electrolysis at 0 V wrt. Pt QRE.. Typically a current of 0.5 A flowed for an electrode area of 3.77 cm^2. Upon removal of the rod, 15 - 20 mins. were allowed for the melt to reach equilibrium, before cyclic voltammetric analysis using tungsten and platinum working electrodes was performed.

4.2.1.Effect of sweep rate.

The cyclic voltammogram Fig.4.2.1.1 shows a typical response at a tungsten electrode. Three cathodic and two anodic processes are observed varying with sweep rate. The first process is a well defined wave occuring at a peak potential (E_p^c) of approx. -0.45 V wrt. Pt. No clear corresponding anodic wave is indicated, although a

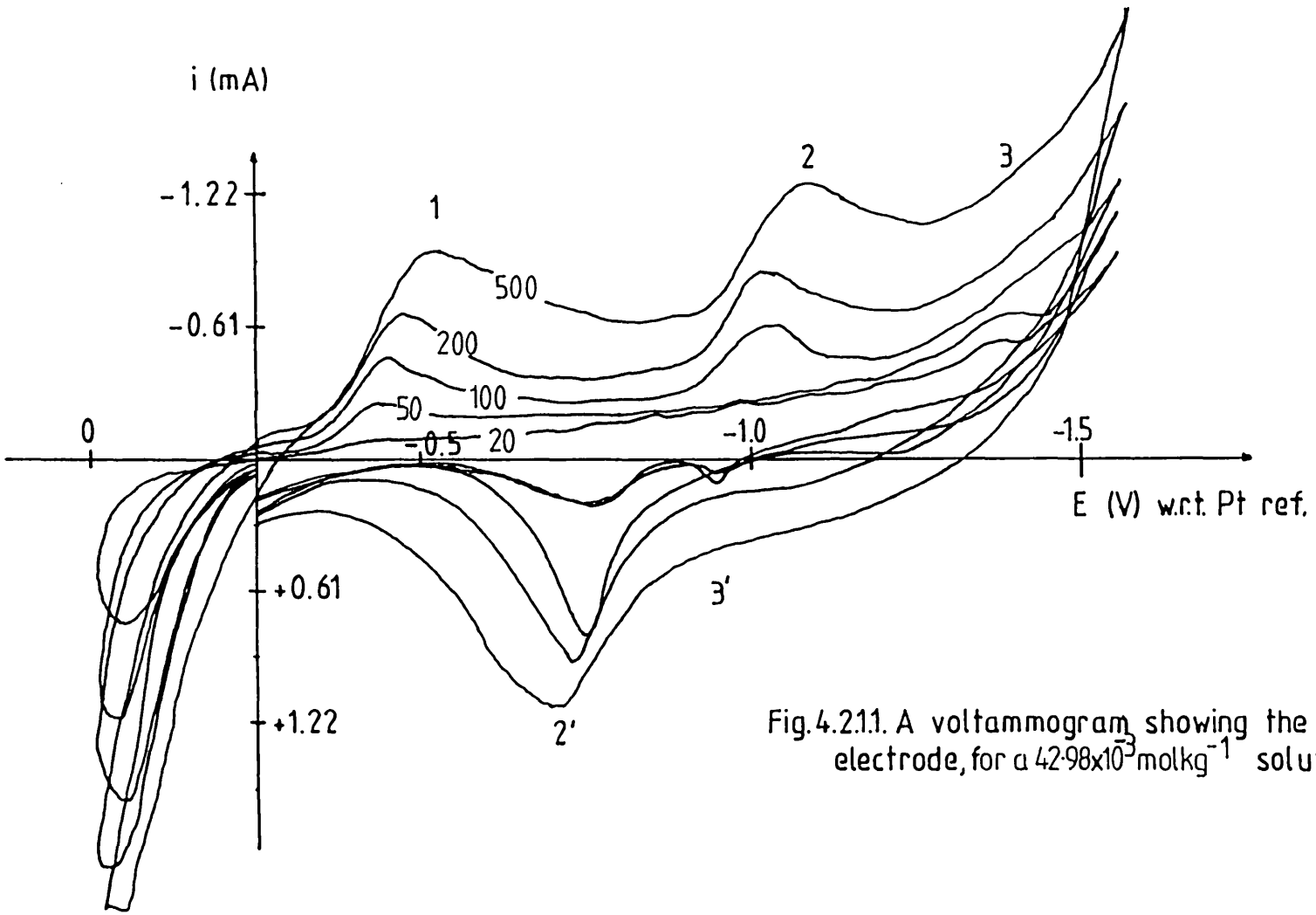

Fig. 4.2.1.1. A voltammogram showing the response at a tungsten electrode, for a $42{\cdot}98 \times 10^{-3}$ molkg^{-1} solution of Mo(III) in $CaCl_2$

reoxidation wave may be mixed with the anodic limit of the melt. At more cathodic potentials a second well defined wave occurs at E_p^c = -0.735 V. At slow sweep rates a even more cathodic process is indicated at E_p^c = -0.945 V wrt. Pt. The influence of sweep rate on these processes is given in table 4.2.1.1.

Peak 1

v (mV/s)	i_p^c (mA)	$\frac{i_p^c}{v^{1/2}}$ ($mAs^{1/2}$ $mV_{1/2}$)	$E_p^c(1)$ (V)	$E_{p/2}^c(1)$ (V)	$E_p^c - E_{p/2}^c(1)$ (mV)
20	0.14	0.0316	-0.430	-0.375	-55
50	0.28	0.040	-0.440	-0.380	-60
100	0.47	0.047	-0.455	-0.390	-65
200	0.56	0.040	-0.485	-0.400	-85
500	0.85	0.038	-0.525	-0.430	-95

Table 4.2.1.1a. VOLTAMMETRIC PARAMETERS FROM Fig 4.2.1.1.

These results indicate that for the first process, that the cathodic peak potential $E_p^c(1)$ shifts cathodic with increasing sweep rate and similarly the half peak width ($E_p^c - E_{p/2}(1)$) increases with increasing sweep rate.

The cathodic peak current $i_p^c(1)$ increases with increasing (sweep rate)$^{1/2}$ ($v^{1/2}$).(Fig.4.2.1.2.), but the more sensitive current function $i_p^c/v^{1/2}$ shows fluctuations with sweep rate, at low sweep rates. Fig.4.2.1.3. As indicated above any anodic response may be "lost" in the anodic limit of the melt, but as no shoulder is observed at low sweep rates, it may be assumed that there is no anodic wave.

The above results can be analysed according to those for a reversible charge transfer, followed by an irreversible chemical reaction.(127) For such a process, the cathodic peak potential is predicted to shift cathodic

Peak 2

v (mV/s)	$i_p^c(2)$ (mA)	$i_p^a(2)$ (mA)	$\frac{i_p^c\ (mAs^{1/2}}{v^{1/2}\ mV^{1/2})}$	i_p^a/i_p^c (mA)	$E_p^c(2)$ (V)	$E_{p/2}^c(2)$ (V)	$E_p^a(2)$ (V)	$E_p^c-E_{p/2}^c(2)$ (mV)	$E_p^c-E_p^a(2)$ (mV)
20	-	-	-	-	undulating plateau		-	-	-
50	-	-	-	-	"	"	-	-	-
100	0.61	1.83	0.061	3.00	-1.015	-0.945	-0.740	-70	-275
200	0.85	2.35	0.060	2.76	-1.030	-0.960	-0.735	-70	-295
500	1.31	3.32	0.059	2.53	-1.080	-0.990	-0.710	-90	-370

Peak 3

v (mV/s)	$i_p^c(3)$ (mA)	$i_p^a(3)$ (mA)	$\frac{i_p^c\ (mAs^{1/2}}{v^{1/2}\ mV^{1/2})}$	i_p^a/i_p^c (mA)	$E_p^c(3)$ (V)	$E_{p/2}^c(3)$ (V)	$E_p^a(3)$ (V)	$E_p^c-E_{p/2}^c(3)$ (mV)	$E_p^c-E_p^a(3)$ (mV)
20	0.38	0.78	0.08	2.06	-1.400	-1.340	-0.945	-60	-455
50	0.47	0.94	0.07	2.00	-1.390	-1.320	-0.940	-70	-450

Table 4.2.1.1b. VOLTAMMETRIC PARAMETERS FROM Fig 4.2.1.1.

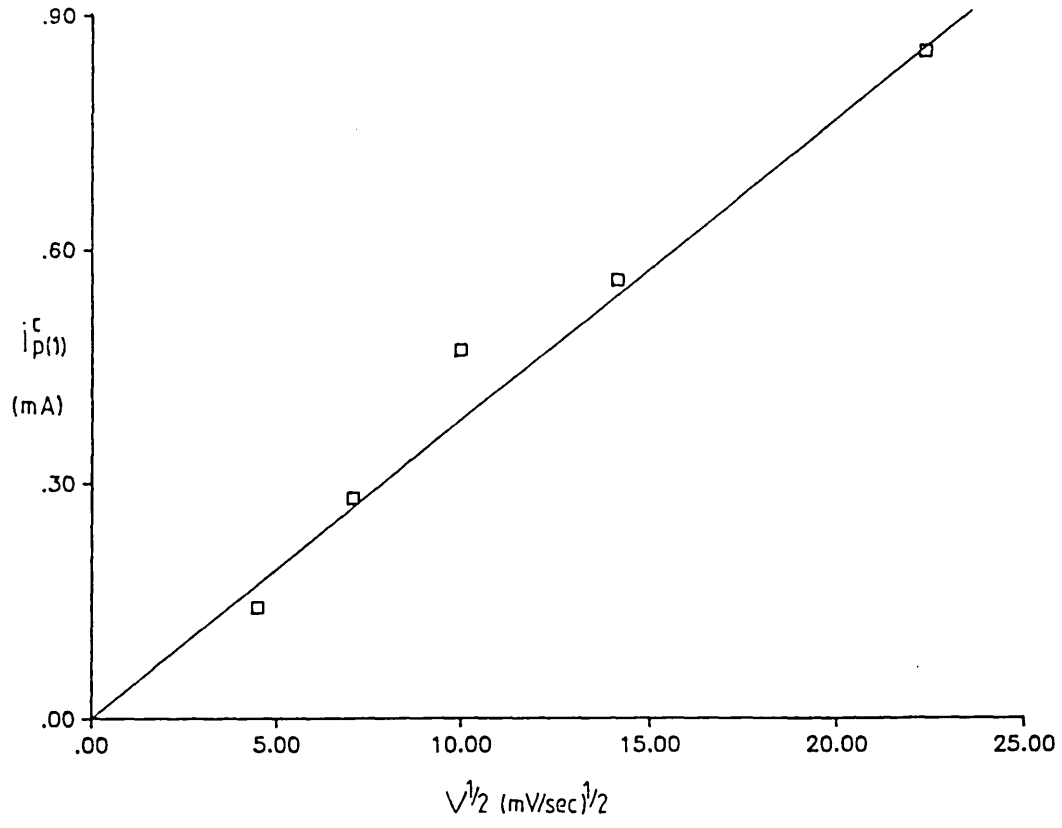

FIG.4.2.1.2. Plot of i_p^c vs $v^{1/2}$ for the 1st. reduction peak at tungsten. [Mo(III)] = $42{\cdot}98 \times 10^{-3}$ molkg^{-1} T=824°C

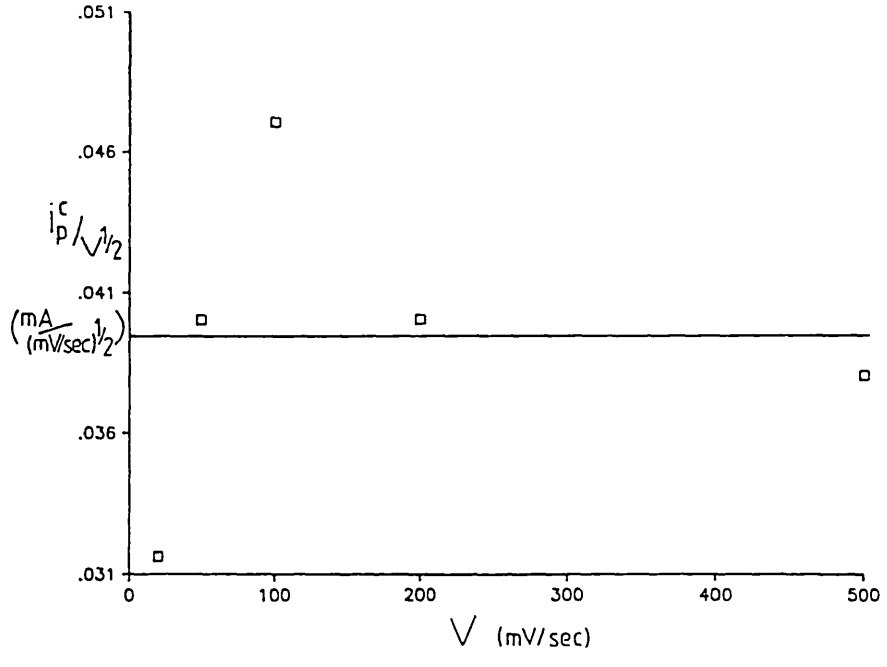

Fig.4.2.1.3. Plot of $i_p^c/v^{1/2}$ vs v for the 1st. reduction peak

by $\frac{-30.T}{298.n}$ mV for a 10 fold increase in sweep rate (v) for small v. Substituting the value of -60mV, an n value of 1.84 can be calculated. If the rate of the chemical reaction is large in comparison with the parameter nFV/RT then no anodic current is observed. Similarly under these conditions, the half peak width ($E_p^c - E_{p/2}$) $= \frac{-48.T}{298.n}$ mV which gives an n value of 2.45 using the mean value.

The above factors could also apply to the special case of the above reaction scheme, of reversible charge transfer followed by an irreversible dimerisation of the reduced product. Using these conditions(128,129), the half peak width$= \frac{-39.T}{298.n}$, substituting the mean value, gives an n value of 1.99. A plots of $\log(\frac{i_p - i}{i})$ against peak potential is linear, with a gradient of 10.55 V^{-1}, giving an αn value of 2.29 and the corresponding $\log(i_p - i)$ plot is curved.(Figs. 4.2.1.4-5)

The main effects of sweep rate on the response are evidenced by the presence and absence of the second and third peaks according to the sweep rate. At low sweep rates the 3rd peak is observed and the 2nd may appear as an undulating plateau, for 20 and 50 $mVsec^{-1}$, whereas at 100, 200 and 500 $mVsec^{-1}$, the 2nd peak is well defined, but the 3rd is not present.

For sweep rates of 100-500 $mVsec^{-1}$ the 2nd cathodic peak potential $E_p^c(2)$ shifts cathodic with increasing sweep rate, and the half peak width ($E_p^c - E_{p/2}(2)$) is constant for 100 and 200 $mVsec^{-1}$ at -70mV, but increases at 500 $mVsec^{-1}$. The anodic peak potential shifts anodic with increasing sweep rate and so the peak to peak potential ($E_p^c - E_p^a(2)$) also increases with increasing sweep rate. The cathodic peak current increases linearly

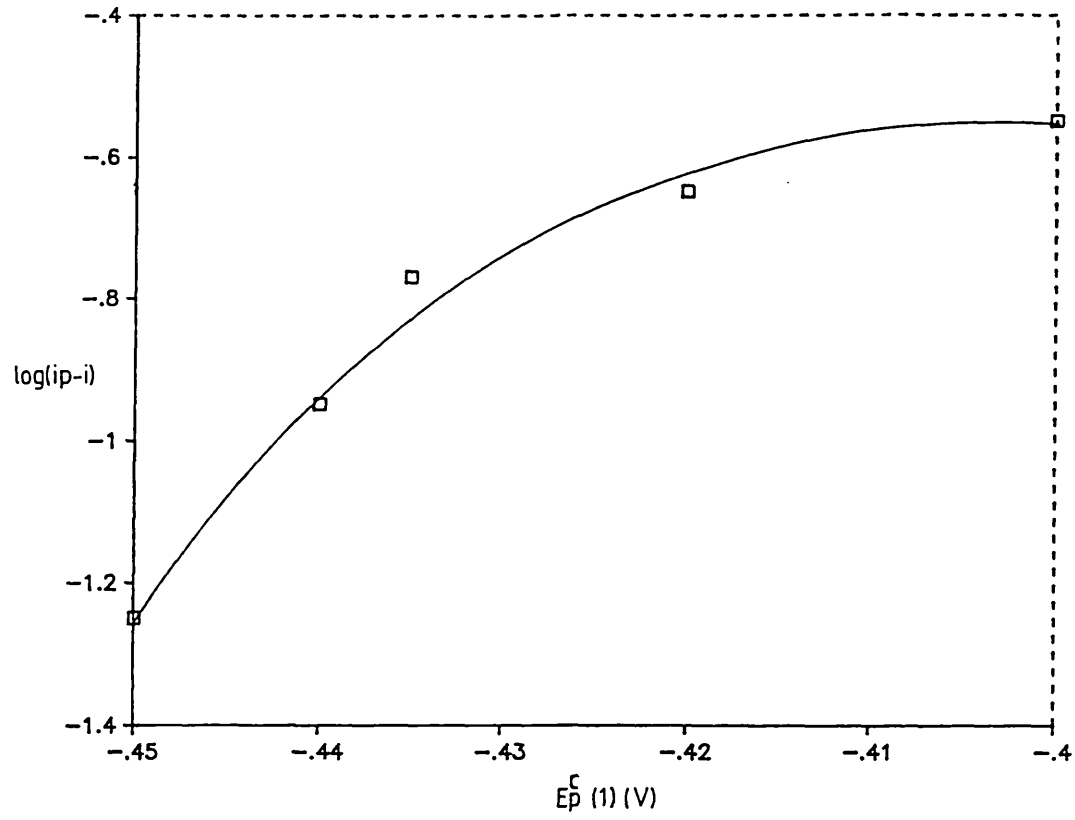

Fig.4.2.1.4. Plot of $\log(i_p-i)$ vs E_p^c in the range $0.5-0.9i_p$, for the 1st. reduction peak at W at 824°C.

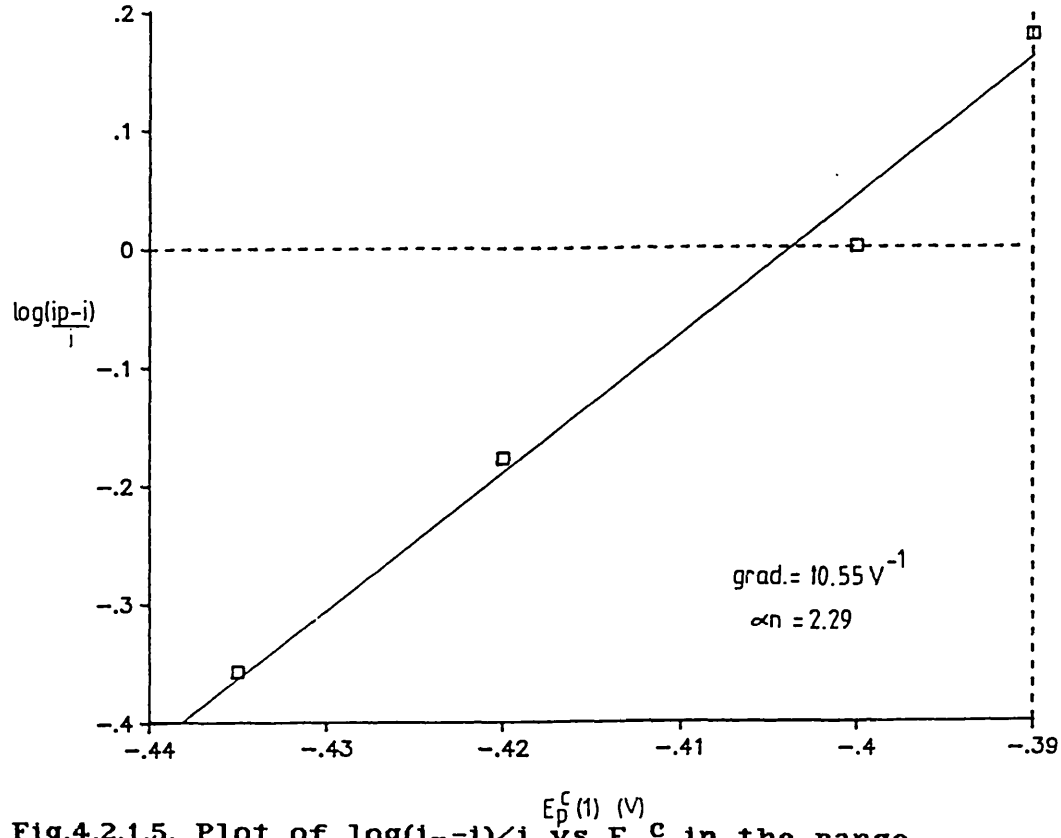

Fig.4.2.1.5. Plot of $\log(i_p-i)/i$ vs E_p^c in the range $0.4-0.7i_p$, for the 1st. reduction peak at W at 824°C.

with (sweep rate)$^{1/2}$, with a zero intercept, (fig.4.2.1.6) but the more sensitive current function ($i_p/v^{1/2}$) decreases with increasing v and thus implies the presence of coupled chemical reactions. The ratio of i_p^a/i_p^c also decreases with increasing v.

These results may be analysed according to a proceeding dissociation reaction followed by a reversible charge transfer, reaction scheme(130, 131), especially for low sweep rates where the undulating plateau current i_p^c is independent of v, and the plateau potential shifts anodic with increasing v. These responses suggest that K for the dimerisation reaction is small. At faster sweep rates (100-500 mVsec^{-1}) the response may approach that for K is large. Plots of $\log(\frac{i_p-i}{i})$ and $\log(i_p-i)$ against potential are linear and curved respectively.(figs.4.2.1.7-8) The gradient of the $\log(\frac{i_p-i}{i})$ plot is 11.28 V^{-1} and gives an αn value of 2.46.

At low sweep rates, 20 and 50 mVsec^{-1} the 3rd cathodic peak appears. For these two peaks the cathodic peak potential $E_p^c(3)$ shifts anodic with increasing sweep rate, whilst the half peak width and the peak to peak separation are almost constant at -65 mV and -425 mV respectively, the latter indicating a reversible process. These factors correspond to the reversible chemical reaction followed by an irreversible charge transfer model.(130, 131) The plots of $\log(\frac{i_p-i}{i})$ and $\log(i_p-i)$ against potential are both linear, indicating the breakdown of the analysis, which is probably due to the presence of coupled chemical reaction preceeding the charge transfer itself. This may manifest itself in the waveform obtained by cyclic voltammetry.(Figs.4.2.1.9-10)

These results indicate an E.C.E. type reaction scheme is occuring:-

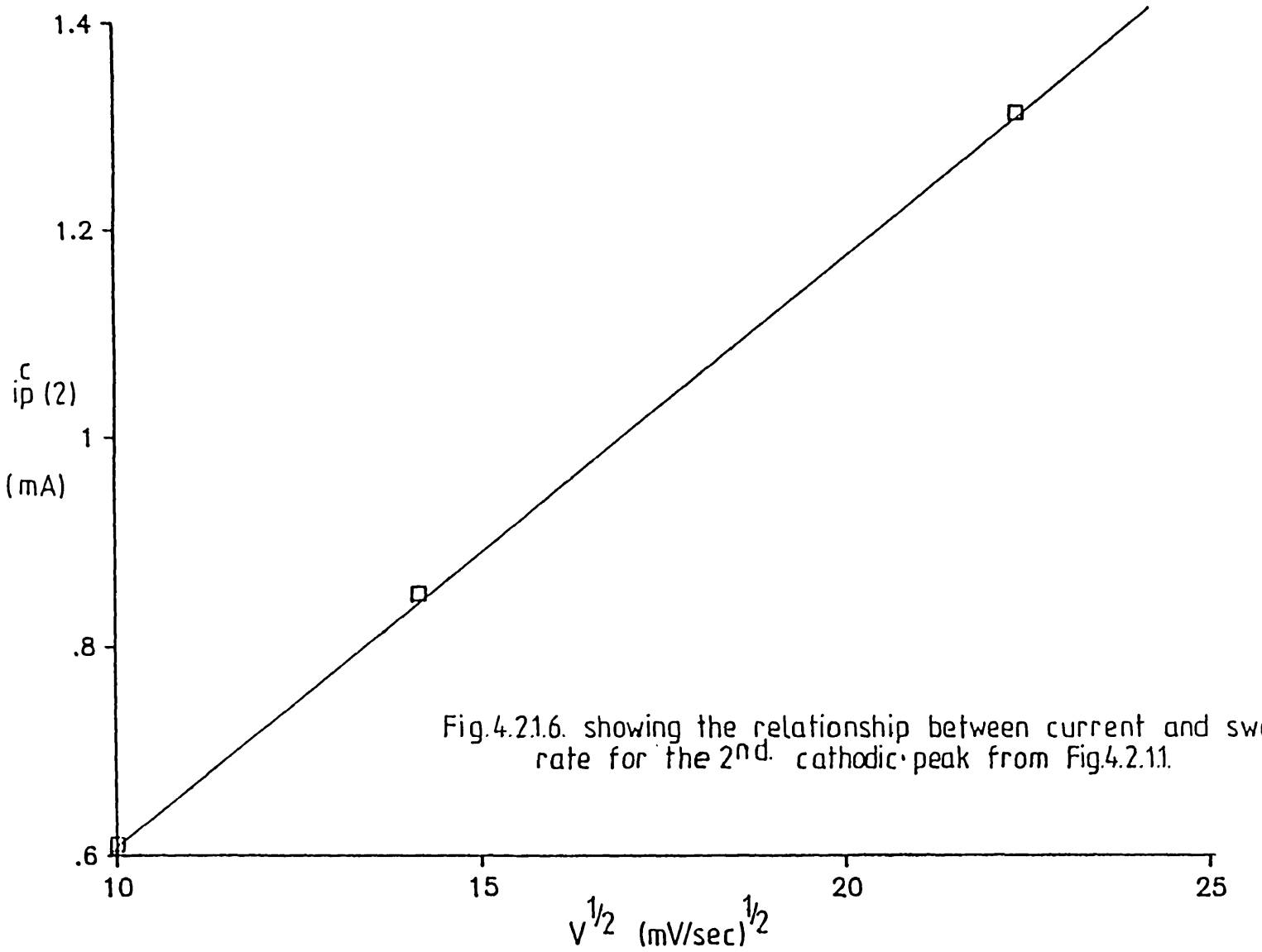

Fig.4.2.1.6. showing the relationship between current and sweep rate for the 2nd. cathodic peak from Fig.4.2.1.1.

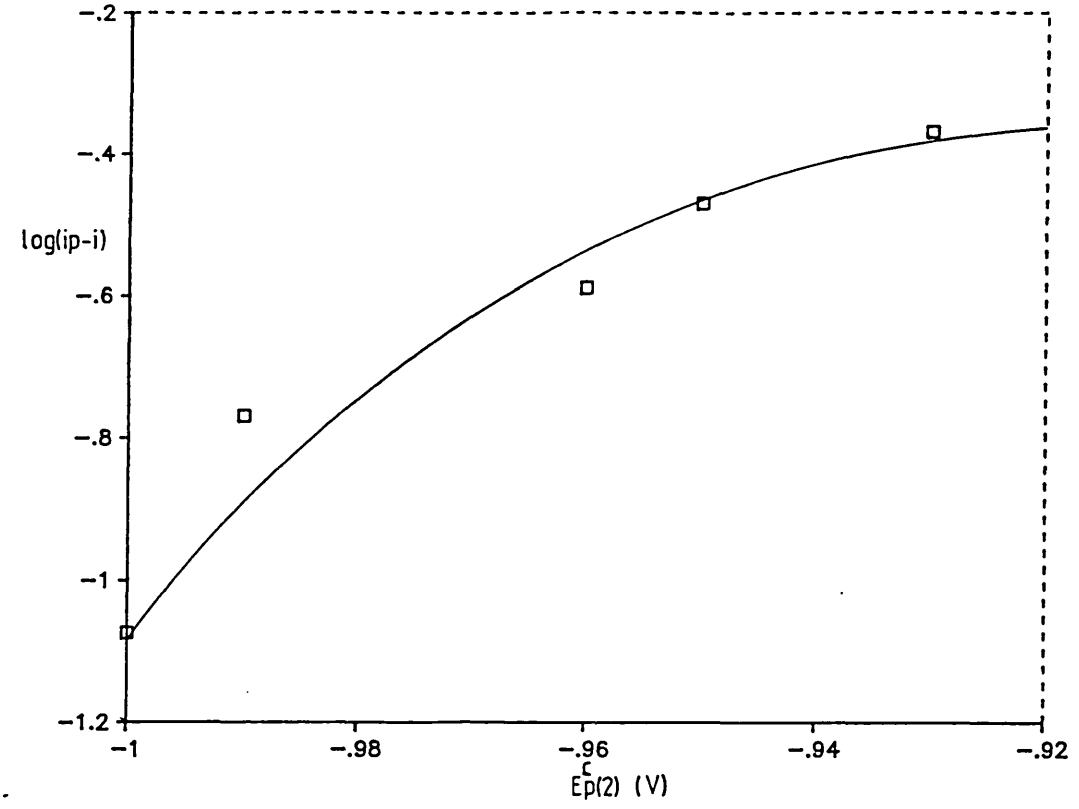

Fig.4.2.1.7. Plot of $\log(i_p-i)$ vs E_p^c in the range $0.5-0.9i_p$, for the 2nd. reduction peak at W at 824°C.

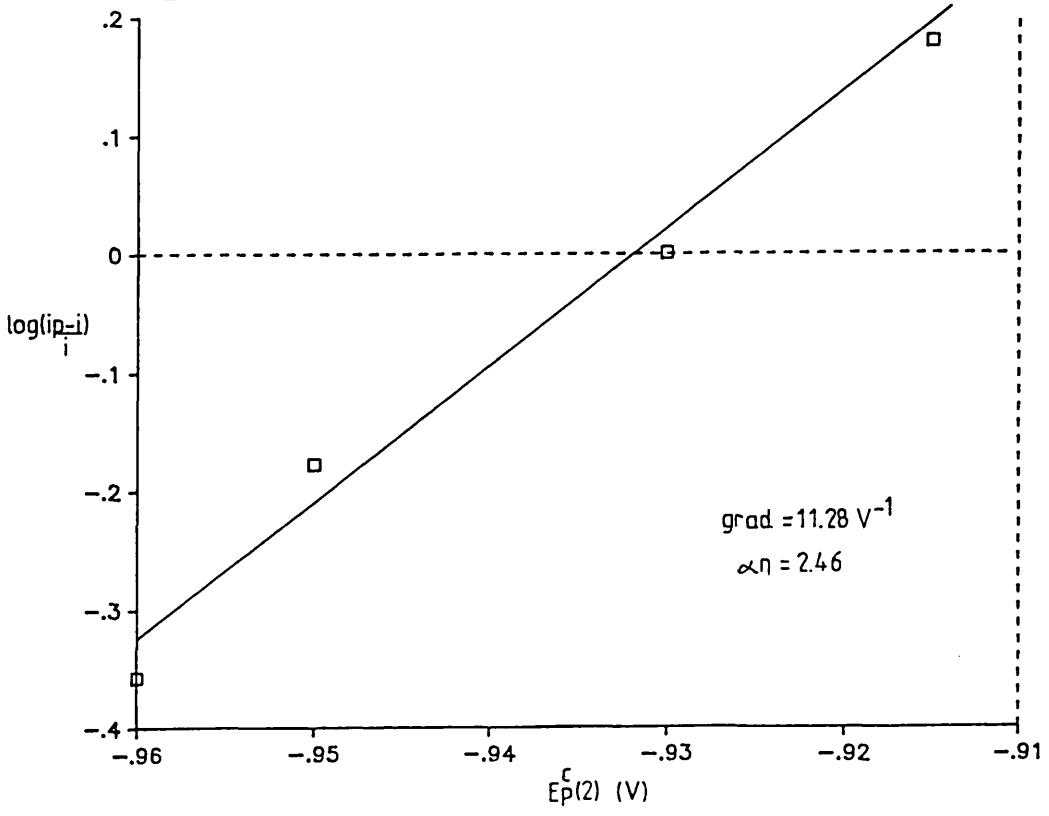

Fig.4.2.1.8. Plot of $\log(i_p-i)/i$ vs E_p^c in the range $0.4-0.7i_p$, for the 2nd. reduction peak at W at 824°C.

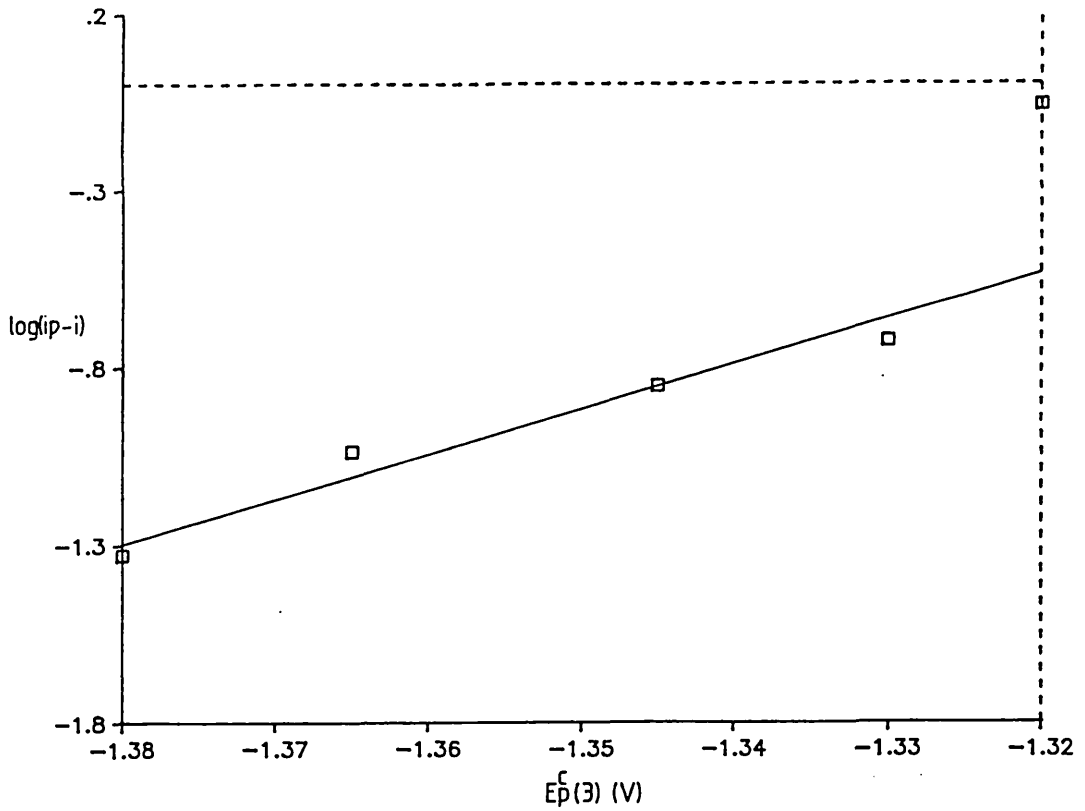

Fig.4.2.1.9. Plot of $\log(i_p-i)$ vs E_p^c in the range $0.5-0.9i_p$, for the 3rd. reduction peak at W at 824°C.

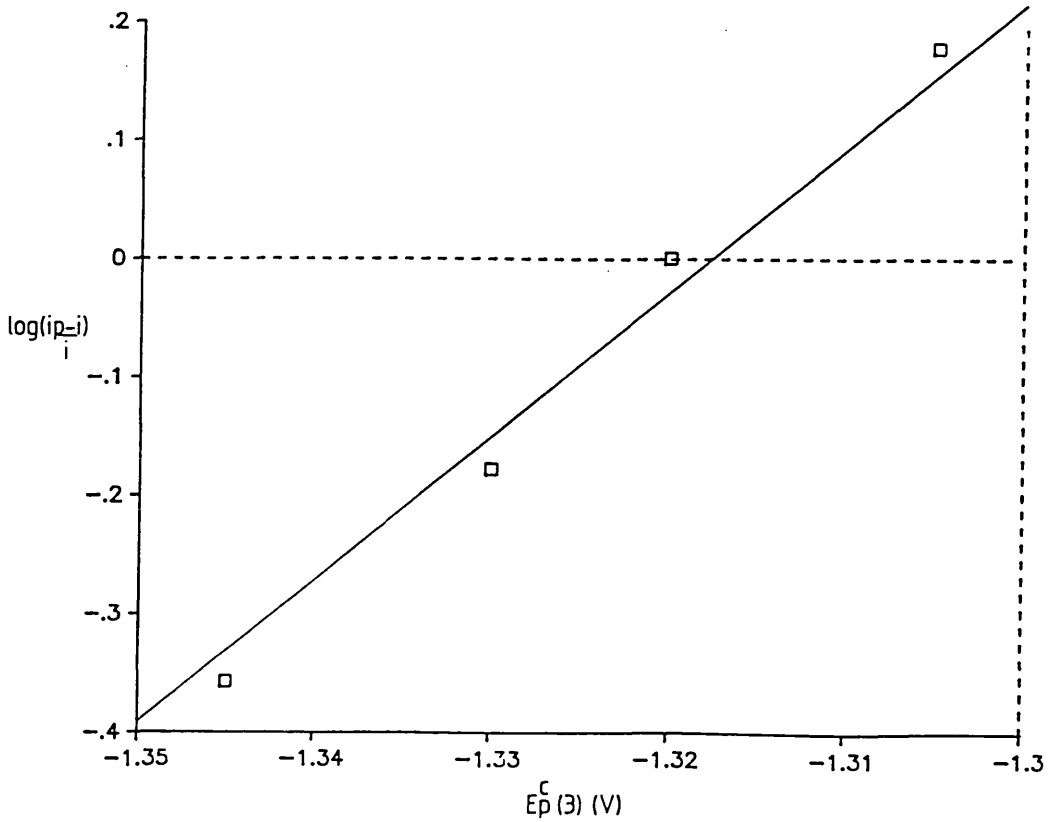

Fig.4.2.1.10. Plot of $\log(i_p-i)/i$ vs E_p^c in the range $0.4-0.7i_p$, for the 3rd. reduction peak at W at 824°C.

$$O + 2e \longrightarrow R \quad (E) \quad (1)$$

$$2R \rightleftharpoons Z \quad (C)$$

$$R + 3e \longrightarrow R' \quad (E) \quad (2) \quad \text{when K is small}$$

$$\text{and/or } Z + 2(3e) \rightleftharpoons 2(R') \quad (E) \quad (3) \quad \text{when K is large}$$

The cyclic voltammetric response at a platinum electrode is shown in Fig.4.2.1.11. It is very similar to that noted at tungsten, with 3 cathodic and 2 anodic waves. The first two waves are less well defined than at tungsten ($E_p^c(1)$ = -0.38 V and $E_p^c(2)$ = -0.86 V with a corresponding oxidation wave at -0.33 V. The 3rd peak is more clearly defined than at tungsten, with a cathodic peak at -1.22 V and a corresponding anodic peak at -0.73 V. This response cannot be considered more rigorously as the voltammograms were found to be difficult to reproduce, and the electrode was observed to lose its "bright" finish during sweeps. Alloy formation is likely to give rise to these effects. The similarity of the responses however indicates that the same reactions are likely to be occuring at both Pt and W electrodes.

4.2.2.Effect of concentration.

Fig.4.2.2.1. shows a typical cyclic voltammogram at tungsten, 15 minutes after the anodic dissolution of molybdenum. This response follows that of Fig.4.2.1.1.but the concentration of molybdenum is half that in Fig.4.2.1.1. Table 4.2.2.1. summarises the various parameters and their variation with sweep rate at this concentration. Table 4.2.2.2. further indicates how some of these parameters vary with concentration from 10.55 - 53.76 mmolal Mo(III), (5.11 - 26.06 x 10^{-3} molar), at sweep rates of 50 and 100 $mVsec^{-1}$.

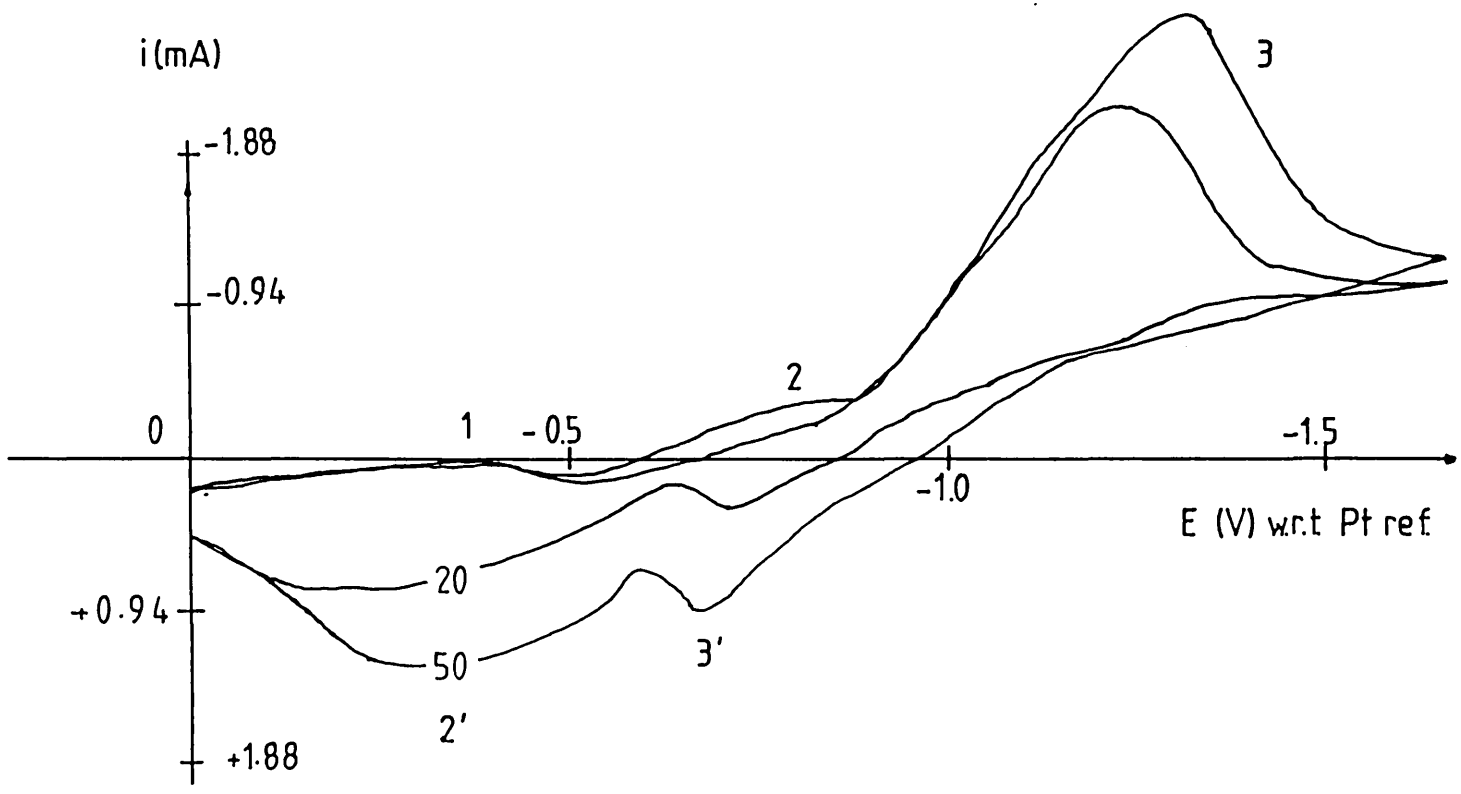

Fig.4.2.1.11. A Voltammogram showing the response at a platinum electrode, for a $28{\cdot}71 \times 10^{-3}$ molkg^{-1} soln. of Mo(III).

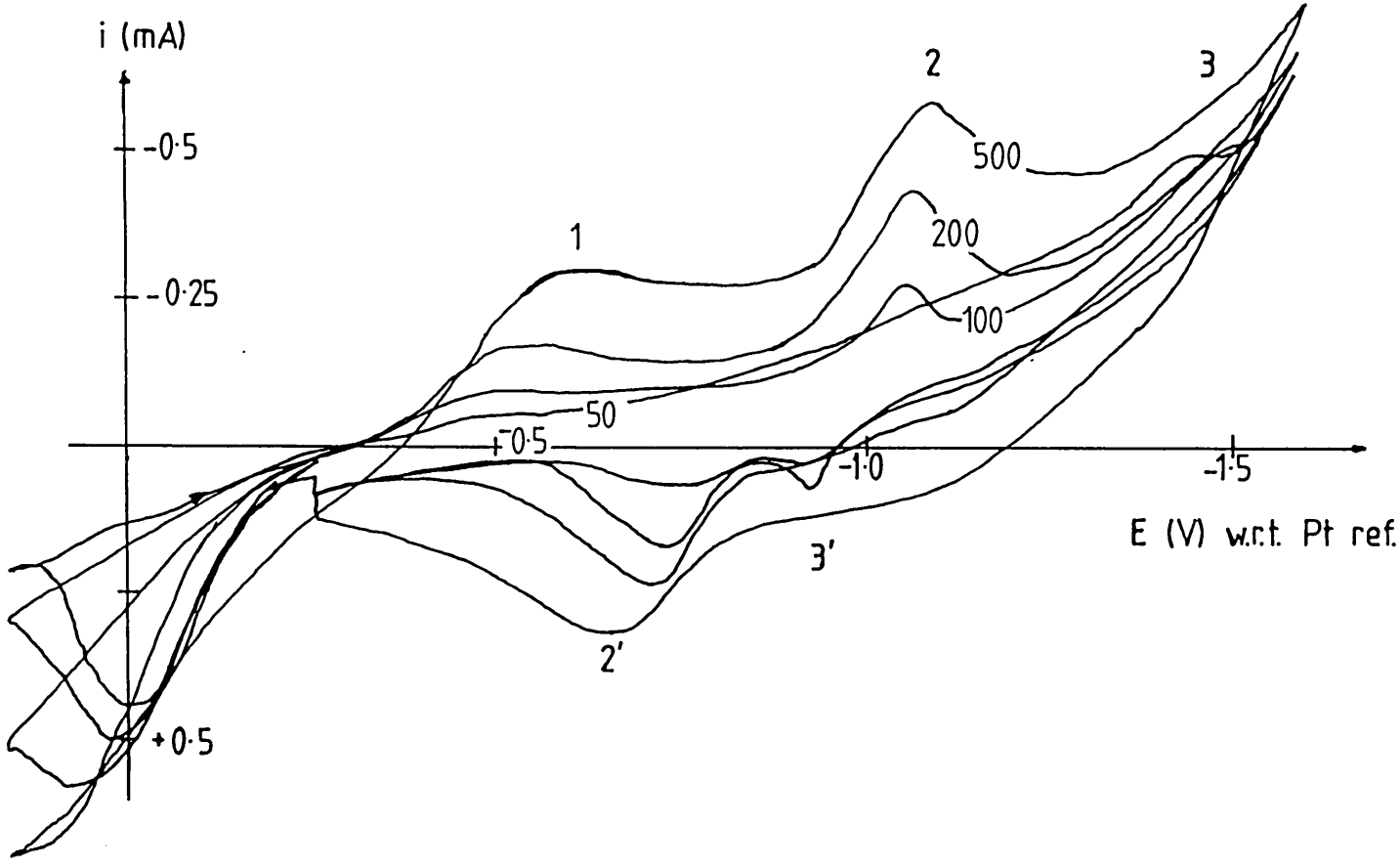

Fig.4.2.2.1. A Voltammogram showing the response at a tungsten electrode, for a $20{\cdot}79 \times 10^{-3}$ molkg^{-1} soln. of Mo(III).

Peak 1

v (mV/s)	$i_p^c(1)$ (mA)	$\frac{i_p^c}{v^{1/2}}$ ($\frac{mAs^{1/2}}{mV^{1/2}}$)	$E_p^c(1)$ (V)	$E_{p/2}^c(1)$ (V)	$E_p^c - E_{p/2}^c(1)$ (mV)
50	0.047	0.007	-0.490	-0.410	-80
100	0.070	0.007	-0.505	-0.420	-85
200	0.117	0.008	-0.530	-0.420	-110
500	0.211	0.009	-0.620	-0.470	-150

Table 4.2.2.1a. VOLTAMMETRIC PARAMETERS FROM Fig 4.2.2.1.

From these tables it can be seen that peaks $E_p^c(1)$ and $E_p^c(3)$ move anodically with increasing concentration, whilst $E_p^c(2)$ appears to move cathodically initally and then anodically at higher concentrations. The half peak width ($E_p^c - E_{p/2}^c(1)$) is essentially constant at -70 mV, but the corresponding half peak widths for peaks 2 and 3 decrease with increasing concentation. The large degree of scatter in these points does not allow any real trend to be noted. The peak current for each peak rises increasingly with concentration, (Figs. 4.2.2.2-4.2.2.3.) the 2nd peak current rising more rapidly than that for the 1st and 3rd. This trend is shown by the increasing ratio of $j_p^c(2)/j_p^c(1)$ and $j_p^c(2)/j_p^c(3)$. The plots of $\log(j_p^c)$ with log(conc.) (figs.4.2.2.4.-5) indicate that a simple power relationship between j_p^c and concentration is unlikely, due to the scatter of the points, but "best line" plots give a markedly longer concentration dependence than 1. Mean gradients of 1.7, 1.3 and 1.3 are determined for $j_p^c(1)$,$j_p^c(2)$and $j_p^c(3)$ respectively.

The anodically shifting potential is further evidence of coupled chemical reactions associated with these peaks, but in a E.C.E. mechanism as suggested in section 4.2.1., j_p^c should be directly proportional to concentration. This markedly longer relationship and the scatter noted above may arise from the disproportionation

Peak 2

v (mV/s)	$i_p^c(2)$ (mA)	$i_p^a(2)$ (mA)	$\frac{i_p^c\ (mAs^{1/2}}{v^{1/2}\ mV^{1/2})}$	i_p^a/i_p^c (mA)	$E_p^c(2)$ (V)	$E_{p/2}^c(2)$ (V)	$E_p^a(2)$ (V)	$E_p^c-E_{p/2}^c(2)$ (mV)	$E_p^c-E_p^a(2)$ (mV)
50	-	-	-	-	-	-	-	-	-
100	0.129	0.246	0.013	1.907	-1.050	-0.920	-0.730	-130	-320
200	0.246	0.364	0.017	1.48	-1.060	-0.930	-0.700	-130	-360
500	0.293	0.587	0.013	2.00	-1.080	-0.930	-0.660	-150	-520

Peak 3

v (mV/s)	$i_p^c(3)$ (mA)	$i_p^a(3)$ (mA)	$\frac{i_p^c\ (mAs^{1/2}}{v^{1/2}\ mV^{1/2})}$	i_p^a/i_p^c (mA)	$E_p^c(3)$ (V)	$E_{p/2}^c(3)$ (V)	$E_p^a(3)$ (V)	$E_p^c-E_{p/2}^c(3)$ (mV)	$E_p^c-E_p^a(3)$ (mV)
50	0.094	0.317	0.013	3.37	-1.425	-1.11	-0.920	-315	-505
100	0.117	0.410	0.012	3.50	-1.430	-1.11	-0.920	-320	-510

Table 4.2.2.1b. VOLTAMMETRIC PARAMETERS FROM Fig 4.2.2.1.

100mVsec^{-1}

conc. (mmolal)	$j_p^c(1)$ (mA/cm^2)	$j_p^c(2)$ (mA/cm^2)	$j_p^c(3)$ (mA/cm^2)	$\frac{j_p^c(2)}{j_p^c(1)}$	$\frac{j_p^c(2)}{j_p^c(3)}$	$\frac{j_p^c(3))}{j_p^c(1)}$	$E_p^c(1)$ (V)	$E_p^c(2)$ (V)	$E_p^c(3)$ (V)	$E_p-E_{p/2}(1)$ (mV)	$E_p-E_{p/2}(2)$ (mV)	$E_p-E_{p/2}(3)$ (mV)
10.55	0.006	0.0030	-	0.5	-	-	-0.555	-0.840	-	-85	-140	-
20.79	0.005	0.0085	0.008	1.70	1.06	1.60	-0.505	-1.050	-1.425	-85	-130	-320
31.91	0.008	0.0090	0.009	1.125	1.00	1.125	-0.475	-1.080	-1.450	-75	-90	-70
42.98	0.018	0.0240	-	1.33	-	-	-0.455	-1.015	-	-70	-60	-
53.76	0.013	-	0.018	-	-	1.30	-0.505	-	-1.390	-85	-	-70

50 mVsec^{-1}

conc. (mmolal)	$j_p^c(1)$ (mA/cm^2)	$j_p^c(2)$ (mA/cm^2)	$j_p^c(3)$ (mA/cm^2)	$\frac{j_p^c(2)}{j_p^c(1)}$	$\frac{j_p^c(2)}{j_p^c(3)}$	$\frac{j_p^c(3))}{j_p^c(1)}$	$E_p^c(1)$ (V)	$E_p^c(2)$ (V)	$E_p^c(3)$ (V)	$E_p-E_{p/2}(1)$ (mV)	$E_p-E_{p/2}(2)$ (mV)	$E_p-E_{p/2}(3)$ (mV)
10.55	0.003	0.004	-	1.33	-	-	-0.530	-0.820	-	-100	-110	-
20.79	0.003	-	0.006	-	-	2.00	-0.490	-	-1.430	-80	-	-315
31.91	0.004	0.012	0.012	3.00	1.00	3.00	-0.460	-1.030	-1.430	-80	-90	-50
42.98	0.011	0.024	0.018	2.18	1.33	1.64	-0.440	-1.015	-1.390	-60	-	-75
53.76	0.007	-	0.018	-	-	2.57	-0.455	-	-1.370	-60	-	-70

Table 4.2.2.2. EFFECT OF CONCENTRATION ON CYCLIC VOLTAMMETERIC PARAMETERS, AT 1097K AT TUNGSTEN ELECTRODES.

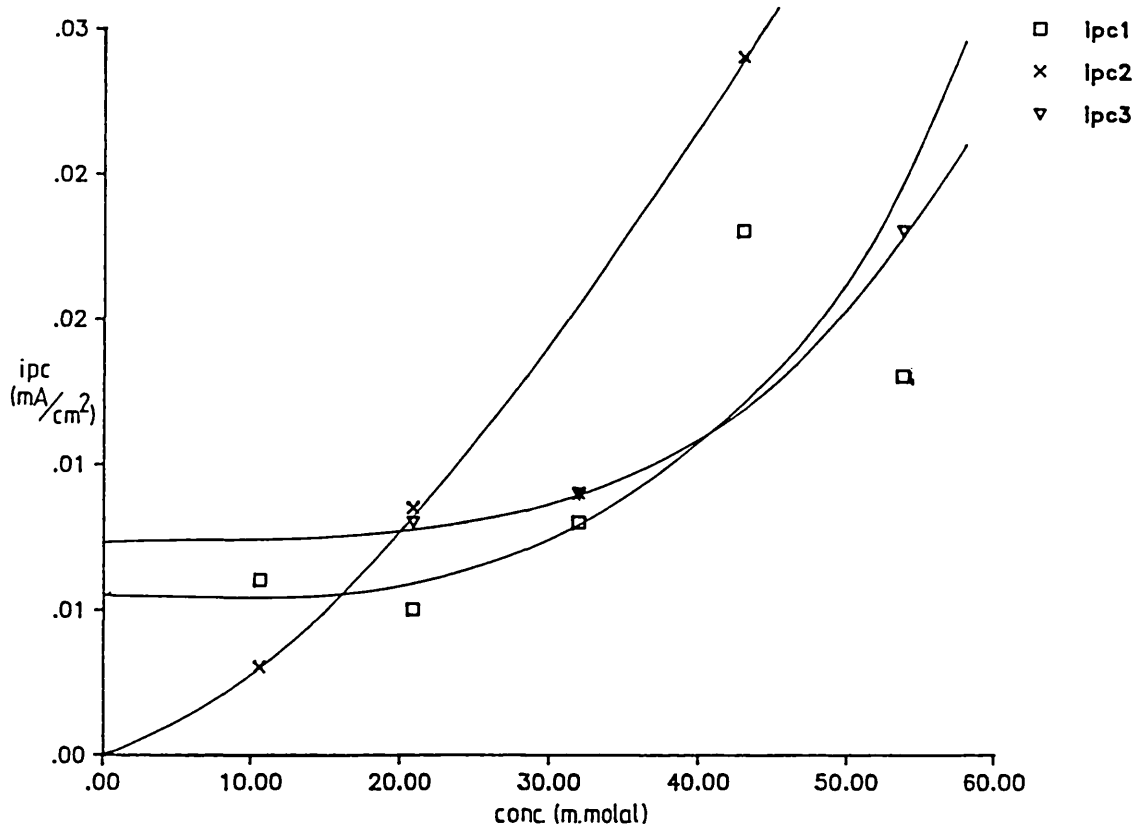

Fig.4.2.2.2. Plot of i_p^c vs conc.(Mo(III)), for reduction peaks 1, 2 and 3 peak. at 100mVsec^{-1} at W.

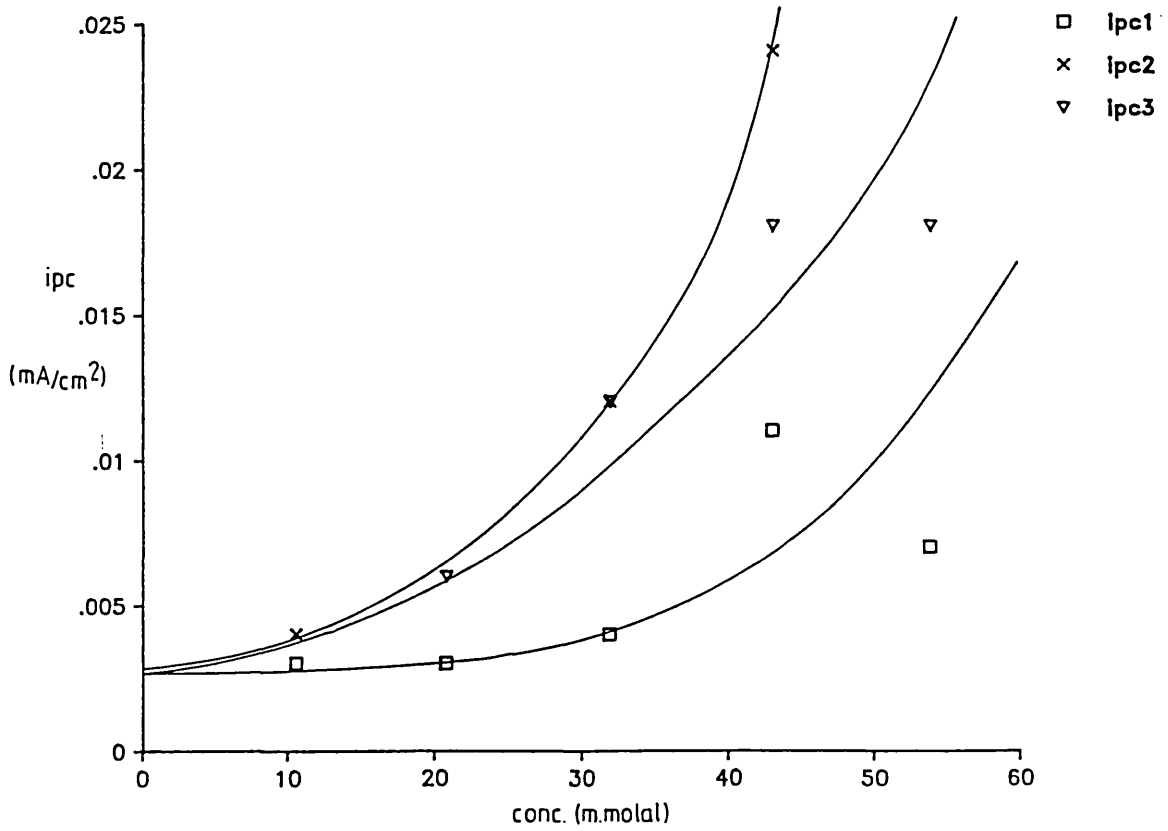

Fig.4.2.2.3. Plot of i_p^c vs conc.(Mo(III)), for reduction peaks 1, 2 and 3 peak. at 50mVsec^{-1} at W.

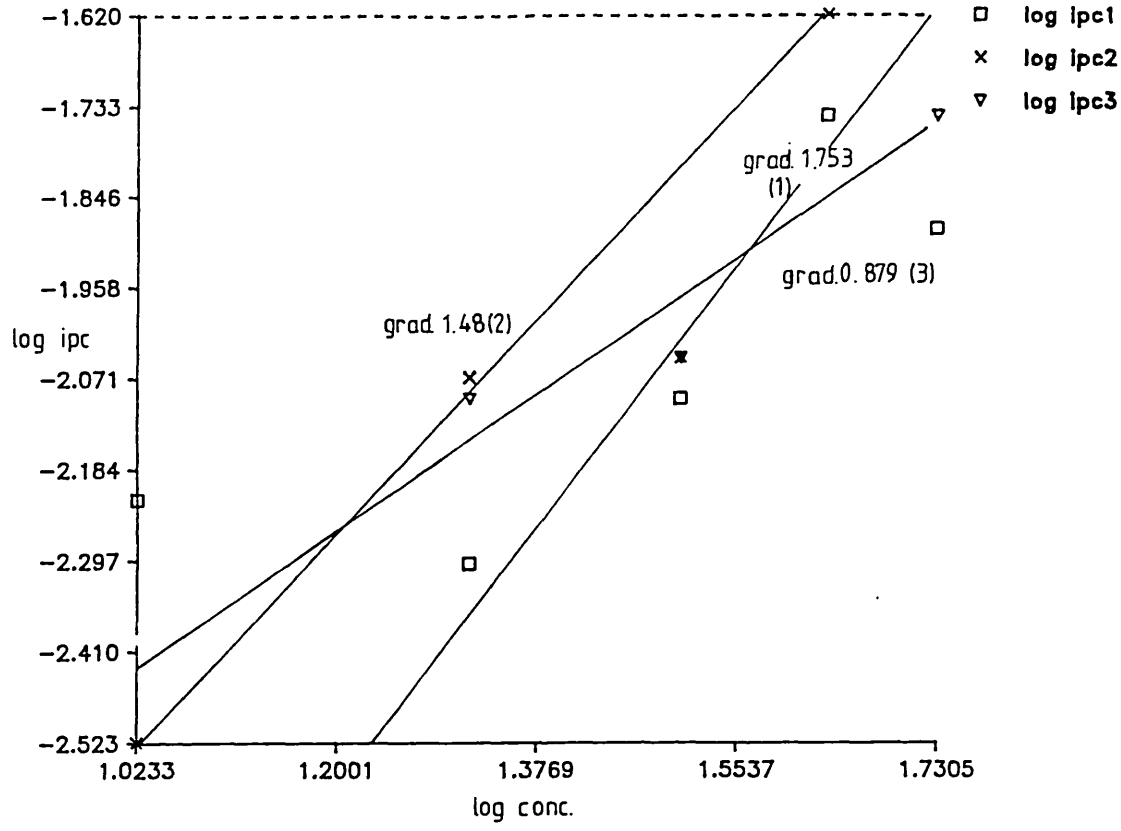

Fig.4.2.2.4. Plot of log(i_p^c) vs log(conc.Mo(III)), for reduction peaks 1, 2 and 3 peak. at 100mVsec^{-1} at W.

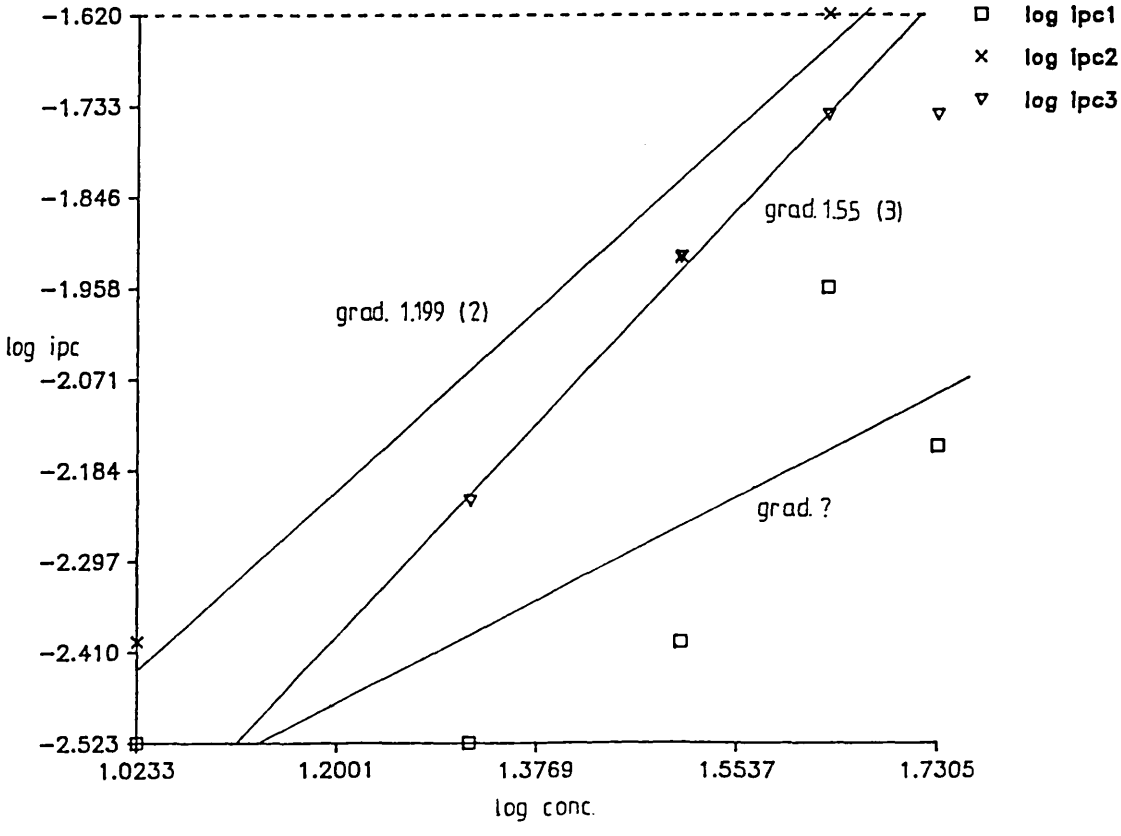

Fig.4.2.2.5. Plot of log(i_p^c) vs log(conc.Mo(III)), for reduction peaks 1, 2 and 3 peak. at 50mVsec^{-1} at W.

reaction indicated in section 4.1., in combination with an E.C.E. reaction scheme.

4.2.3.Effect of temperature

The marked effect of temperature on the cyclic voltammetric response at a tungsten electrode is shown in Fig.4.2.3.1. At 864^{o}C (c) both the 1st and 2nd peaks shown in (a) and (b), at 824^{o}C and 851^{o}C, are no longer observed. Table 4.2.3.1. indicates how the current density varies with temperature and concentration at a sweep rate of 200 mVsec^{-1}.

Temp. (^{o}C)	$j_p^c(1)$ (mAcm^{-2})	$j_p^c(2)$ (mAcm^{-2})	$j_p^c(3)$ (mAcm^{-2})	conc. (mol/dm^{-3})	conc./T$^{1/2}$ (mol/l.K$^{1/2}$)
812	1.06	1.06	1.59	3.83x10^{-3}	1.16x10^{-4}
824	0.429	0.86	-	5.11x10^{-3}	1.54x10^{-4}
851	0.429	0.62	0.62	4.40x10^{-3}	1.31x10^{-4}
864	-	-	1.72	6.79x10^{-3}	2.01x10^{-4}

Table 4.2.3.1. VARIATION OF CURRENT DENSITY WITH TEMPERATURE

A relative drop in current density for increasing temperature for the 1st and 2nd peaks is observed, when accounting for the concentration differences. The 3rd peak current density however, decreases and then increases. This temperature effect is complex. One would expect the current density to rise with temperature as electrode reactions should occur more readily, but changes in the stability of the species giving rise to the peaks may bring about this sort of behaviour, especially as a disproportionation reaction is observed to occur. Similarly disassociation reactions will occur more readily at higher temperatures. Only the most stable species will remain in solution and thus a loss of species can give rise to a falling current density. This variation of temperature with current density allows the diffusion coefficient for the reacting species for each peak to be

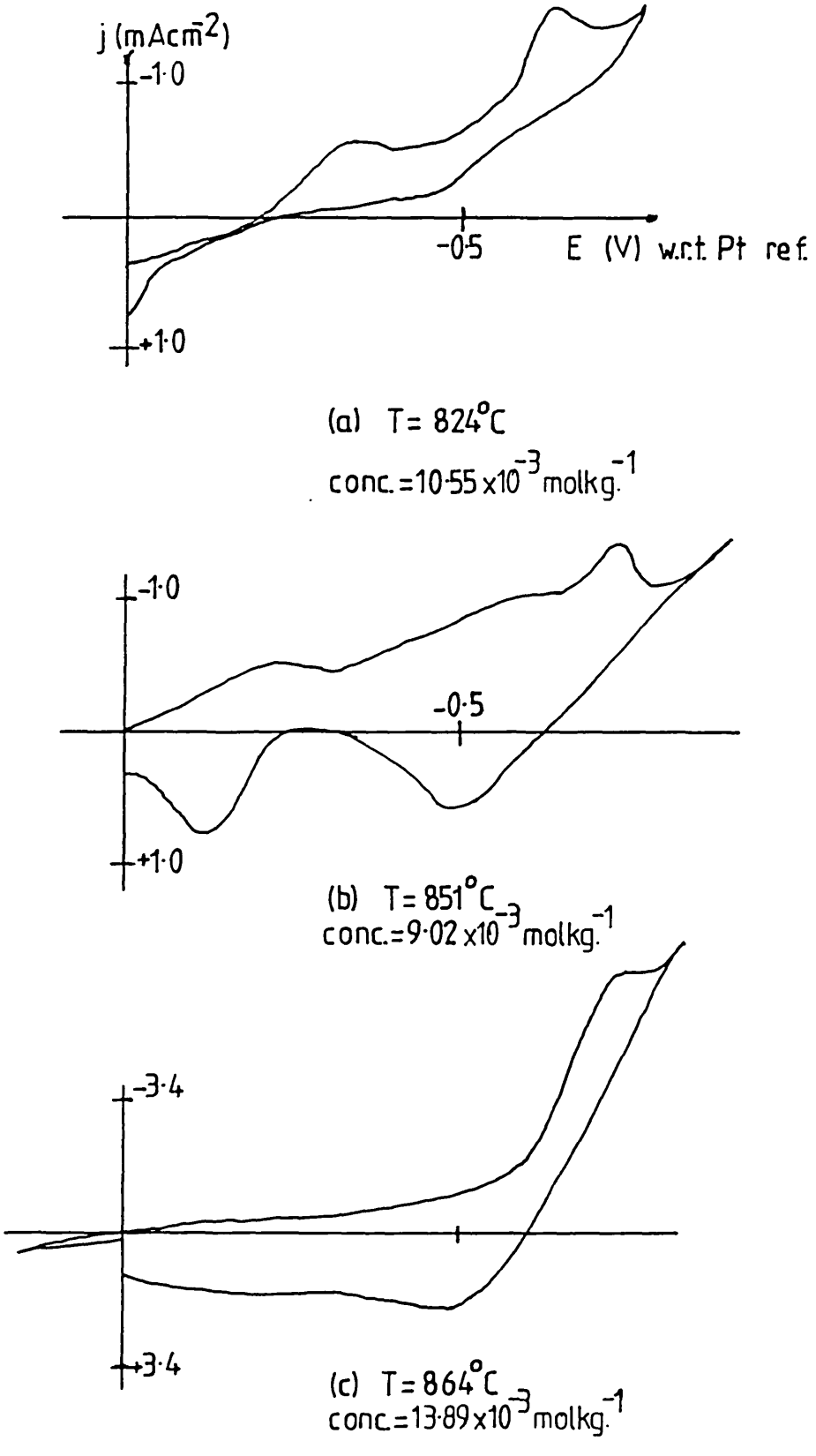

Fig.4.2.3.1. Voltammograms showing the responses at tungsten electrodes for different temperatures. v = 200 mVsec.$^{-1}$

calculated, if the electrochemical reactions are those indicated in section 4.2.1.

peak 1

$$O + 2e \rightleftharpoons R \qquad (a)$$

$$2R \rightleftharpoons Z \qquad (b)$$

when K is small (b) becomes more irreversible:

then $j_p = 0.53(nF)^{3/2}.(Dv)^{1/2}.C/(RT)^{1/2}$ applies to this peak, using the mean values of j_p and $C/T^{1.2}$, 0.661 $mAcm^{-2}$,1.34x10^{-4} $mol/lK^{1/2}$ and that v = 0.2 $Vsec^{-1}$ and n = 2, the diffusion coefficient becomes 8.77x10^{-6} cm^2sec^{-1} at approx. 829^oC.

peak 2 and 3

$$Z \rightleftharpoons 2R \qquad (c)$$

$$R + 3e \rightleftharpoons R' \qquad (d)$$

when K is large, peak 3, dissociation occurs less readily and $j_p = 1.087(nF)^{3/2}.(D_Zv)^{1/2}.C/(RT)^{1/2}$ applies to this peak, using the mean values of j_p and $C/T^{1.2}$,1.31 $mAcm^{-2}$,1.49 x10^{-4} $mol/lK^{1/2}$ and substituting as above, D_Z becomes 6.62x10^{-6} cm^2sec^{-1} at approx. 842^oC.

when K is small, peak 2, dimerisation is not favoured and $j_p = 1.155(nF).(D_ovk_b)^{1/2}.(KC)^{3/4}/(RT)^{1/2}$ as the value of K and K_b are unknown, D in this case cannot be calculated.

4.2.4.Effect of time

Figs.4.2.4.1.-2 show the effect of 15 hours on a melt containing 53.76x$10^{-3}$$molkg^{-1}$ solution of Mo(III). Loss of the 2nd cathodic peak is indicated and the relative peak currents decrease. These results indicate the instability of the anodically dissolved species. Table 4.2.4.1. shows the main changes after 15 hours at a sweep rate of 200 $mVsec^{-1}$.

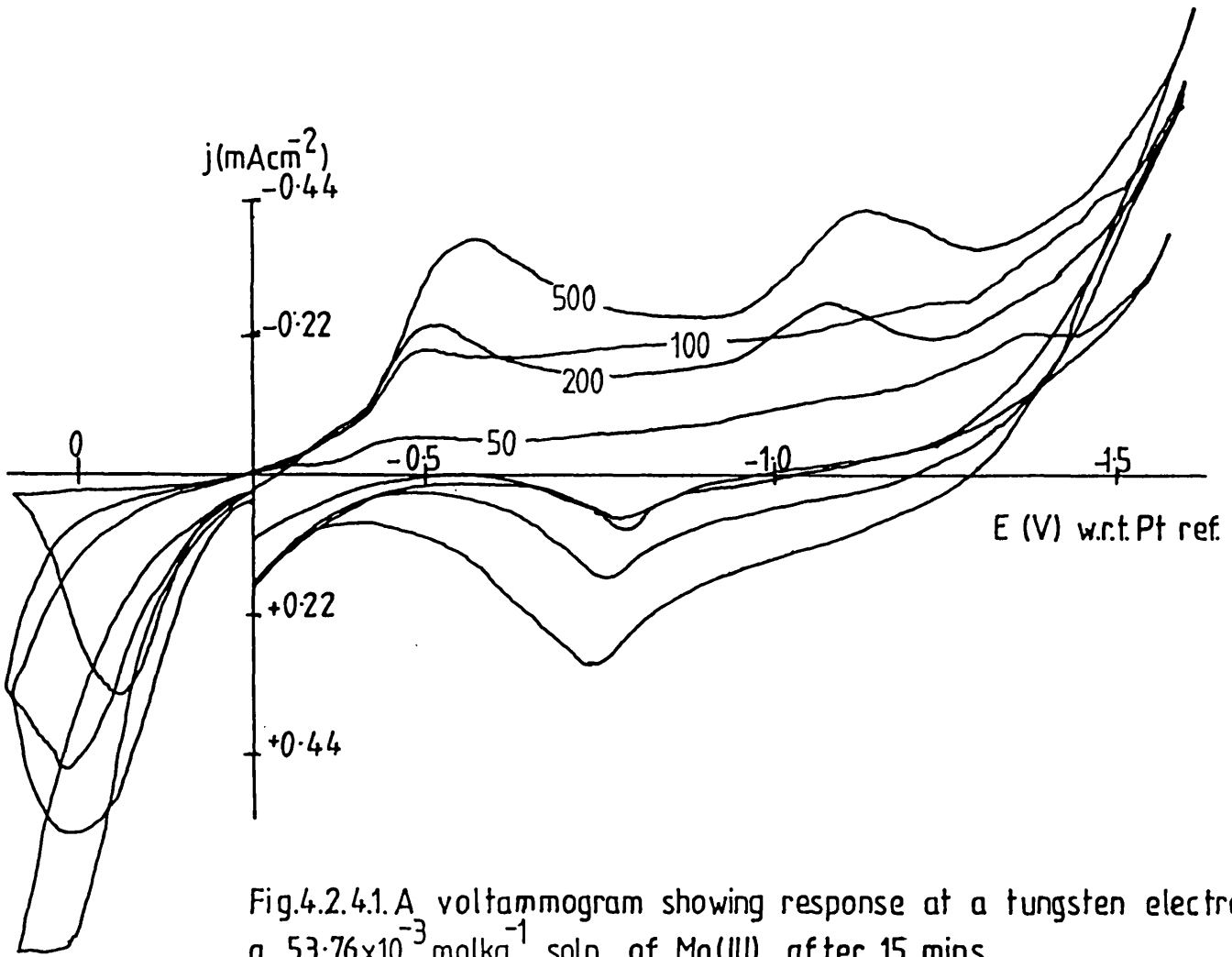

Fig.4.2.4.1. A voltammogram showing response at a tungsten electrode for a $53{\cdot}76 \times 10^{-3}$ molkg^{-1} soln. of Mo(III), after 15 mins.

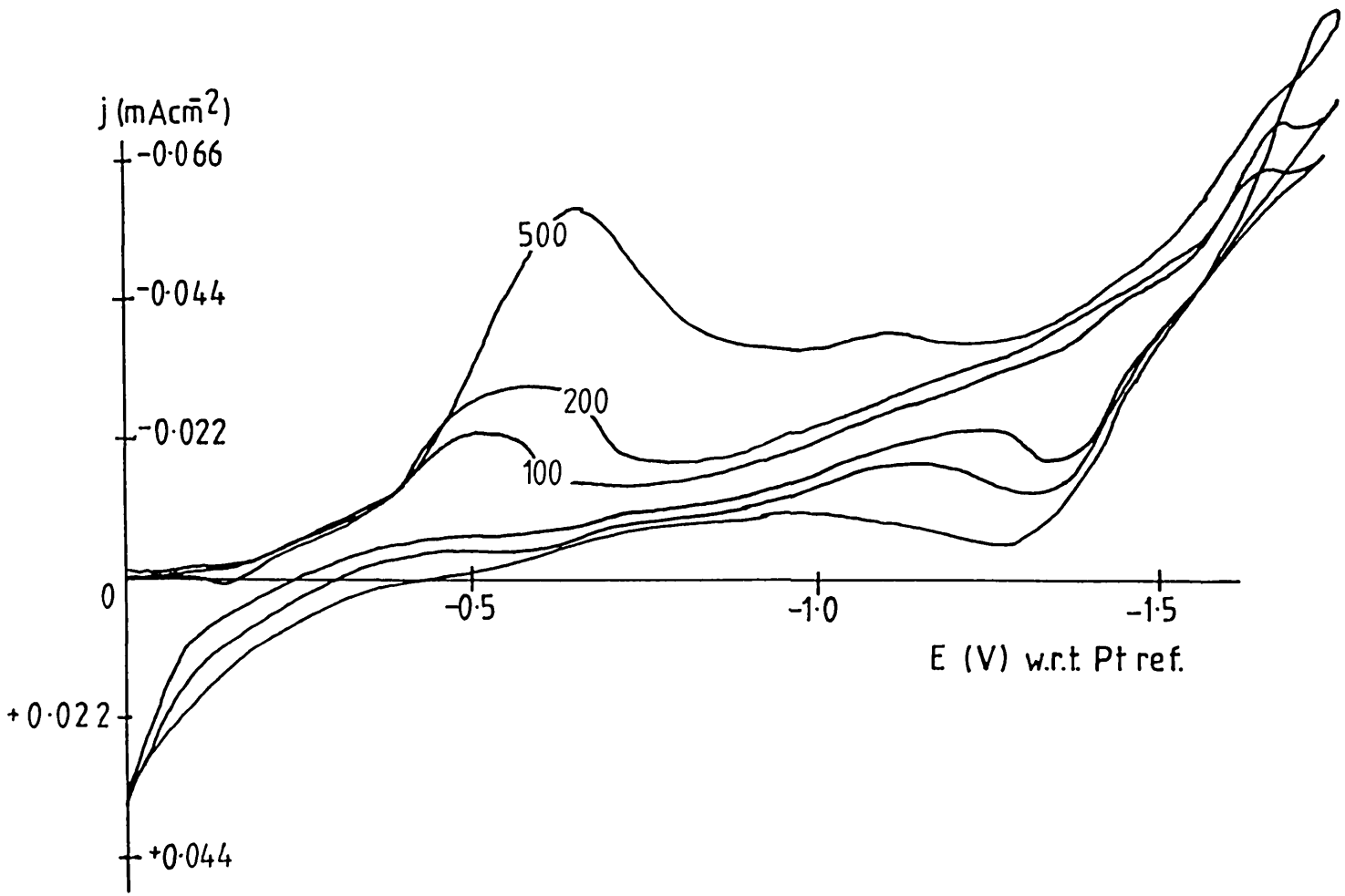

Fig.4.2.4.2. A voltammogram showing the response at a tungsten electrode for a $53{\cdot}76 \times 10^{-3}$ molkg^{-1} soln. of Mo(III), after 15 hours.

t (hrs.)	$j_p^c(1)$ (mA/cm^2)	$j_p^c(2)$ (mA/cm^2)	$j_p^c(3)$ (mA/cm^2)	$E_p^c(1)$ (V)	$E_p^c(2)$ (V)	$E_p^c(3)$ (V)
0.25	0.24	0.169	-	-0.51	-1.085	-
15.00	0.061	-	0.047	-0.57	-	-1.52

Table 4.2.4.1.THE EFFECT OF TIME ON VOLTAMMETRIC PARAMETERS

The substantial current drop in the net current reveals that electroactive species are lost with time and thus must be unstable at these temperatures. Almost complete loss of the species giving rise to peak two is shown, and the clearly defined 3rd peak after 15 hours, indicates the probable formation of the species corresponding to this peak from a proportion of that which after 15 minutes was the species giving rise to the 2nd peak. The disproportionation reaction indicated in 4.1. is likely to be responsible for the above behaviour.

4.3.DISCUSSION.

A possible reaction scheme to give the above responses is:-

A disproportionation reaction:-

$$5(MoCl_6)^{3-} \longrightarrow 2Mo + 3MoCl_5 + 15Cl^-$$

and electrochemical/ chemical reactions:-

$$Mo^{5+} + 2e \rightleftharpoons Mo^{3+}$$

$$2(MoCl_6)^{3-} \rightleftharpoons (Mo_2Cl_9)^{3-} + 3Cl^-$$

$$(MoCl_6)^{3-} + 3e \rightleftharpoons Mo + 6Cl^-$$

The disproportionation of the $(MoCl_6)^{3-}$ species added by anodic dissolution would give rise to the Mo^{5+} species and thus the presence of the first cathodic peak observed. The variation of the response with sweep rate reveals the nature of the E.C.E. reaction scheme indicated above, so that at slow sweep rates the monomer species $(MoCl_6)^{3-}$ which is produced by the reduction of the Mo^{5+} is able to dimerise before reaching its reduction potential (to molybdenum) and then dissociation is required before

reduction to Mo. Thus the 3rd cathodic peak can be accounted for. At faster sweep rates, there is insufficient time for this dimerisation to occur before the reduction potential to Mo is reached and thus the 2nd cathodic peak is formed. Mixtures of this behaviour are also observed as might be expected if these reactions can occur to some extent. The calculated n values 2,3 and 3 for peaks 1,2 and 3 respectively also support the above reaction scheme.

The effect of concentration also indicates the monomer/dimer equilibrium, as increasing the concentration should enhance the formation of dimers and thus the noted increase in the peak current for the 3rd peak. Similarly increasing the concentration of $(MoCl_6)^{3-}$ should increase the amount of Mo^{5+} produced by disproportionation and thus the rise in the 1st peak cathodic current. The anodic shifts of peak potential with increasing concentration also indicate an E.C.E. scheme is occuring.

Increasing the temperature gives rise to what might appear anomalous effects, as the dimer/monomer equilibrium should favour the monomer at higher temperatures, but it is the 3rd peak (dimer) that is observed at the highest temperatures. However this does not consider the stability of the monomer species itself. The disproportionation reaction forming volatile $MoCl_5$ and Mo noted at all temperatures will be enhanced at higher temperatures and thus the only electrochemically active species remaining in the melt will be the dimer. The stability of the dimer at > 850°C may also be due to the acidity of $CaCl_2$. The calcium ion "capturing" chloride ions and thus reduces the available chloride ions for complexing with the Mo, and so favours the dimer. This effect has been noted by Phillips and Osteryoung (93) using NaCl-$AlCl_3$ melts, who found that as the acidity of the melt

was increased, loss of $MoCl_6^{3-}$ occurred. The effects noted with time may arise from the same factors. This behaviour, dimer/monomer formation, disproportionation and melt cation effects have been noted by other workers (94-97). Senderoff and Mellors(95) also calculated the diffusion coefficient of the monomer at 800°C in a LiCl-KCl solvent and determined a value of 3.87×10^{-5} cm^2/sec. The values calculated for the Mo^{5+} species and the dimer in section 4.2.3. of 8.77×10^{-4} and 6.62×10^{-4} appear reasonable for the increase in charge and size of the ions compared with the monomer. The effect of melt cation is noted by White and Twardoch (94) in CsCl-LiCl and KCl-LiCl melts at 450°C,shifting the monomer/dimer equilibrium. These workers also note only one anodic process for both monomer and dimer, but at the slow sweep rates in this melt, two peaks are observed. The sharp peak correponding to the dimer peak may indicate a stripping phenomena rather than an oxidation reaction.

5.THE ELECTROCHEMICAL BEHAVIOUR OF CALCIUM CARBONATE

5.1.INTRODUCTION

This chapter investigates the electrochemical behaviour of calcium carbonate additions dissolved in $CaCl_2$ at temperatures from 824 to 844 ^{o}C and for concentrations from 9.75 to 183.09 $x10^{-3}molkg^{-1}$ calcium carbonate.

The instablity of calcium carbonate at these temperatures was expected and thus the probable loss of carbonate ion by thermal decomposition to the oxide and carbon dioxide. The observation of gas evolution and the voltammograms obtained after carbonate addition indicated this sort of reaction was occuring. In order to suppress this decomposition the use of a carbon dioxide, rather than argon atmosphere over the melt, was considered.

Cyclic voltammetric investigations of this decomposition reaction and the electrochemistry of carbonate ions ,in molten calcium chloride are considered below, showing the effects of varying sweep rates, electrode material, carbonate concentration and melt atmosphere.

5.2.CYCLIC VOLTAMMETRIC ANALYSIS OF $CaCO_3$ IN $CaCl_2$.

Pellets of calcium carbonate were added to pure molten calcium chloride and analysed at tungsten and platinum electrodes. These responses were markedly affected by both the time after addition and the condition of the electrode surface. After cycling, subsequent cycles were inconsistent with the first. The carbon coating observed on the electrode was assumed to be responsible for this effect. The time after addition, although not revealing a change in the morphology of the voltammogram, gave rise to increased peak heights, and slight cathodic shifting of the peaks with increasing time after addition. This is most likely due to the time required for the

pellet to dissolve. The use of freshly polished electrodes for each sweep and allowing two hours for the dissolution of the pellets gave reproducible voltammograms.

5.2.1.Effect of sweep rate.

The cyclic voltammogram (Fig 5.2.1.1.) shows a typical response obtained at a tungsten electrode, for various sweep rates. Two cathodic and one anodic wave can be observed. The first couple appears at approx. -0.62 V w.r.t. Pt Q.R.E. and a single more cathodic wave is found at approx. -1.08 V at 100 $mVsec^{-1}$. After sweeping past this potential a black carbon coating is formed on the electrode, which is not removed on reversing the potential sweep. These three processes are observed for all sweep rates and the effect of sweep rate on cyclic voltammetric parameters is given in tables 5.2.1.1,5.2.1.2., for the 1^{st} peak (cathodic and anodic) and the 2^{nd} peak respectively, for a solution containg 60.22 $x10^{-3}molkg^{-1}$ calcium carbonate.

Table 5.2.1.1. indicates that for the first peak, the peak cathodic potential (E_p^c) shifts more cathodic with increasing sweep rate, and that both the half peak width ($E_p^c-E_{p/2}^c(1)$) and the peak to peak potential ($E_p^c-E_p^a(1)$) increase with increasing sweep rate. This implies that the process becomes more irreversible with increasing sweep rate. The peak current is directly proportional to $v^{1/2}$, (Fig.5.2.1.2.) and the current function $ip^c/v^{1/2}$ is virtually independent of v, especially at lower sweep rates.

This response may be analysed according to the quasi reversible charge transfer model(132,133). According to this model the peak to peak separation is equal to

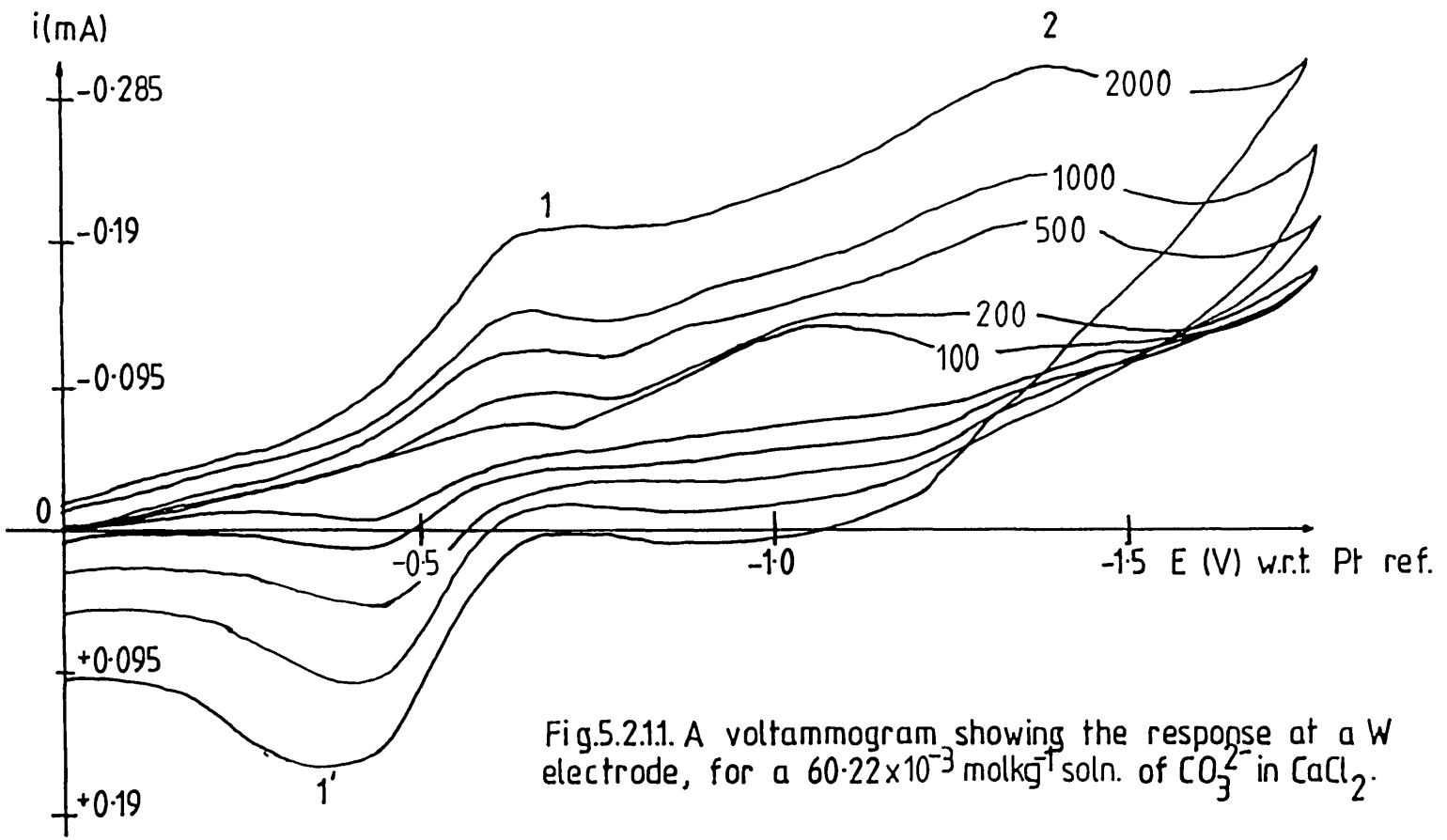

Fig.5.2.1.1. A voltammogram showing the response at a W electrode, for a $60{\cdot}22 \times 10^{-3}$ molkg^{-1} soln. of CO_3^{2-} in $CaCl_2$.

Peak 1

v (mV/s)	$i_p^c(1)$ (mA)	$i_p^a(1)$ (mA)	$\frac{i_p^c\ (mAs^{1/2}}{v^{1/2}\ mV^{1/2})}$	i_p^a/i_p^c (mA)	$E_p^c(1)$ (V)	$E_{p/2}^c(1)$ (V)	$E_p^a(1)$ (V)	$E_p^c-E_{p/2}^c(1)$ (mV)	$E_p^c-E_p^a(1)$ (mV)
100	0.047	0.038	0.005	0.8	-0.62	-0.41	-0.47	-210	-150
200	0.070	0.047	0.005	1.5	-0.64	-0.45	-0.44	-190	-200
500	0.108	0.075	0.005	1.44	-0.645	-0.46	-0.43	-185	-215
1000	0.117	0.117	0.004	1.00	-0.655	-0.47	-0.42	-185	-235
2000	0.155	0.164	0.003	1.06	-0.68	-0.51	-0.39	-170	-290

Table 5.2.1.1. VOLTAMMETRIC PARAMETERS FROM Fig 5.2.1.1.

Peak 2

v (mV/s)	$i_p^c(2)$ (mA)	$\frac{i_p^c\ (mAs^{1/2}}{v^{1/2}\ mV^{1/2})}$	$E_p^c(2)$ (V)	$E_{p/2}^c(2)$ (V)	$E_p^c-E_{p/2}^c(2)$ (mV)
100	0.056	0.006	-1.08	-0.85	-230
200	0.080	0.006	-1.15	-0.87	-280
500	0.127	0.006	-1.27	-1.03	-240
1000	0.164	0.005	-1.36	-1.04	-320
2000	0.174	0.004	-1.40	-1.065	-335

Table 5.2.1.2. VOLTAMMETRIC PARAMETERS FROM Fig 5.2.1.1.

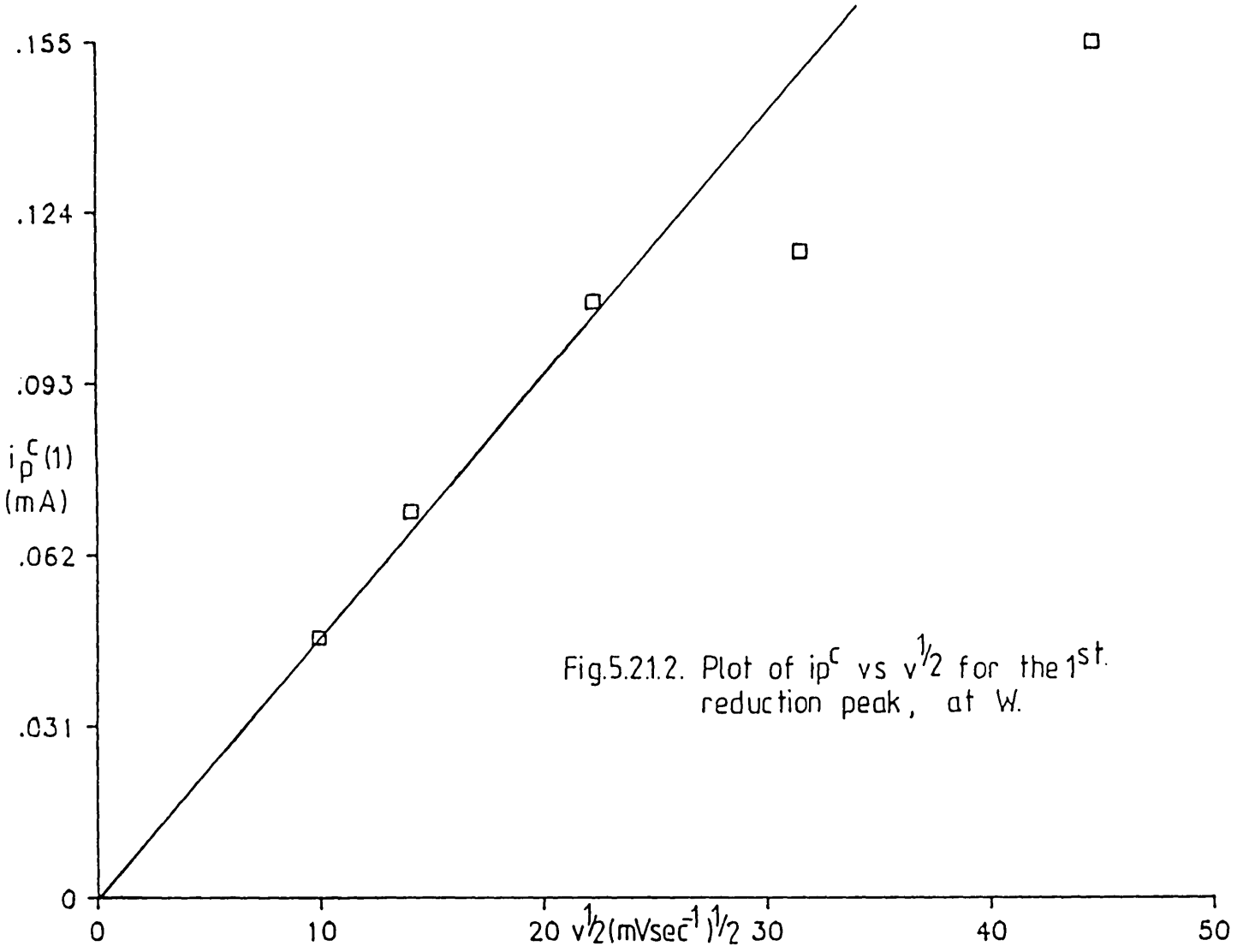

Fig.5.21.2. Plot of ip^c vs $v^{1/2}$ for the 1st. reduction peak, at W.

$-(60.T)/(298.n)$mV. At the lowest sweep rate this gives an n value of 1.47. Plots of $\log\frac{(ip-i)}{i}$ and log(ip-i) against E_p^c are shown in Figs 5.2.1.3,5.2.1.4. The linear $\log\frac{(ip-i)}{i}$ has a gradient of 5.44 V^{-1}, which gives an αn value of 1.18.

Similarly considering peak two, table 5.2.1.2., the lack of anodic response indicates that this process is irreversible. Both the cathodic peak potential and the cathodic half peak potential shift cathodic with increasing sweep rate, and the peak potential is proportional to the natural log. of v.(Fig.5.2.1.5). The peak cathodic current is directly proportional to $v^{1/2}$ (Fig.5.2.1.6.) and the current function ($i_p^c/v^{1/2}$) is constant at lower sweep rates, but increases as v increases.

These factors all indicate that a reversible process with an insoluble product is occuring at the electrode. According to this model, the cathodic peak potential and the cathodic half peak potential should shift by $-(30.T)/(\alpha n.298)$mV for a ten fold increase in sweep rate. Taking the mean value of 229mV an αn value of 0.48 is calculated. Also the cathodic half width should be equal to $-1.857(RT)/(\alpha nF)$ V and similarly gives an αn value of 0.62. The plot of E_p^c against ln v gives an αn value of 1.16. Plots of $\log\frac{(ip-i)}{i}$ and log(ip-i) against E_p^c are shown to be non linear in Figs 5.2.1.7 and 5.2.1.8. This also indicates the irreversibility of this process.

These responses indicate that a quasi reversible process is occuring at approx. -0.62 V :-

$$O + 2e \rightleftharpoons R$$

and that an irreversible process occurs at approx. -1.08 V.

$$O + ne \longrightarrow R$$

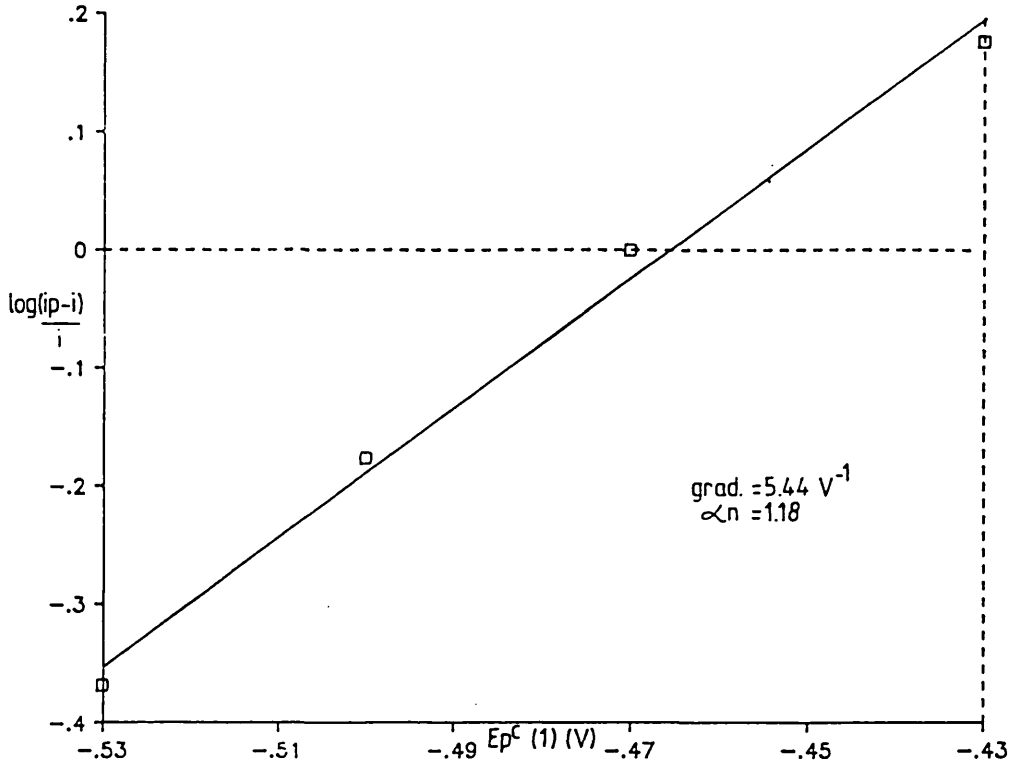

Fig.5.2.1.3. Plot of $\log(i_p-i)/i$ vs E_p^c in the range $0.4-0.7i_p$, for the 1st. reduction peak at tungsten.

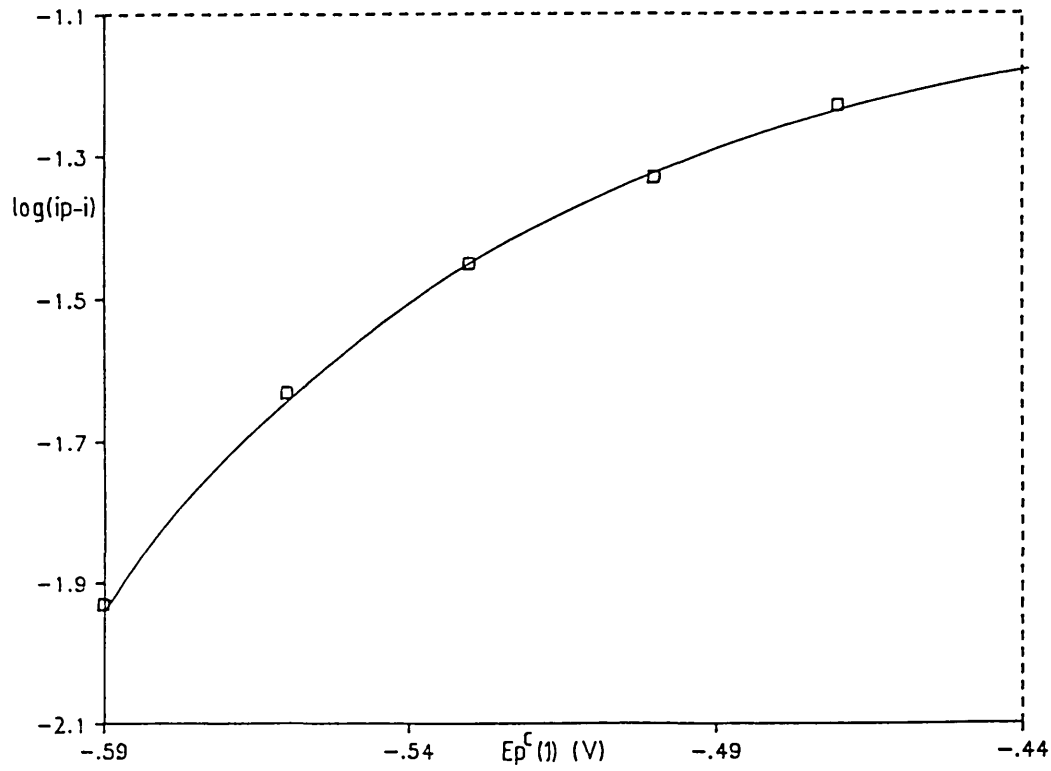

Fig.5.2.1.4. Plot of $\log(i_p-i)$ vs E_p^c in the range $0.5-0.9i_p$, for the 1st. reduction peak at tungsten.

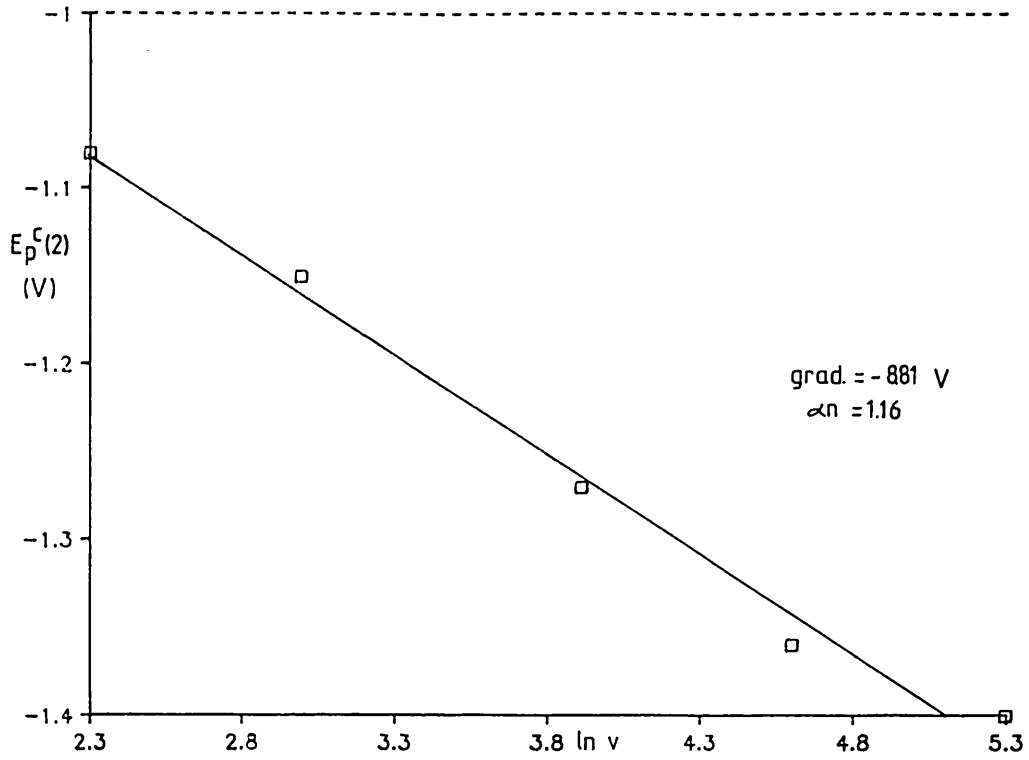

Fig.5.2.1.5. Plot of ln(v) vs $E_p^c(2)$, for the 2nd. reduction peak at W.

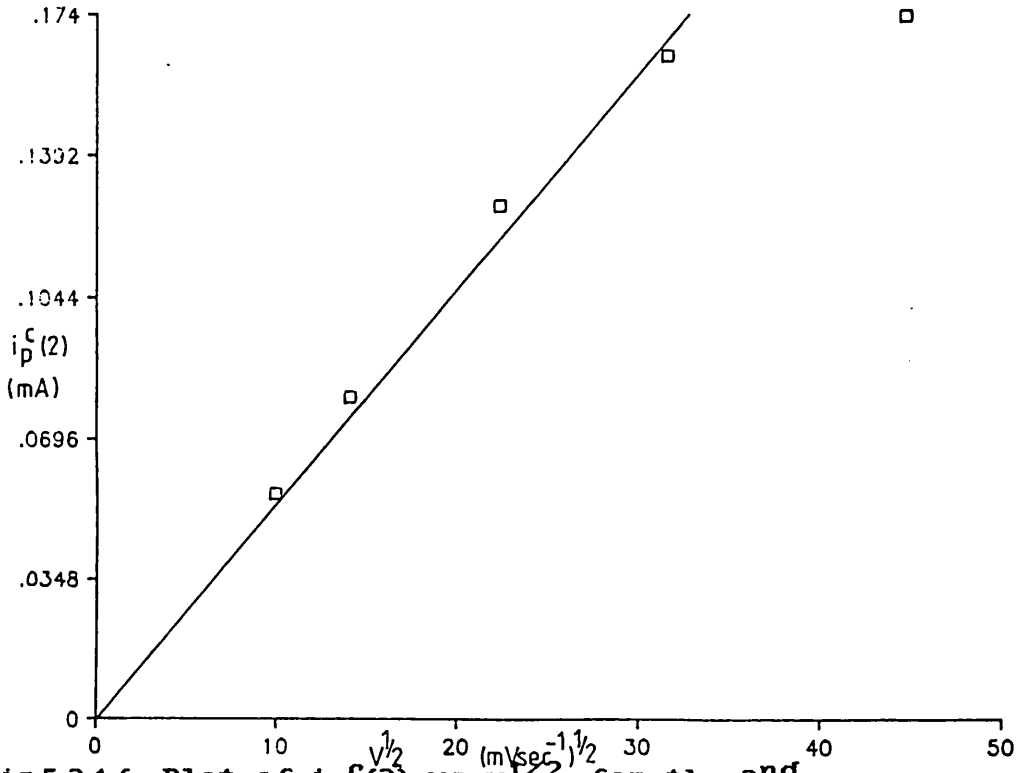

Fig.5.2.1.6. Plot of $i_p^c(2)$ vs $v^{1/2}$, for the 2nd. reduction peak at W.

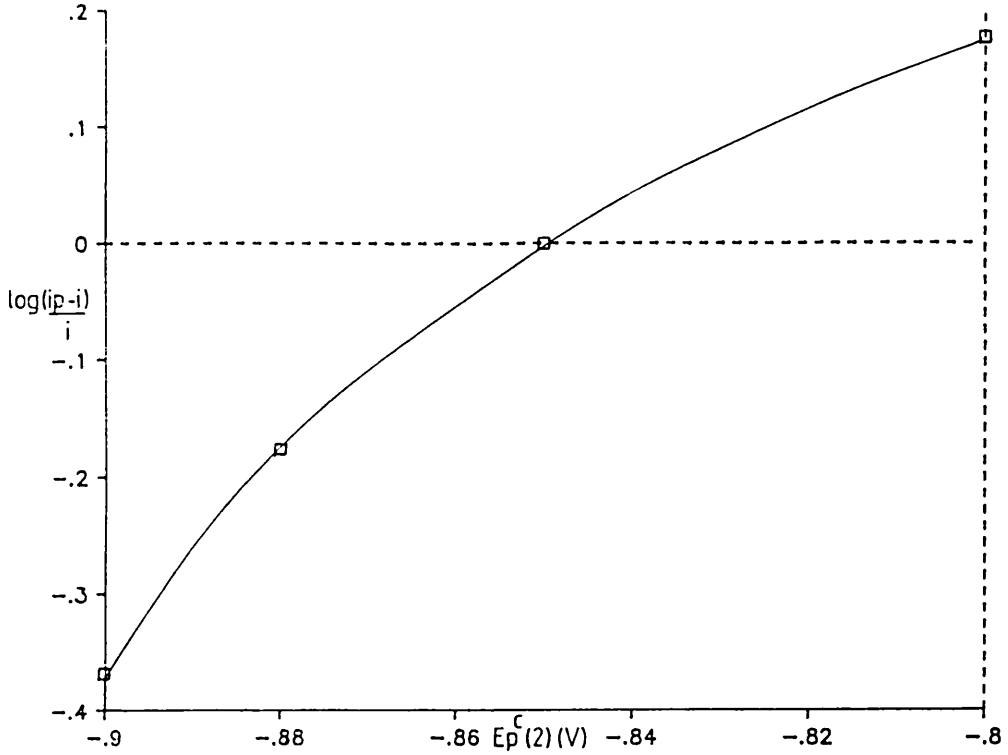

Fig.5.2.1.7. Plot of $\log(i_p-i)/i$ vs E_p^c in the range $0.4-0.7i_p$, for the 2nd. reduction peak at W.

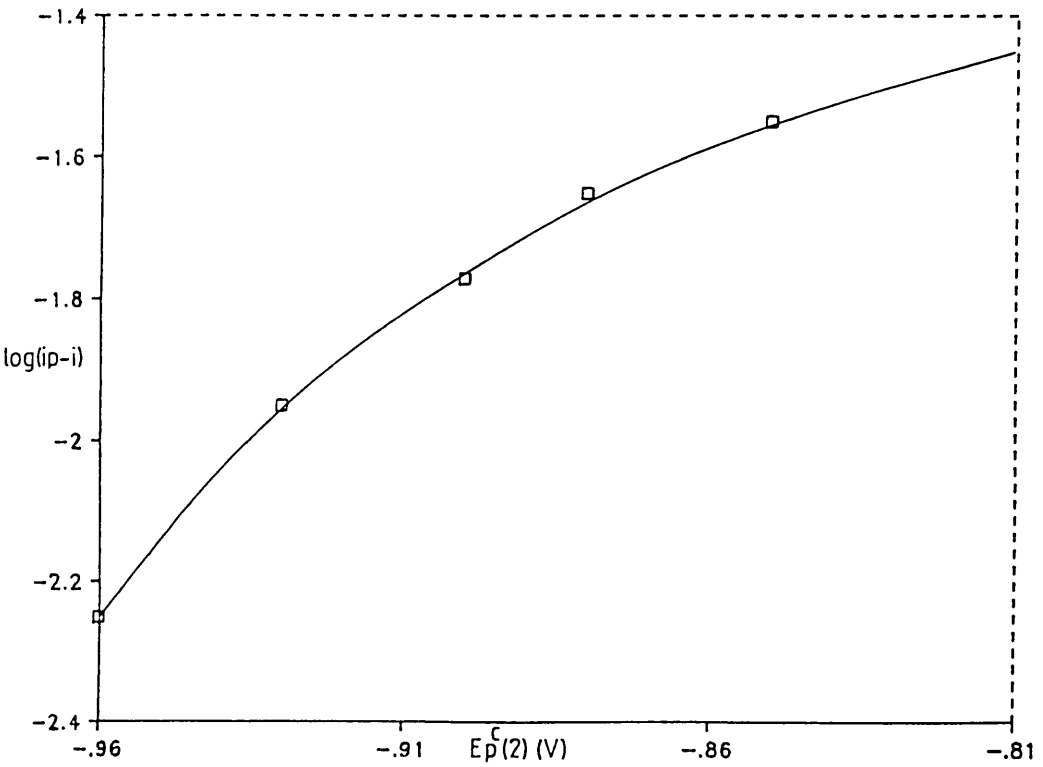

Fig.5.2.1.8. Plot of $\log(i_p-i)$ vs E_p^c in the range $0.5-0.9i_p$, for the 2nd. reduction peak at W.

A very similar response is noted at a Pt electrode. Fig.5.2.1.9. The cathodic peak corresponding to the first peak at tungsten is not observed, the waves are displaced to more cathodic potentials. Table 5.2.1.3. shows the variation of cyclic voltammetric parameters with sweep rate.

Table 5.2.1.3. shows that as at the tungsten electrode the cathodic peak potential and the cathodic half peak potential shift cathodic with increasing sweep rate. The cathodic peak potential is proportional to ln v, Fig.5.2.1.10. The cathodic peak current is directly proportional to $v^{1/2}$ (Fig.5.2.1.11) and the current function is independent of the sweep rate. The above factors again indicate that an irreversible process is occuring at the electrode, with an insoluble product. αn values can be calculated as before:-

method	$E_p^c - E_{p/2}^c$	10x v shift $E_p^{c\prime} - E_{p/2}^c$	E_p^c v lnv
αn	0.56	1.36	3.53

5.2.2.Effect of concentration.

The response of carbonate ions in $CaCl_2$ at a tungsten electrode is essentially the same for varying concentration. Table 5.2.2.1. indicates the effect of increasing concentration. The main effects are that, the cathodic peak potentials (1),(2) shift cathodic with increasing concentration and the peak currents increase with increasing concentration. Fig.5.2.2.1. indicates that j_p^c is proportional to the concentration. These factors are consistent with an irreversible charge transfer with an insoluble product.

To further investigate the relationship between the two peaks observed at tungsten, the potential of the electrode was held at -1.25 V w.r.t. Pt for varying times and the effect on the 1st peak noted. Table 5.2.2.2. shows the relative increase in the anodic current with increasing holding time. Fig.5.2.2.2. shows how i_p^a/i_p^c

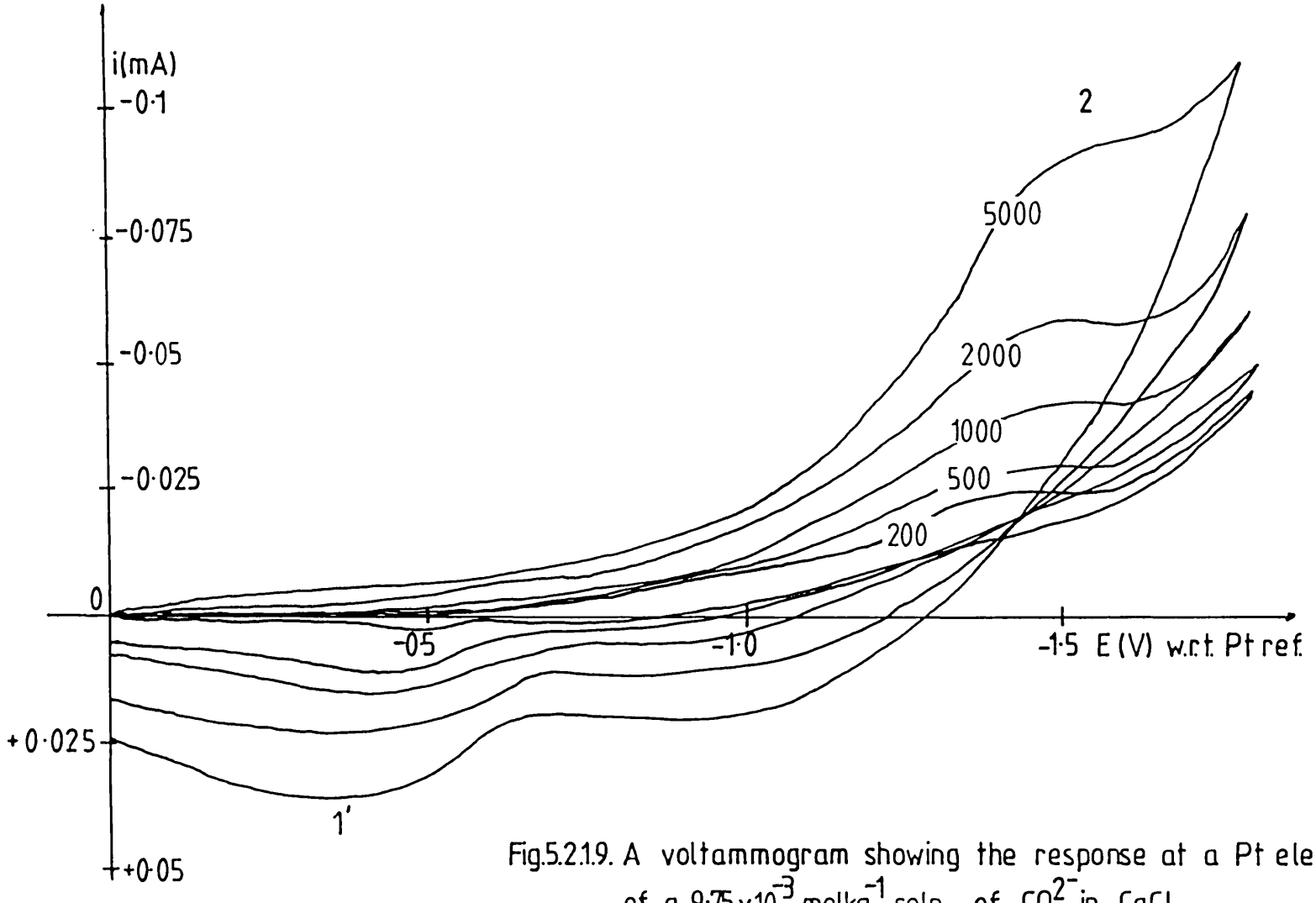

Fig.5.2.1.9. A voltammogram showing the response at a Pt electrode, of a $9{\cdot}75 \times 10^{-3}$ molkg^{-1} soln. of CO_3^{2-} in $CaCl_2$.

v (mV/s)	$i_p^c(2)$ (mA)	$i_p^a(1)$ (mA)	$\frac{i_p^c(2)(mAs^{1/2}}{v^{1/2}\ mV^{1/2})}$	i_p^a/i_p^c (mA)	$E_p^c(2)$ (V)	$E_{p/2}^c(2)$ (V)	$E_p^a(1)$ (V)	$E_p^c-E_{p/2}^c(2)$ (mV)	$E_p^c(2)-E_p^a(1)$ (mV)
200	0.021	0.002	0.001	0.095	-1.38	-1.08	-0.49	-300	-890
500	0.028	0.009	0.001	0.335	-1.41	-1.095	-0.46	-315	-950
1000	0.038	0.016	0.001	0.432	-1.44	-1.12	- 0.44	-320	-1000
2000	0.054	0.026	0.001	0.684	-1.46	-1.15	-0.43	-310	-1030
5000	0.085	0.038	0.001	0.447	-1.50	-1.18	-0.40	-320	-1100

Table 5.2.1.3. VOLTAMMETRIC PARAMETERS FROM Fig 5.2.1.9.

conc. (mmolal)	$j_p^c(1)$ (mA)	$j_p^c(2)$ (mA)	$j_p^a(1)$ (mA)	$E_p^c(1)$ (V)	$E_p^c(2)$ (V)	$E_p^a(1)$ (V)
9.75	0.143	0.065	0.075	-0.61	-1.06	-0.53
60.22	0.171	0.205	0.098	-0.62	-1.08	-0.45
121.55	0.434	0.788	0.359	-0.63	-1.10	-0.41
150.43	0.458	0.830	0.544	-0.64	-1.11	-0.32
183.09	0.771	0.962	0.701	-0.64	-1.12	-0.34

Table 5.2.2.1. EFFECT OF CONCENTRATION ON VOLTAMMETRIC PARAMETERS

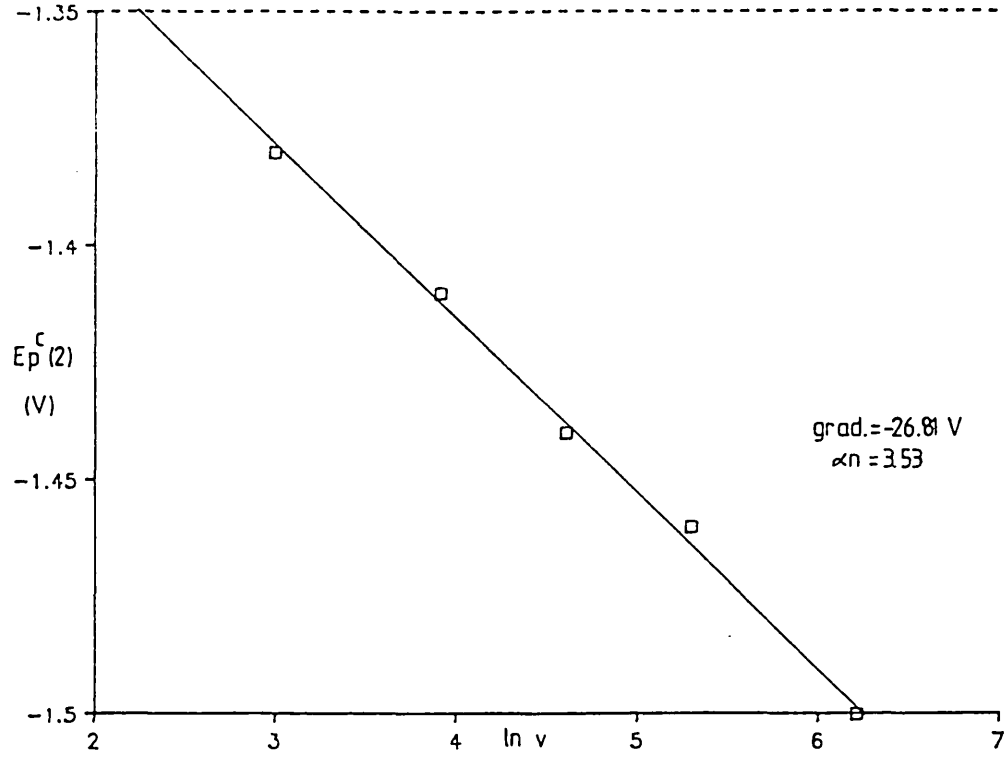

Fig.5.2.1.10. Plot of lnv vs $E_p^c(2)$, for the reduction of CO_3^{2-} at Pt.

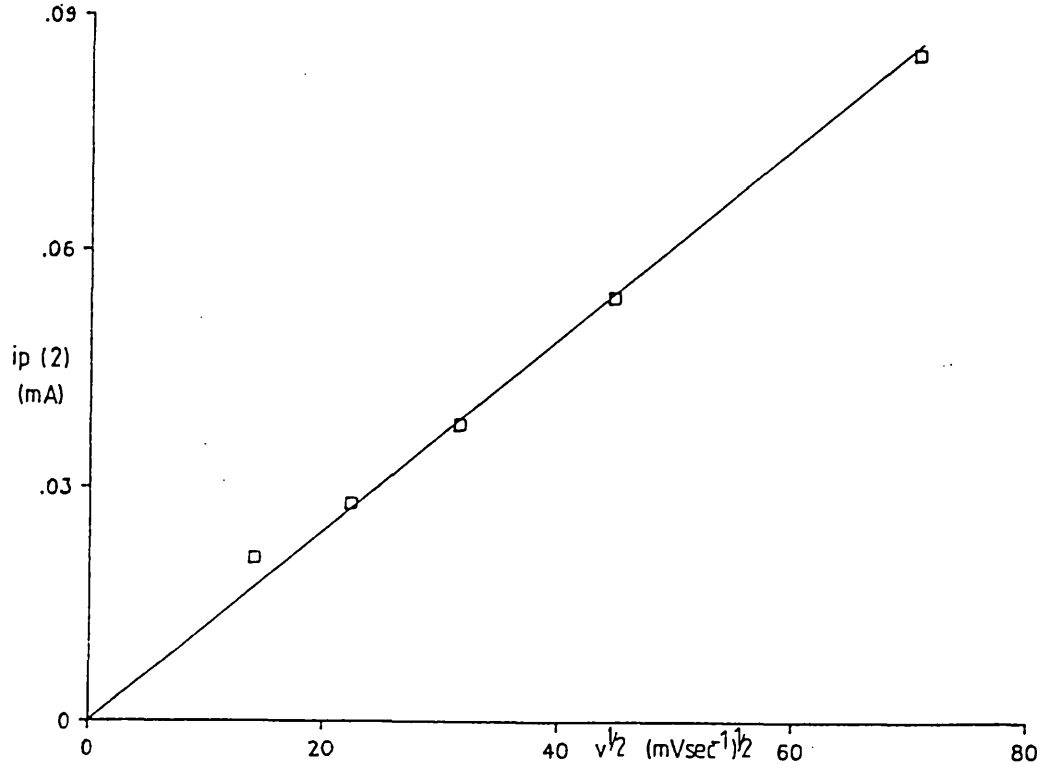

Fig.5.2.1.11. Plot of $i_p^c(2)$ vs $v^{1/2}$, for the reduction of CO_3^{2-} at Pt.

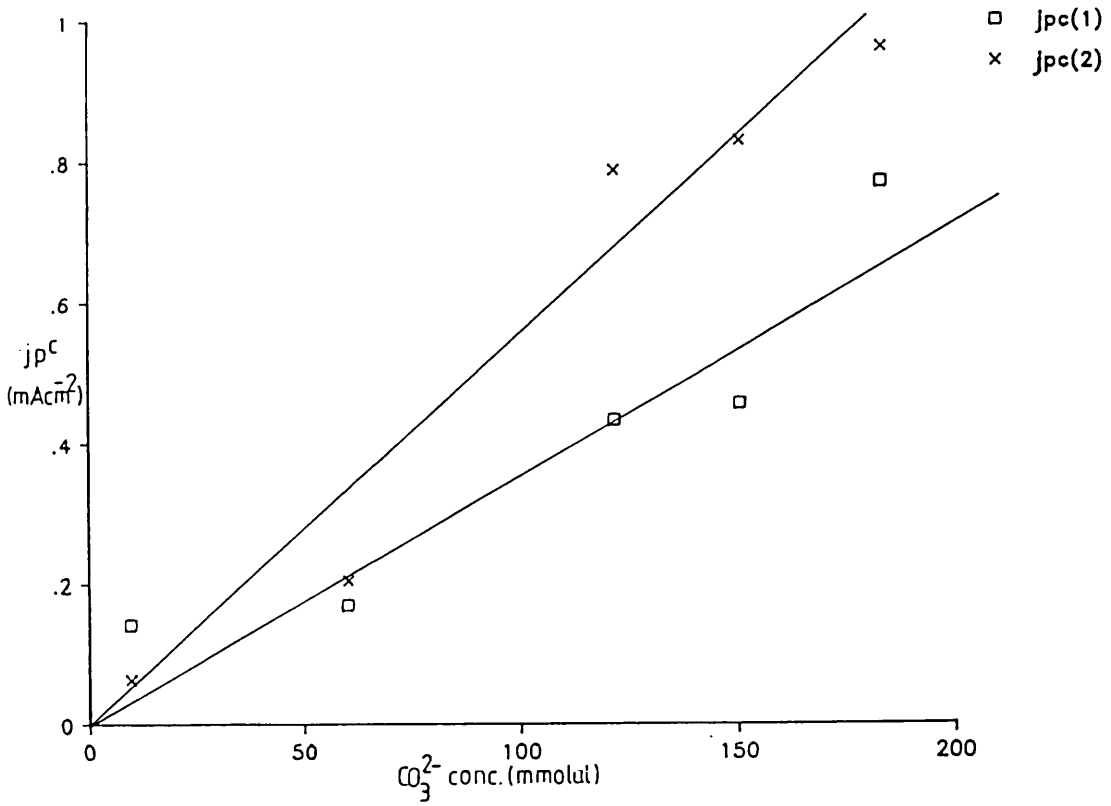

Fig.5.2.2.1. Plots of j_p^c vs conc.(CO_3^{2-}), the reduction peaks 1 and 2 at tungsten.

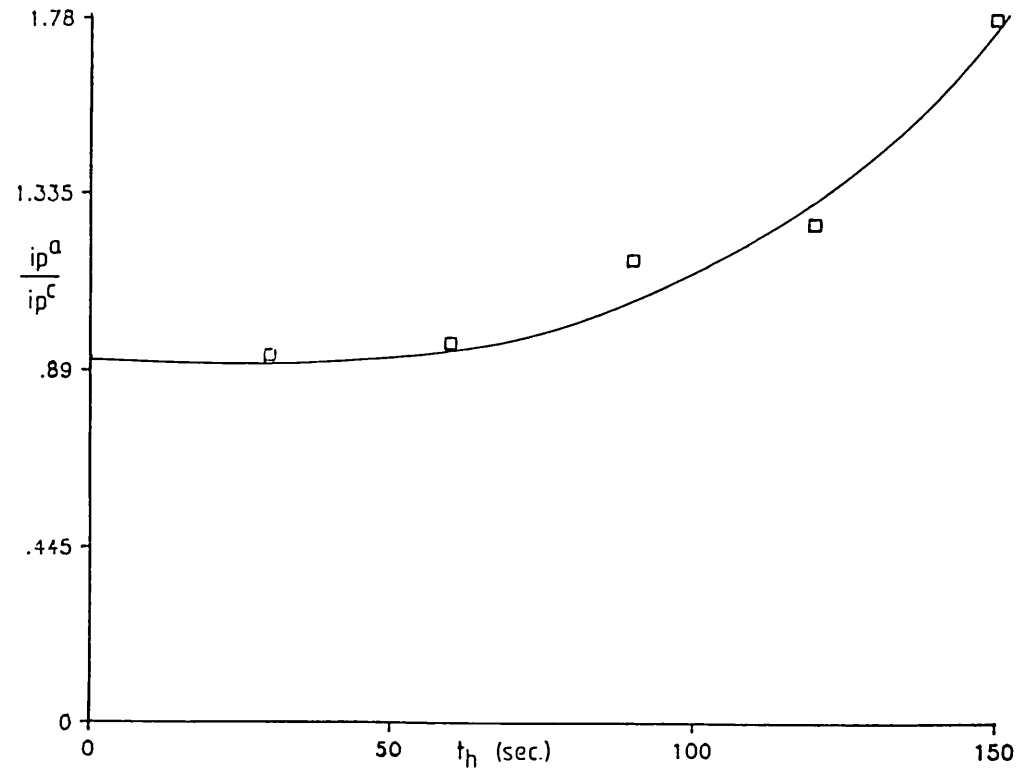

Fig.5.2.2.2. Plot of i_p^a/i_p^c vs holding time for the 1st. reduction peak at tungsten.

varies with holding time. These results suggest that the species giving rise to the 1st peak are generated during the process occuring giving rise to the second irreversible peak.

$t_{holding}$ (sec)	$i_p^c(1)$ (mA)	$i_p^a(1)$ (mA)	$i_p^a/i_p^c(1)$
30	0.027	0.025	0.93
60	0.027	0.026	0.96
90	0.023	0.027	1.17
120	0.023	0.029	1.26
150	0.023	0.041	1.78

Table 5.2.2.2. EFFECT OF HOLDING TIME ON CURRENT PARAMETERS

5.2.3.Discussion.

The results indicated above may be explained by an irreversible carbonate reduction, giving rise to carbon at the electrode. The 1st peak which has a probable 2 electron quasi reversible transfer, is generated upon addition of carbonate ions. The species giving rise to the anodic peak is generated upon the reduction of the carbonate ion at the 2nd reduction peak. Thus a possible reaction scheme giving rise to the above factors may be:-

$$2O^{2-} \rightleftharpoons O_2^{2-} + 2e \text{ at } -0.62 \text{ V}$$

$$CO_3^{2-} + 4e \rightleftharpoons 3O^{2-} + C \text{ at } -1.08 \text{ V}$$

The thermal decomposition of carbonate:-

$$CO_3^{2-} \rightleftharpoons O^{2-} + CO_2$$

hence the generation of the 1st peak and its enhancement by the reduction of the carbonate ion. The formation of peroxide and its reduction in $CaCl_2$-NaCl has been investigated by Brookes and Inman(134), although the potentials indicated for this process in the above work are inconsistent with those found by Brookes and Inman. The irreversibility and the response noted at a Pt electrode are very similar to those noted by Mo(110), but

again the reduction is somewhat anodic of the potentials indicated in her work. These effects may arise due to the use of a quasi reference electrode, which although self consistent for a particular experiment, the concentration of other species especially oxide content affect the actual equilibrium potential the electrode attains. Direct comparison of potentials against those on a controlled scale is not strictly possible, unless using the cathodic limit as a comparison point. As indicated earlier in section 3.3.2. the presence of free calcium in the melt does not allow this process to be clearly defined in this melt, and hence the difficulty in comparing potentials. However even considering these difficulties the carbonate reduction peak is somewhat anodic of that found by other workers, but the acidity of the Ca^{2+} ion may destabilise the carbonate ion and thus reduction of this complex ion can occur more readily. The varying αn values calculated for carbonate reduction at Pt and W can be explained by the possible formation of carbides at the electrode, giving rise to distortions in the wave morphology, particularly between the response for different electrode materials.

5.2.4.Effect of carbon dioxide.

The thermal decomposition of carbonate ions theoretically can be supressed by using a CO_2 environment, pushing the equilibrium back to the left:-

$$CO_3^{2-} \rightleftharpoons CO_2 + O^{2-}$$

Voltammograms obtained under CO_2 environments are markedly different to those obtained under Ar. Fig.5.2.4.1a and b. show the response at W and Pt at a sweep rate of $50mVsec^{-1}$. Table 5.2.4.1. indicates the effect of sweep rate on these responses. The activation/deactivation peaks noted over the region -0.5 to -1.0 V w.r.t. Pt and the well defined peak at -1.5 V w.r.t. Pt do not have corresponding oxidation peaks. The response of the pure melt under a CO_2 environment was considered. In order to see whether these activation/deactivation peaks were due

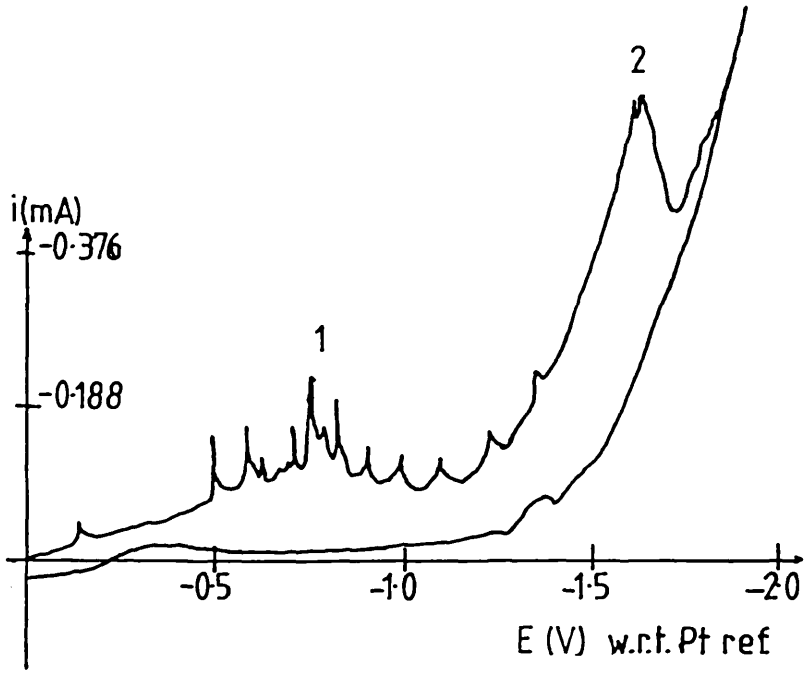

(a) at W.

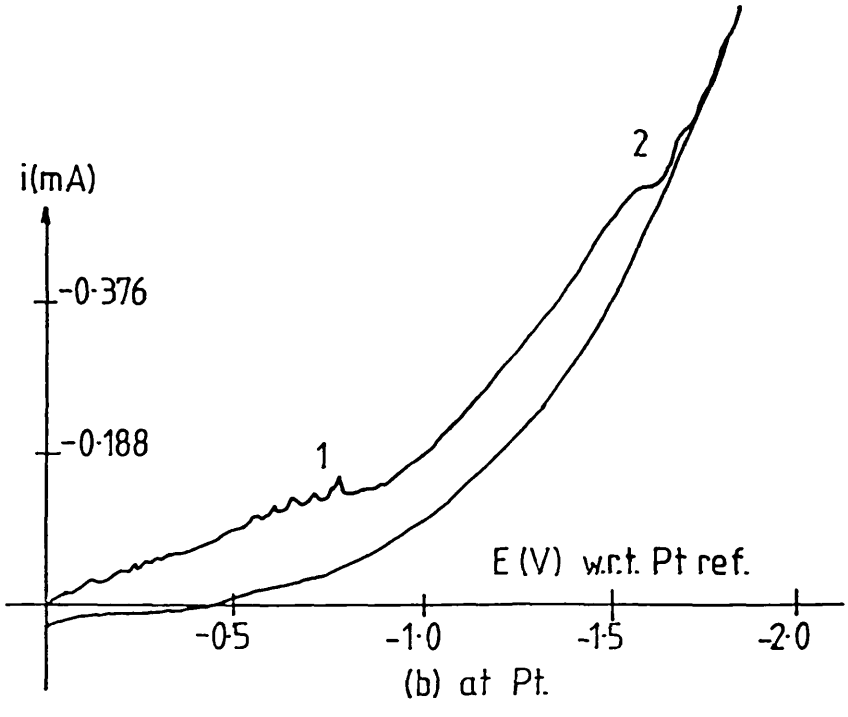

(b) at Pt.

Fig.5.2.4.1. Voltammograms showing the reduction of CO_3^{2-} under a CO_2 atmosphere, sweeping at 50 $mVsec^{-1}$

At W

v (mV/s)	$i_p^c(2)$ (mA)	$\frac{i_p^c\ (mAs^{1/2}}{v^{1/2}\ mV^{1/2})}$	approx $E_p^c(1)$ (V)	$E_p^c(2)$ (V)	$E_{p/2}^c(2)$ (V)	$E_p^c - E_{p/2}^c(2)$ (mV)
20	0.206	0.047	-0.71	-1.52	-1.17	-350
50	0.573	0.081	-0.80	-1.62	-1.42	-200
100	0.488	0.048	-0.80	-1.64	-1.46	-180
200	0.563	0.040	-1.00	-1.82	-1.65	-170

At Pt

v (mV/s)	$i_p^c(2)$ (mA)	$\frac{i_p^c\ (mAs^{1/2}}{v^{1/2}\ mV^{1/2})}$	approx $E_p^c(1)$ (V)	$E_p^c(2)$ (V)	$E_{p/2}^c(2)$ (V)	$E_p^c - E_{p/2}^c(2)$ (mV)
50	0.516	0.073	-0.82	-1.56	-1.13	-430
100	0.535	0.054	-0.90	-1.58	-1.13	-250
200	0.600	0.042	-0.80	-1.60	-1.19	-510
500	0.507	0.023	-1.12	-1.62	-1.28	-430

Table 5.2.4.1. EFFECT OF CO_2 ON VOLTAMMETRIC PARAMETERS.

to the CO_2 alone or by interaction with the carbonate ions in the melt.

Fig.5.2.4.2. shows that these peaks are present without the carbonate ion at a tungsten electrode. Pt electrodes gave similar responses. This activation/deactivation is similar to that observed for gas formation at the electrode, so a possible explaination for this behaviour is the reduction of CO_2 to carbon monoxide, the more cathodic peak observed in the presence of the carbonate ion being due to its reduction. This peak is more cathodic than those noted under Ar. This may be due to the increased stability of the carbonate ion under CO_2 and thus the more cathodic potentials required for its reduction. Bartlett and Johnson (106) considering the thermodynamics of CO_2 and CO_3^{2-} in chloride melts, showed that CO_2 is reduced more readily than CO_3^{2-}, and furthermore, that CO_2 is reduced to CO rather than C and the CO_3^{2-} to C, at these temperatures. The solubility of CO_2 in the melt gives rise to the observed response.

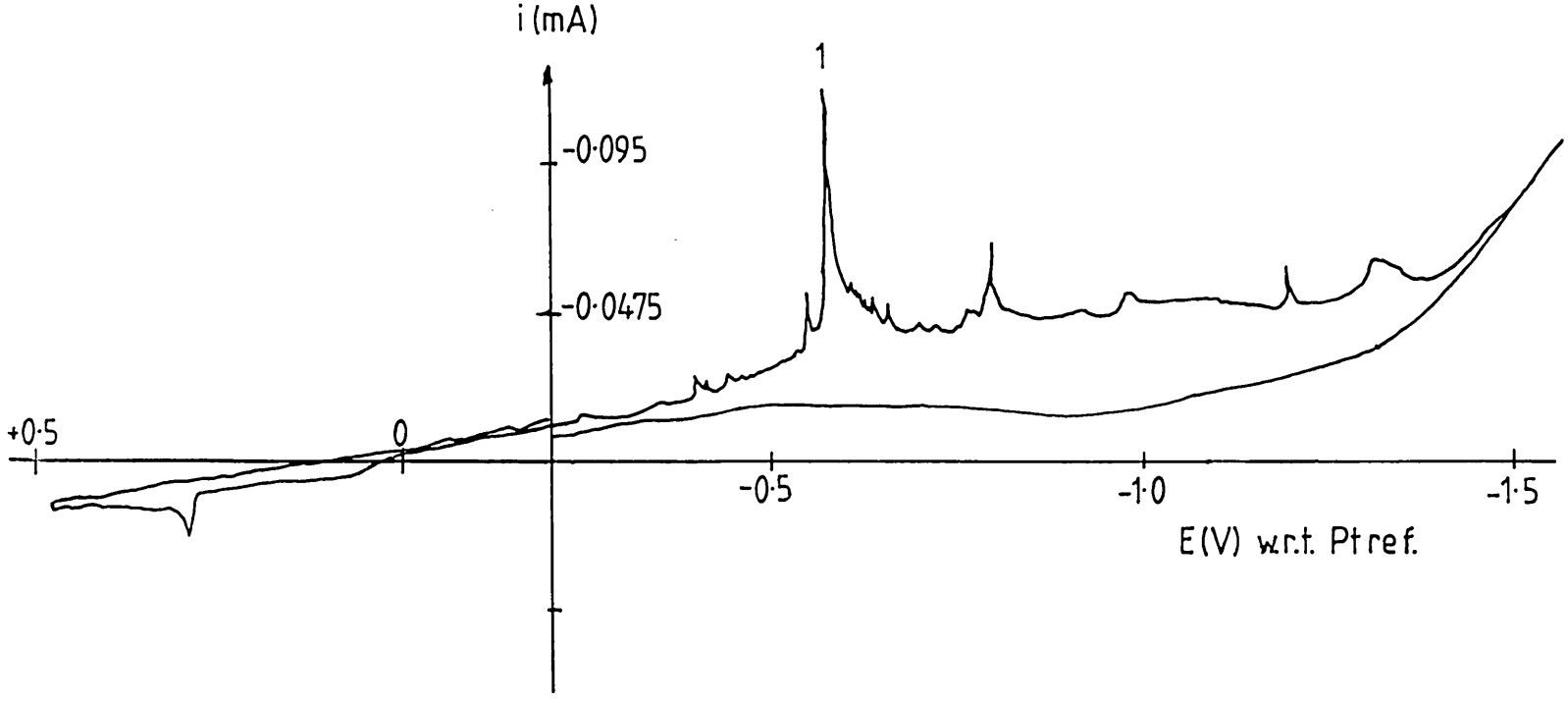

Fig.5.5.4.2. A voltammogram showing the response of pure $CaCl_2$ at tungsten under a CO_2 atmosphere.

6.THE ELECTROCHEMICAL BEHAVIOUR OF BOTH CALCIUM CARBONATE AND ANODICALLY DISSOLVED MOLYBDENUM IN CALCIUM CHLORIDE.

6.1. INTRODUCTION.

This chapter investigates the effects of calcium carbonate and anodically dissolved molybdenum on the cyclic voltammetric response at tungsten and platinum electrodes, for the temperature and concentration ranges noted in chapters 4 and 5. Again chemical reactions may be expected to occur and the formation of a pale yellow volatile species condensed on the cell head was noted after the addition of the second solute to the solvent.

6.2.CYCLIC VOLTAMMETRIC ANALYSIS OF $CaCO_3$ AND $MoCl_3$

As indicated previously in sections 4.2 and 5.2 pellets of calcium carbonate were added to the melt and molybdenum rod dissolved into the melt. The responses at W and Pt were found to be dependent upon the condition of the electrode surface and on the time after addition. As noted with the carbonate approx. 2 hours were required for complete dissolution of the pellets and thus cyclic voltammetric analysis was only undertaken after this time had elapsed. Similarly, due to the formation of coatings on the electrode after scanning, freshly cleaned electrodes were used for each sweep.

6.2.1.Response at tungsten.

Fig.6.2.1.1. shows a typical response of a $MoCl_3$ and CO_3^{2-} containing solution. The complex morphology revealed does not readily lend itself to rigorous cyclic voltammetric analysis, because the superposition of peaks gives rise to difficulties with determining the base line for anodic and cathodic currents. However the morphology is generally similar to that previously noted for $MoCl_3$ and CO_3^{2-}. Table 6.2.1.1. indicates the effect of sweep rate on the peak potentials shown in Fig.6.2.1.1. and from this some trends can be noted, namely that the cathodic peak potentials, $E_p^c(1)$,$E_p^c(2)$,$E_p^c(3)$,$E_p^c(4)$ shift

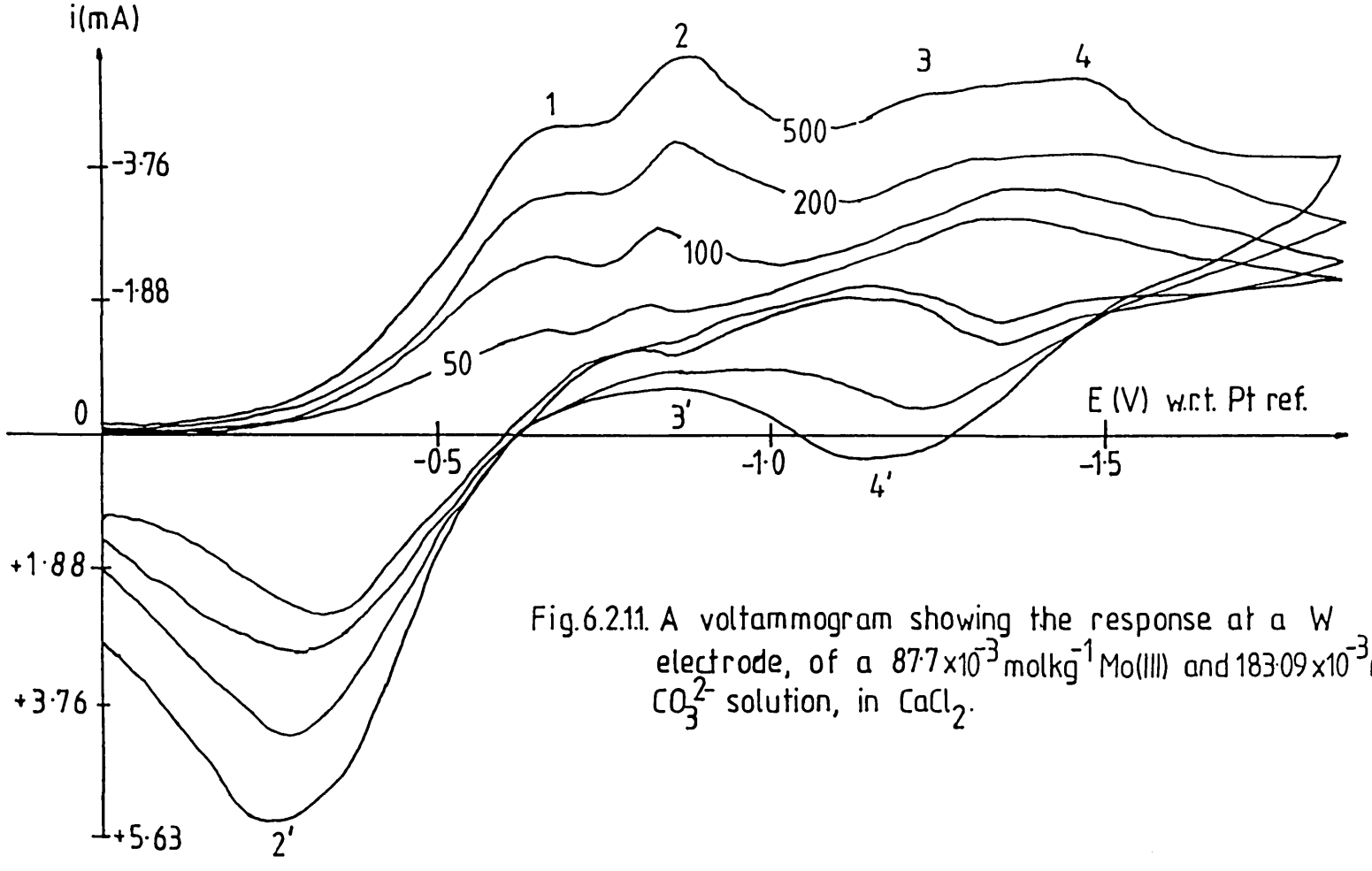

Fig.6.2.1.1. A voltammogram showing the response at a W electrode, of a $87{\cdot}7 \times 10^{-3}$ molkg^{-1} Mo(III) and $183{\cdot}09 \times 10^{-3}$ molkg^{-1} CO_3^{2-} solution, in $CaCl_2$.

cathodic with increasing sweep rate and $E_p^a(2')$,$E_p^c(3')$, $E_p^c(4')$ shift anodic with increasing sweep rate. Comparison of these data with those in table 5.2.1.1. and 4.2.1.1 and 4.2.2.2. show similarities for the Mo^{5+},Mo^{3+} monomer and dimer, and the O_2^{2-} and CO_3^{2-} peaks.

v (mV/s)	$E_p^c(1)$ (V)	$E_{pc}(2)$ (V)	$E_p^c(3)$ (V)	$E_p^c(4)$ (V)	$E_p^a(2')$ (V)	$E_p^a(3')$ (V)	$E_p^c(4')$ (V)
50	-0.62	-0.79	-1.04	-1.40	-0.34	-0.72	-1.36
100	-0.64	-0.82	-1.25	-1.45	-0.30	-0.75	-1.30
200	-0.64	-0.78	-1.10	-1.45	-0.38	-	-1.25
500	-0.67	-0.88	-1.25	-1.45	-0.25	-	-1.15

Table 6.2.1.1. VOLTAMMETRIC PARAMETERS FROM Fig 6.2.1.1.

Qualitatively the cyclic voltammogram, generated by similar concentrations for each solute, Fig.6.2.1.2., and the addition of these curves, yields a response very similar to that noted in Fig.6.2.1.1. Comparing these curves, reveals that the 3rd and 4th anodic peaks are merged in Fig.6.2.1.2., with a much smaller 3rd anodic peak than is expected. At this concentration for $MoCl_3$ in melts containing only $MoCl_3$ as a solute, the monomer peak was not observed.(3rd peak) The presence of this peak implies a shift in the equilbrium:-

$$Mo_2Cl_9^{3-} + 3Cl^- \rightleftharpoons 2MoCl_6^{3-}$$

in favour of the monomer and hence the ease by which reduction of Mo can occur. This shift may be due to the carbonate ion, as the acidity of the calcium ion may give rise to the favouring of the dimer in the absence of carbonate, but the basicity of this complex oxyanion, in comparison with chloride ions, will encourage calcium ions to "capture" them rather than the chloride ions and thus allow more "complexing" of the Mo and favouring of the monomer.

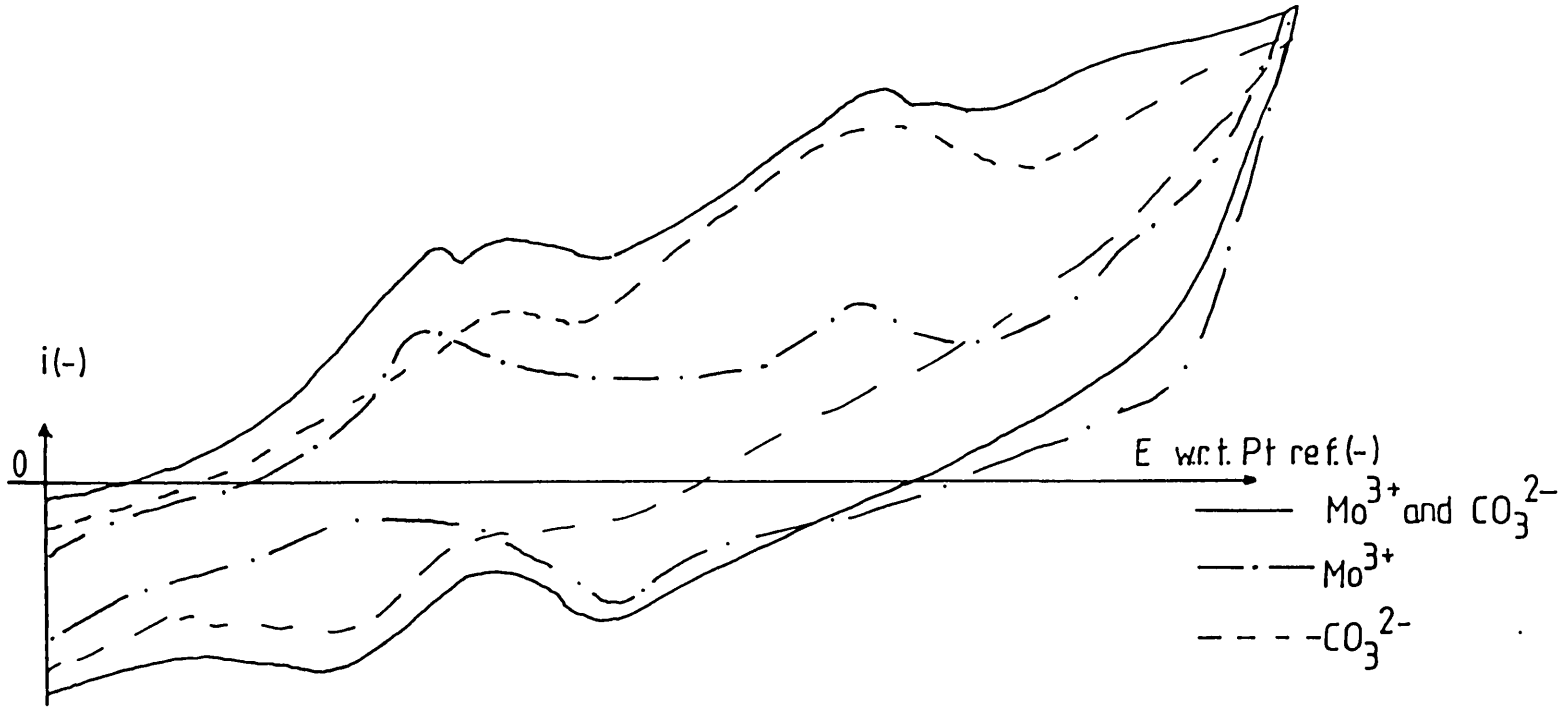

Fig.6.2.1.2. Voltammograms showing the responses for $53{\cdot}76 \times 10^{-3}$ molkg^{-1} soln. of Mo(III), a $183{\cdot}09 \times 10^{-3}$ molkg^{-1} soln. of CO_3^{2-} and the predicted sum of these two solutions, at a tungsten electrode, at 200 mVsec^{-1}.

Fig.6.2.1.3 shows the response for CO_3^{2-} and Mo^{3+} in solution at a Pt electrode. Comparison with Figs.4.2.1.11 and 5.2.1.9. shows that this response may approximate that for the addition of Mo^{3+} and CO_3^{2-} separately, as for the response at W.

6.2.2.Effect of concentration.

The variation of the concentration of CO_3^{2-} in comparison with the Mo^{3+} was studied in order to investigate, the possible effect on the acidity of the Ca^{2+} ion w.r.t. the Mo^{3+} ion. Fig.6.2.1.1. shows the response for a solution with a CO_3^{2-}conc./Mo^{3+}conc. of 2.09 and Fig.6.2.2.1. shows the response for a ratio of 0.75. The lower carbonate concentration gives rise to a relatively larger Mo^{5+} peak and the anodic peak correponding to the dimer reduction is enhanced. These effects are consistent with a change in the Mo^{3+} equilibrium so favouring the dimer at relatively lower carbonate concentrations. Less oxide and peroxide ions are generated by the decomposition of the carbonate and thus more chloride ions are required to complex the calcium ion, encouraging the formation of the dimer. The increased stability of the monomer at higher CO_3^{2-}conc./Mo^{3+}conc. ratios may also enhance the formation of $MoCl_5$ by disproportionation, but the observed peak is smaller for higher ratios. This effect may arise by the reaction of $MoCl_5$ with oxide and peroxide, generating volatile oxychlorides.

6.2.3.Effect of temperature.

At higher temperatures, 841^{o}C compared with 820^{o}C the response at W approaches that for carbonate alone. (Fig.6.2.3.1.) This effect is probably due to the loss of the unstable $MoCl_3$ species as volatile Mo(V) oxychlorides, this would leave only the dimer peak, which is obscured by the broad carbonate peak.

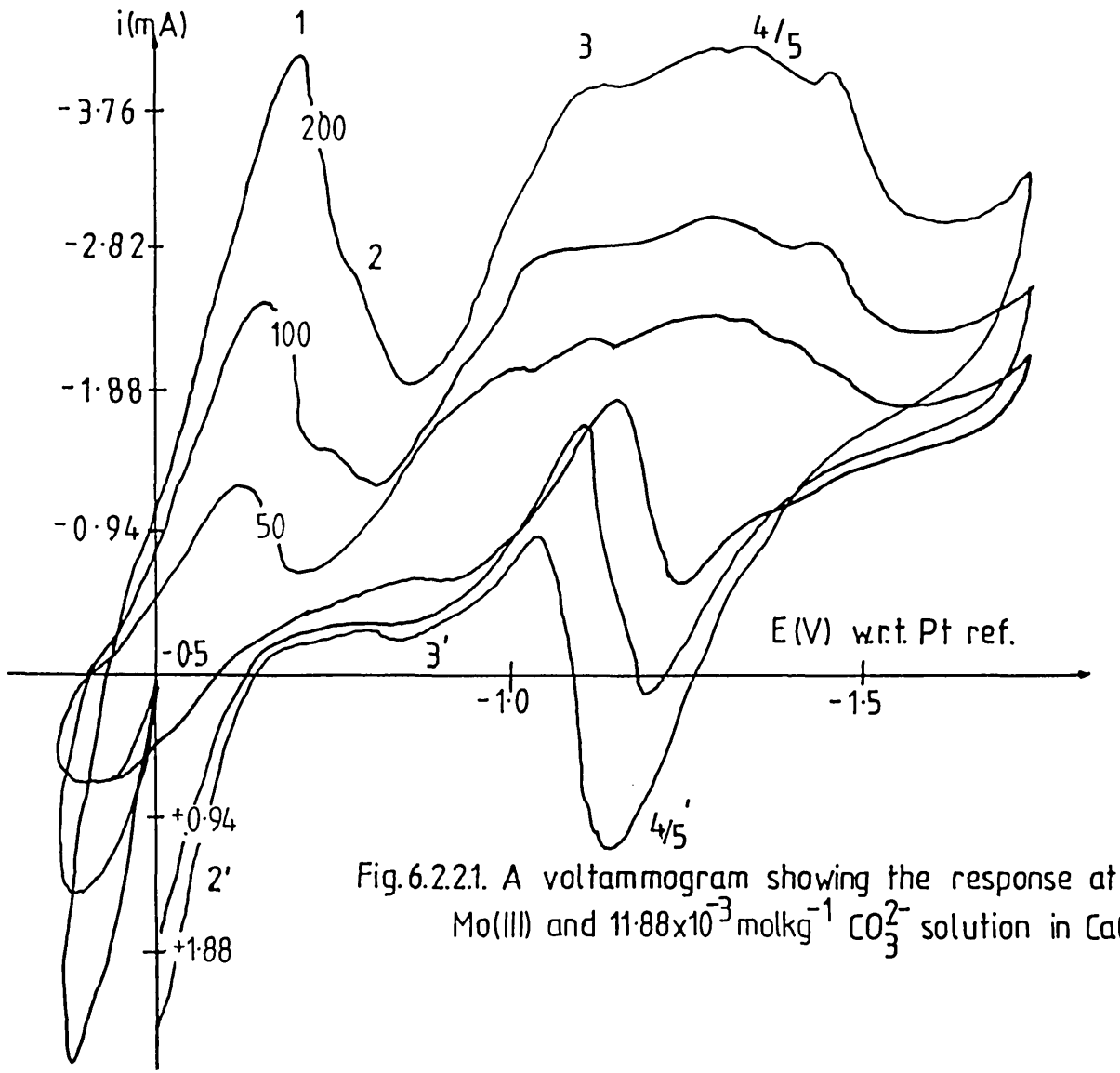

Fig. 6.2.2.1. A voltammogram showing the response at W, for a $16{\cdot}93\times10^{-3}$ molkg^{-1} Mo(III) and $11{\cdot}88\times10^{-3}$ molkg^{-1} CO_3^{2-} solution in $CaCl_2$.

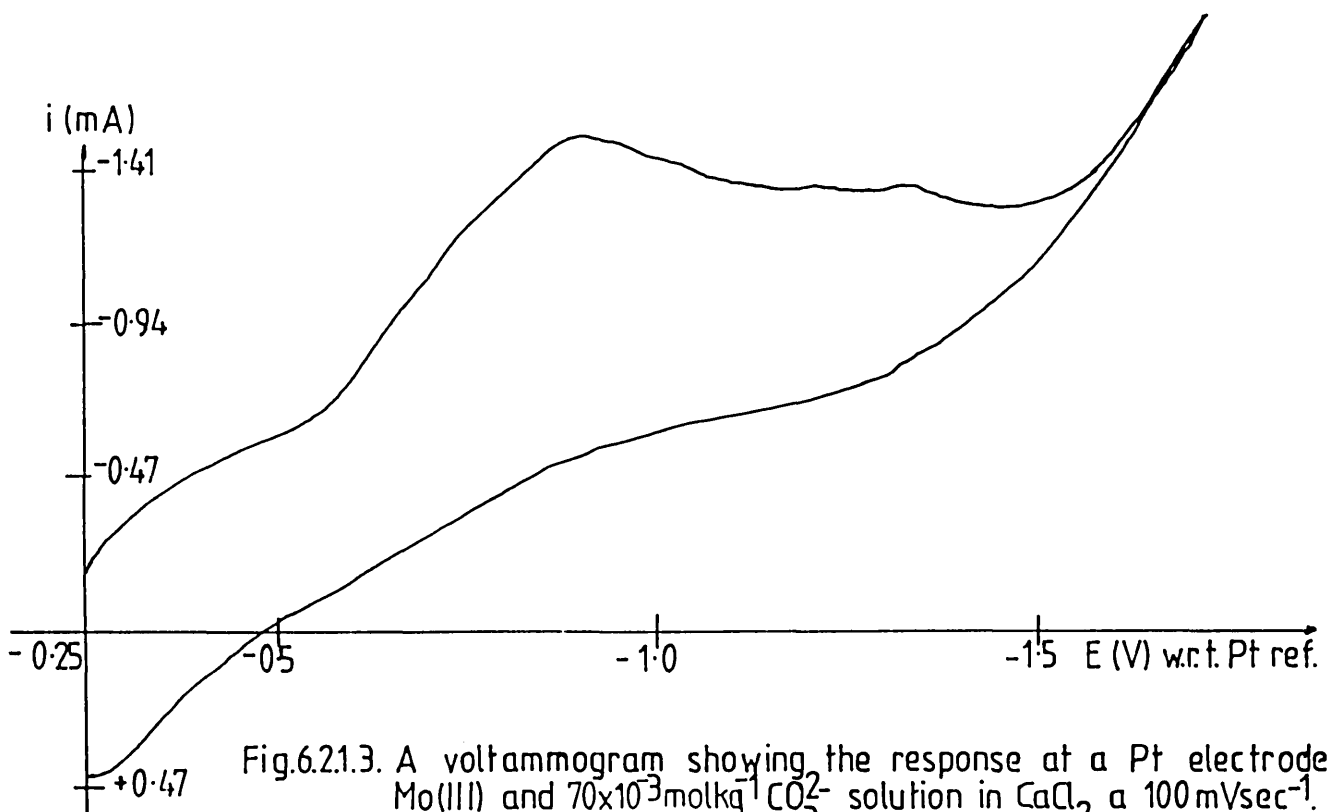

Fig.6.2.1.3. A voltammogram showing the response at a Pt electrode, for a $52{\cdot}14\times10^{-3}$ molkg^{-1} Mo(III) and 70×10^{-3}molkg^{-1} CO_3^{2-} solution in $CaCl_2$ a 100 mVsec^{-1}.

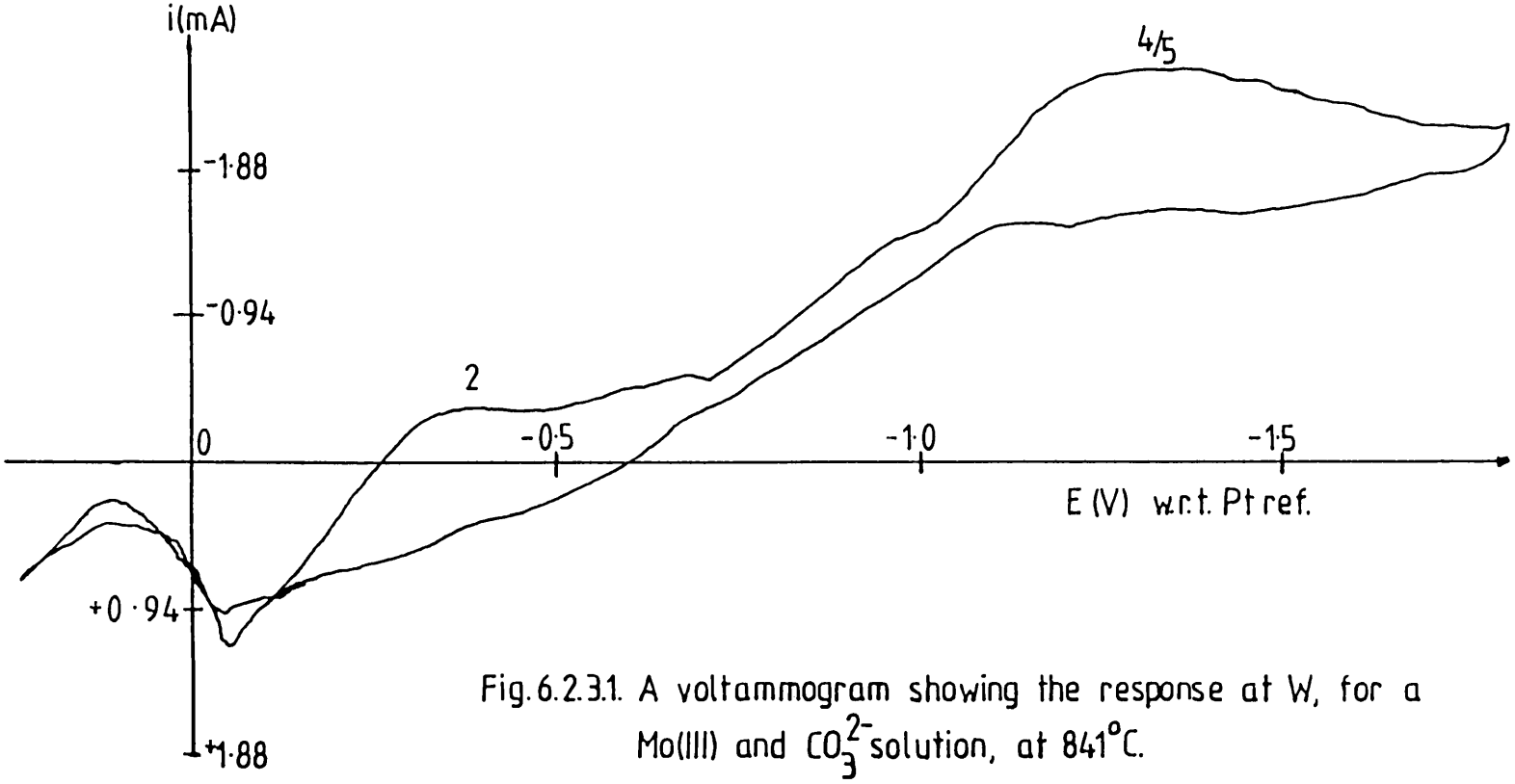

Fig. 6.2.3.1. A voltammogram showing the response at W, for a Mo(III) and CO_3^{2-} solution, at 841°C.

6.3.SUMMARY

The responses indicated in this chapter possibly show how the interaction of carbonate ions with molybdenum ions affects the electrochemistry of molybdenum in $CaCl_2$. The major factor appears to be the generation of O^{2-} and O_2^{2-} from the thermal decomposition of the carbonate ion, reducing the acidity of the Ca^{2+} ion in comparision with the Mo^{3+} ion. This increases the availability of Cl^- ions for complexing, favouring the monomer form of Mo^{3+}, when the $CaCO_3$ concentration exceeds that for $MoCl_3$. The formation of oxychlorides leads to the loss of volatile Mo^{5+} species. The complex response noted above and the possible relationships between cyclic voltammetric behaviour and the melt chemistry have been speculated. This can only be justified by the observed co-deposition of carbon and molybdenum for potentials more cathodic than -1.0 V.

7.ELETRODEPOSITION OF MOLYBDENUM AND CARBON

7.1.INTRODUCTION

In this chapter aspects of the formation of electrodeposits of molybdenum or carbon are considered. The type of electrochemical and nucleation processes for these reductions were investigated by chronoamperometry at tungsten and platinum electrodes for a range of overpotentials. Similarly the coatings produced at stainless steel coupon electrodes, for large overpotentials were examined by X-ray diffraction and scanning electron microscopy to determine the type of coating produced for various conditions.

7.2.CHRONOAMPEROMETRY

In order to obtain reproducible i-t transients for Mo and C deposition at low overpotentials, the electrode surface was initially cleaned by applying an anodic pulse compared to the equilibrium potential prior to the nucleation pulse. The equilibrium potential for the couple Mo(III)/Mo)(0), was taken as -0.6V w.r.t. Pt quasi ref. at 824^{o}C in this melt, using the cyclic voltammetric parameters indicated in chapter 4. A wave form shown in Fig.7.2. was applied to the working electrode. The rest potential allows the electrode to reach equilibrium without the reduction process proceeding.(135) After this nucleation pulse, another cleaning pulse was applied to help stop alloy formation.

Fig.7.2 Waveform applied for chronoamperometry.

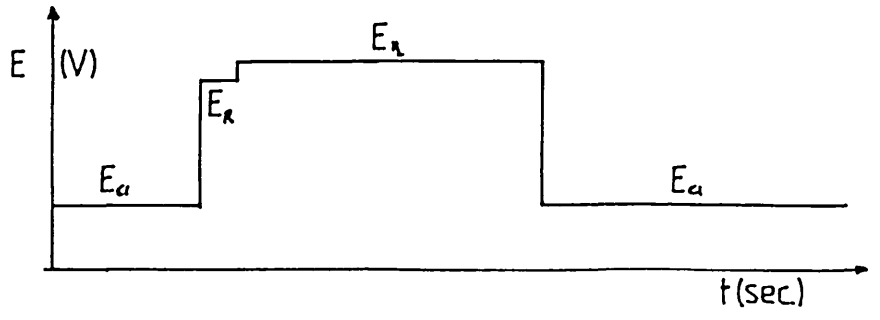

For carbon deposition the irreversiblity of this process does not allow an equilibrium potential to be determined and a cleaning pulse does not remove the deposit. Freshly polished eletrodes were used for each new overpotential.

7.2.1.Characteristics of the i-t transients developed for molybdenum deposits.

The involvement of a well defined nucleation stage in the formation of molybdenum electrodeposits is revealed in the potentiostatic i-t transients obtained for different overpotentials. Instead of a typical current decay according to $t^{-1/2}$, as expected for a diffusion controlled process,the response shows a rising current region.Fig.7.2.1.1 shows the more complex response. After an initial high current peak corresponding to double layer charging, the current decays and then increases again, before decaying according to a $t^{-1/2}$ dependence. The rising current region corresponds to the formation of stable nuclei, which becomes arrested when the diffusional zones around each nucleus overlap and for further growth diffusion from the bulk electrolyte is required.

These curves are dependent upon the overpotential as might be expected, due to the dependency of nucleation on overpotential.(section 1.3.) The rising sections of these curves were analysed to give detail of the nature of the nucleation process occuring. Plots of log i vs log t for transients obtained at a tungsten electrode for a $MoCl_3$ concentration of 7.28 $x10^{-3}molkg^{-1}$ are shown in Fig.7.2.1.2. yielding a gradient of 3/2 for each potential. From the theory noted in section 1.4.2., this slope corresponds to simultaneous formation and growth of nuclei. Fig.7.2.1.3. shows this relationship and reveals that for larger overpotentials the gradients become greater, indicating the more favoured nucelation at these potentials. At longer times this relationship tends to

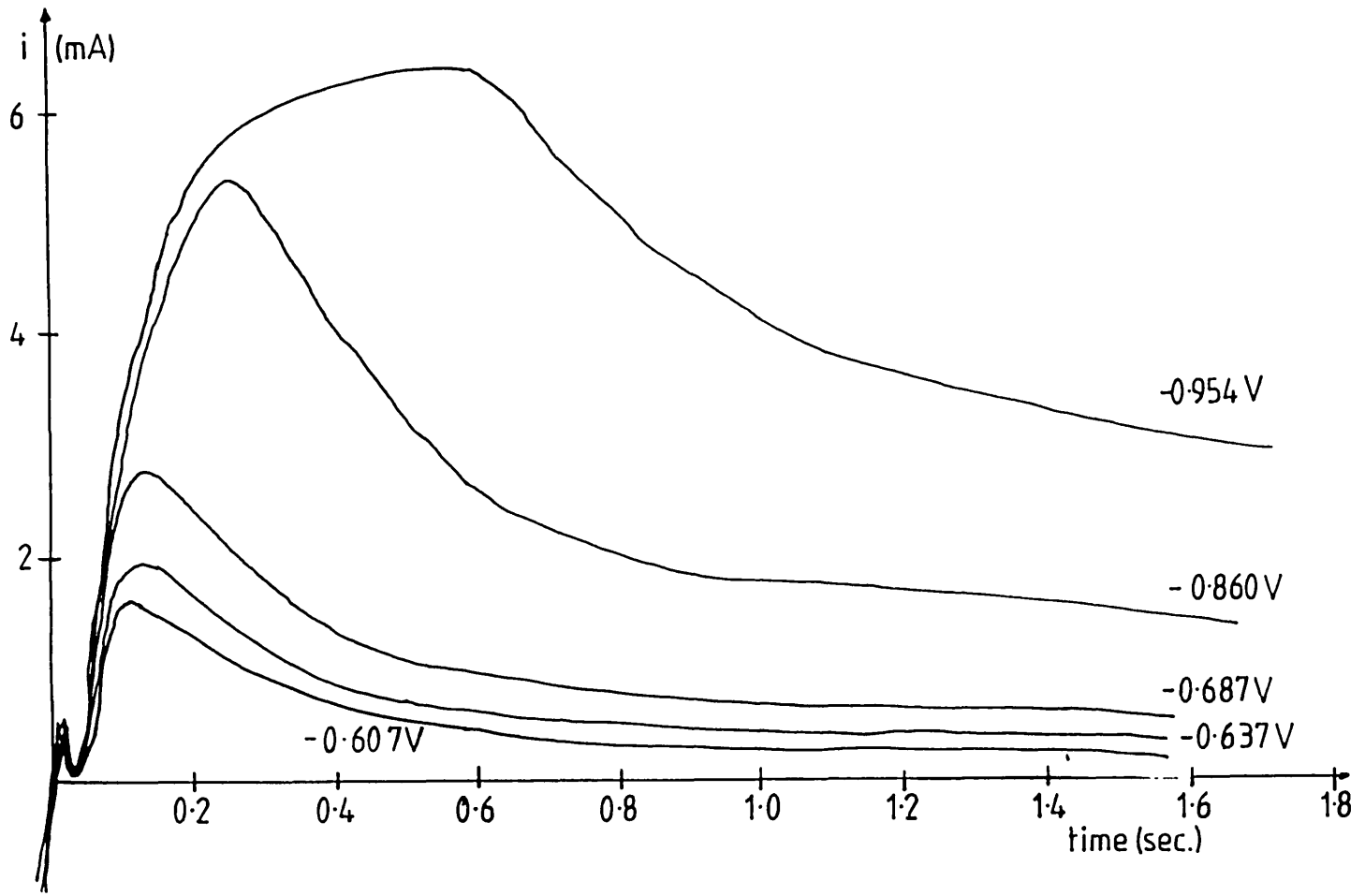

Fig. 7.2.1.1. i-t potentiostatic transients for the electrodeposition of Molybdenum at tungsten, from a $7{\cdot}28 \times 10^{-3}$ molkg^{-1} soln. of $MoCl_6^{3-}$.

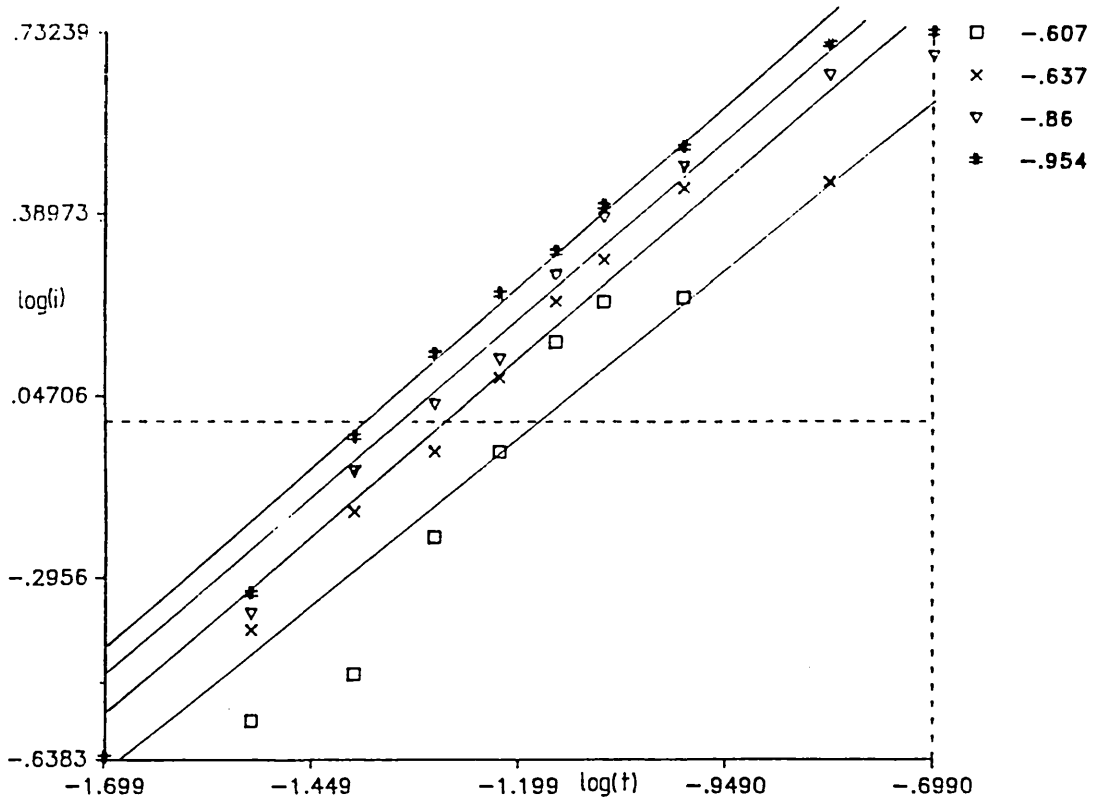

Fig.7.2.1.2. Plots of log i vs log t, for the rising current region corresponding to Mo deposition at W.

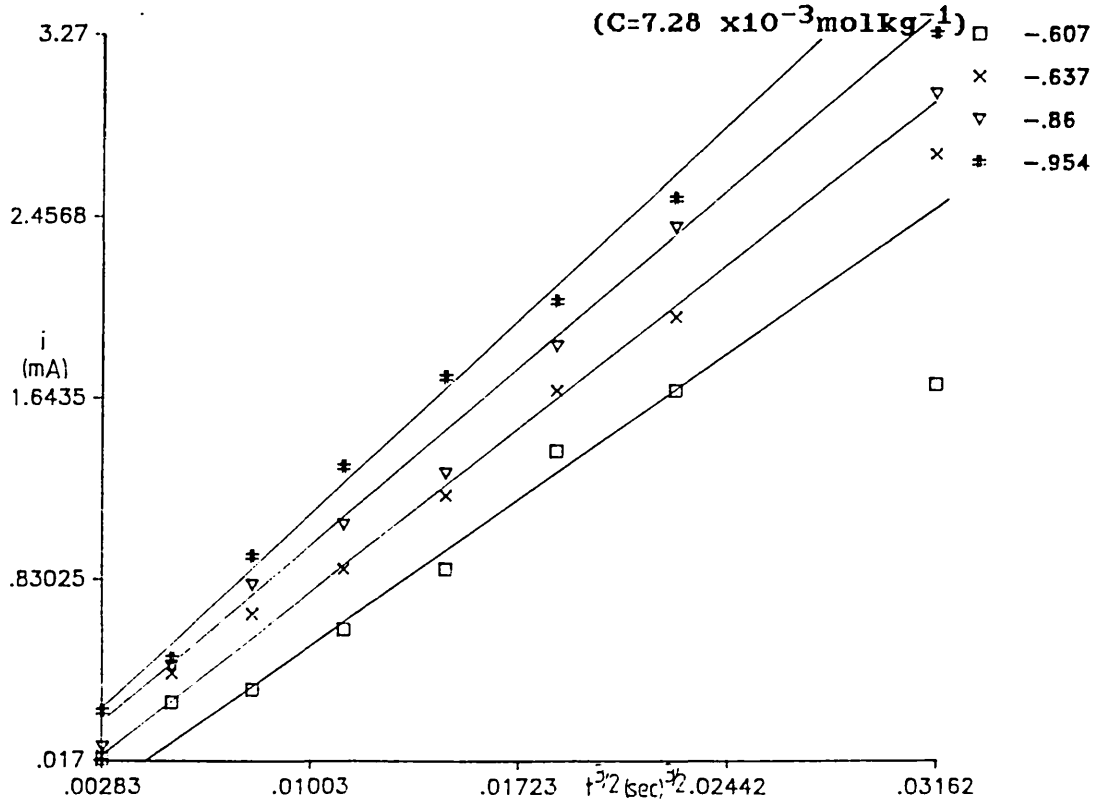

Fig.7.2.1.3. Plots of i vs $t^{3/2}$, for the rising current region corresponding to Mo deposition at W. (C=7.28 x10^{-3}molkg^{-1})

$t^{1/2}$ coresponding to growth of the nuclei. After the rising current stage, the current decays according to $t^{1/2}$ shown in Fig.7.2.1.4. Similar responses for the rising and falling sections of the curves are found for a 28.7 $x10^{-3}$ $molkg^{-1}$ solution of $MoCl_3$ at a tungsten electrode. (Figs.7.2.1.5-7.2.1.9). At a Pt electrode the same effects are observed.(Figs.7.2.1.10-7.2.1.12)

7.2.2.Characteristics of the i-t transients developed for carbon deposits.

The potentiostatic transients produced for carbon deposition revealed no rising current region.(Fig.7.2.2.1) After the initial sharp rise in current corresponding to the double layer charging, then a decaying current is observed. The overpotential scales the response, but does not alter its shape, which may be due to the charge transfer process being slow and should reveal a $t^{-1/2}$ decay for short times. Figs.7.2.2.2. and 7.2.2.3. show this dependence. This relationship does not hold at long times, again indicating the irreversiblity of the charge transfer process.(section 1.4.2.) This lack of nucleation phenomena indicates the irreversiblity that might be expected for the reduction of an oxyanion.

7.3.CHARACTERISTICS OF MOLYBDENUM AND CARBON DEPOSITED ON STAINLESS STEEL SUBSTRATES.

As the most versatile and widely used bulk metal, stainless steel, offers a good combination of properties for unit cost. But in situations requiring high wear resistance, surface treatments are used, to keep cost low, but achieve the required characteristics.(e.g. drill bits) Thus the deposition of molybdenum and carbon on to this metal was investigated, rather than on to "inert" metals W,Pt, used for cyclic voltammetry and chronoamperometry. Stainless steel was not used in these experiments as the oxidation potential for iron is very cathodic(-1.0 V)to that for the reduction of $MoCl_6^{3-}$,Mo^{5+}

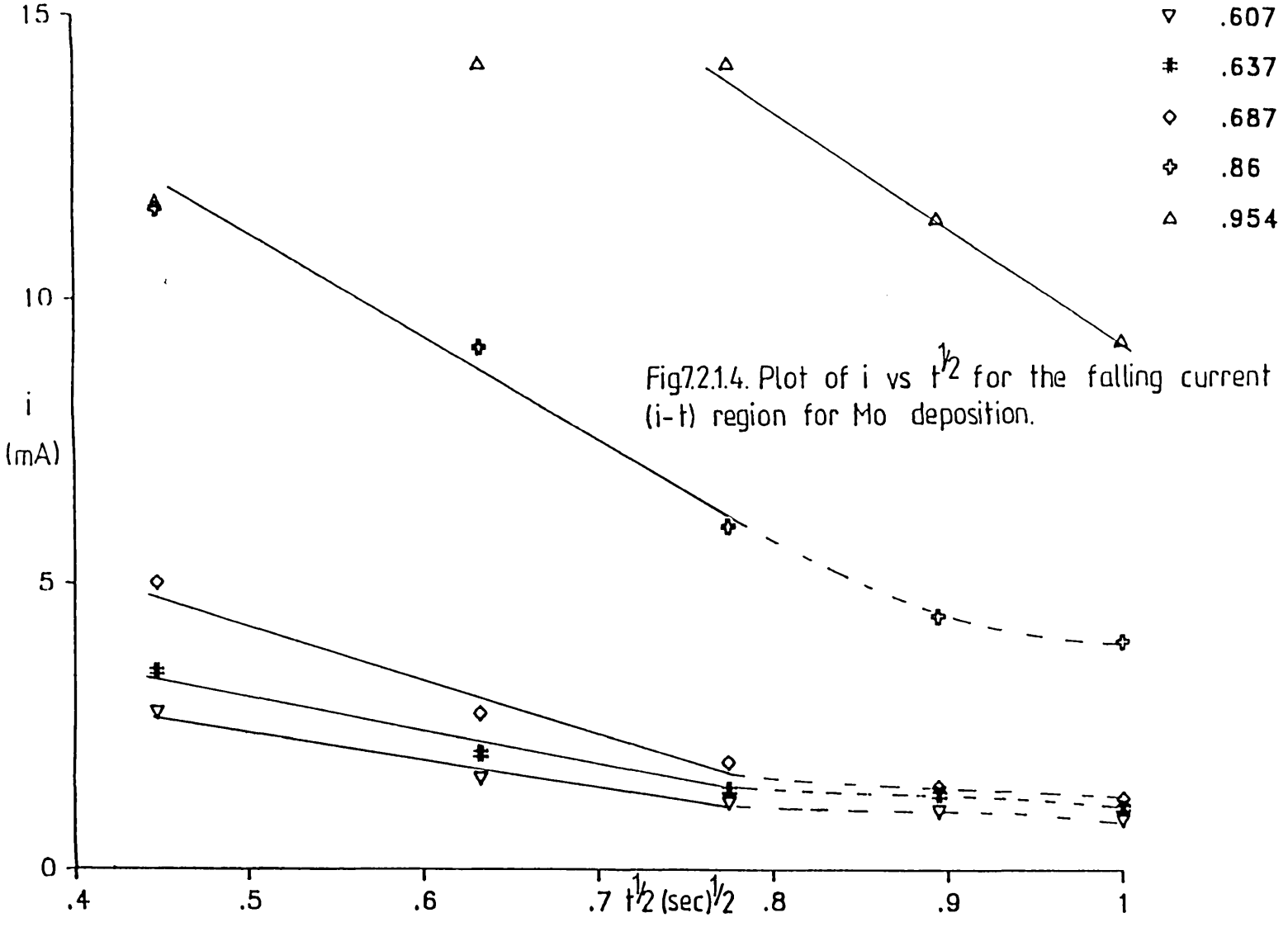

Fig.7.2.1.4. Plot of i vs $t^{1/2}$ for the falling current (i-t) region for Mo deposition.

Fig.7.2.15. i-t potentiostatic transients for the electrodeposition of molybdenum at tungsten, from a $28{\cdot}7 \times 10^{-3}$ molkg^{-1} soln. of $MoCl_6^{3-}$.

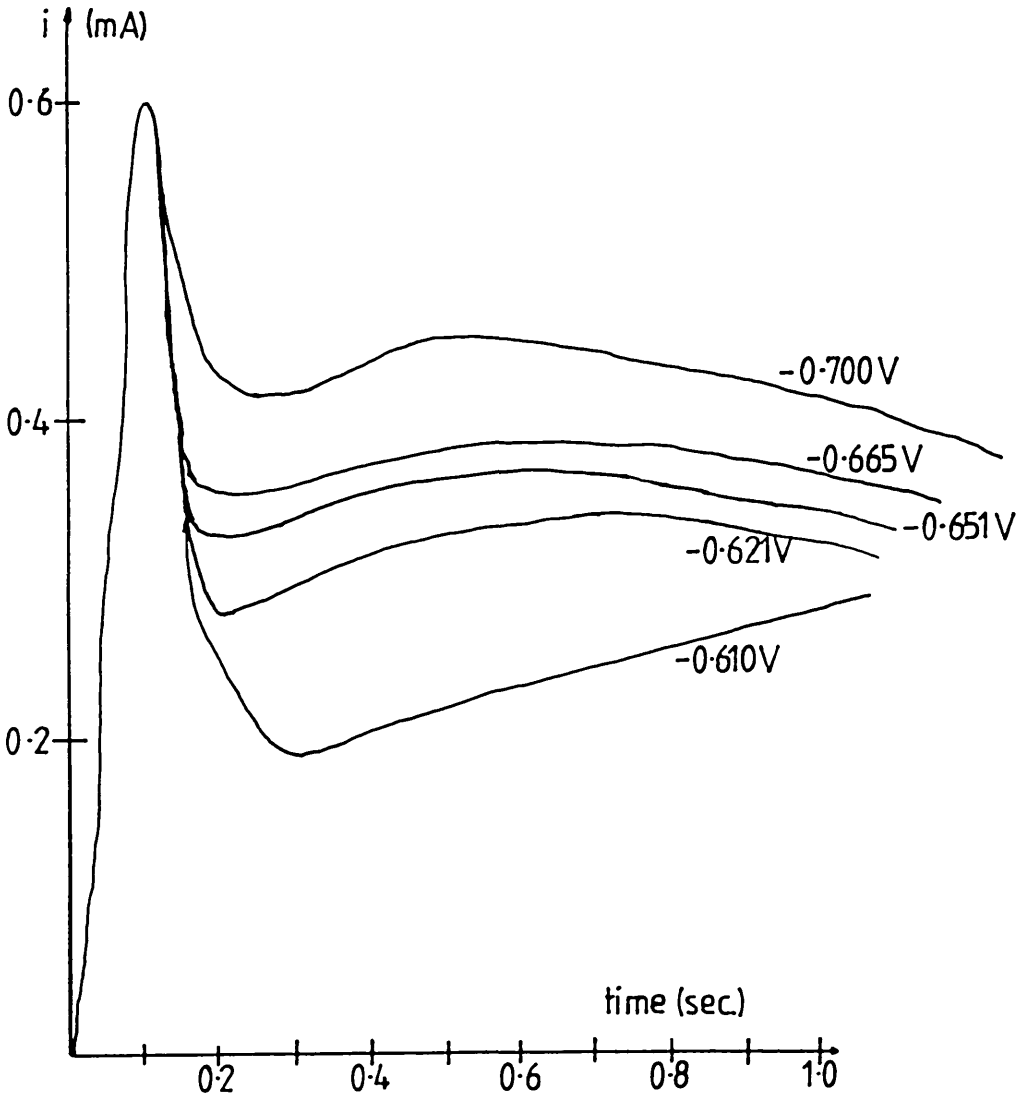

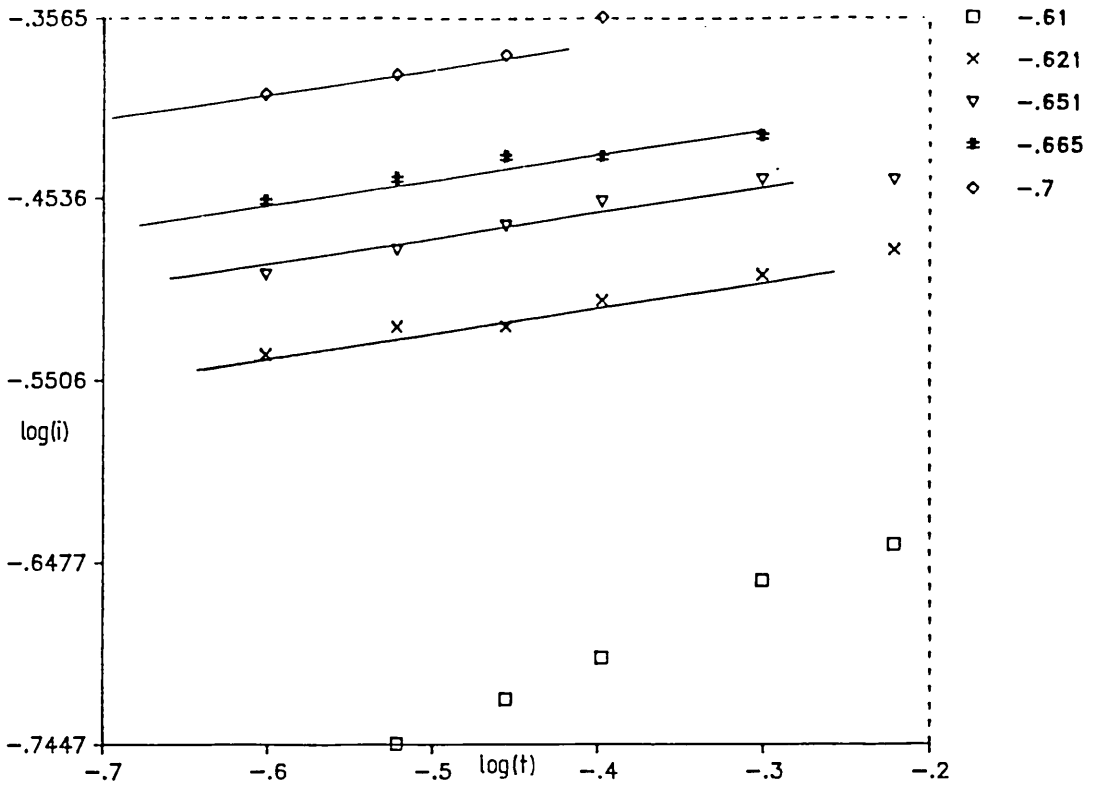

Fig.7.2.1.6. Plots of log i vs log t, for the rising current region corresponding to Mo deposition at W.

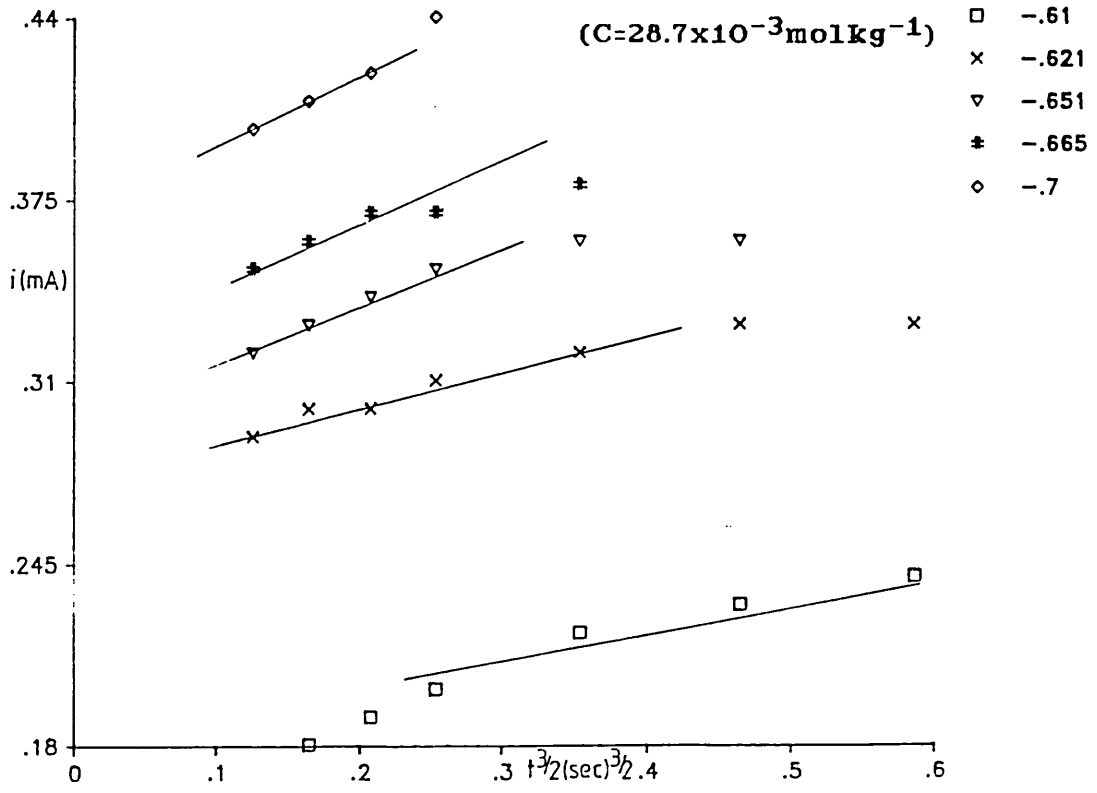

Fig.7.2.1.7. Plots of i vs $t^{3/2}$, for the rising current region corresponding to Mo deposition at W. ($C=28.7\times10^{-3}molkg^{-1}$)

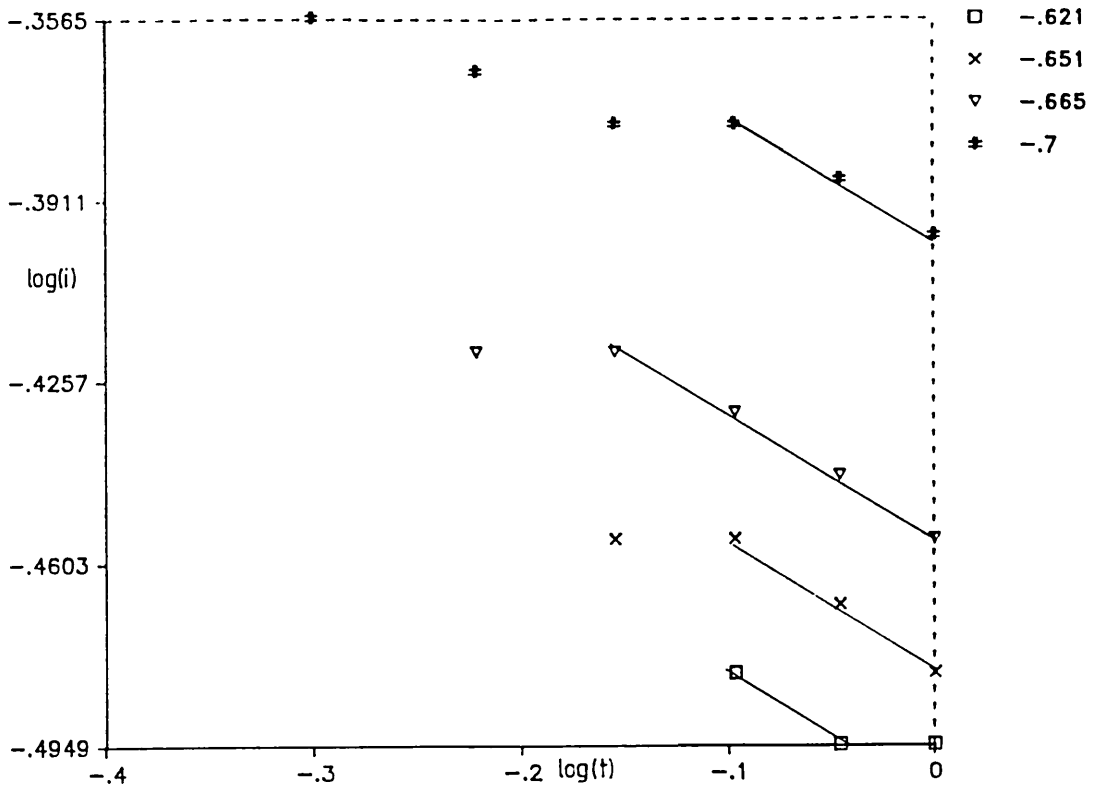

Fig.7.2.1.8. Plots of log i vs log t, for the falling current region corresponding to Mo deposition at W. ($C=28.7x10^{-3}molkg^{-1}$)

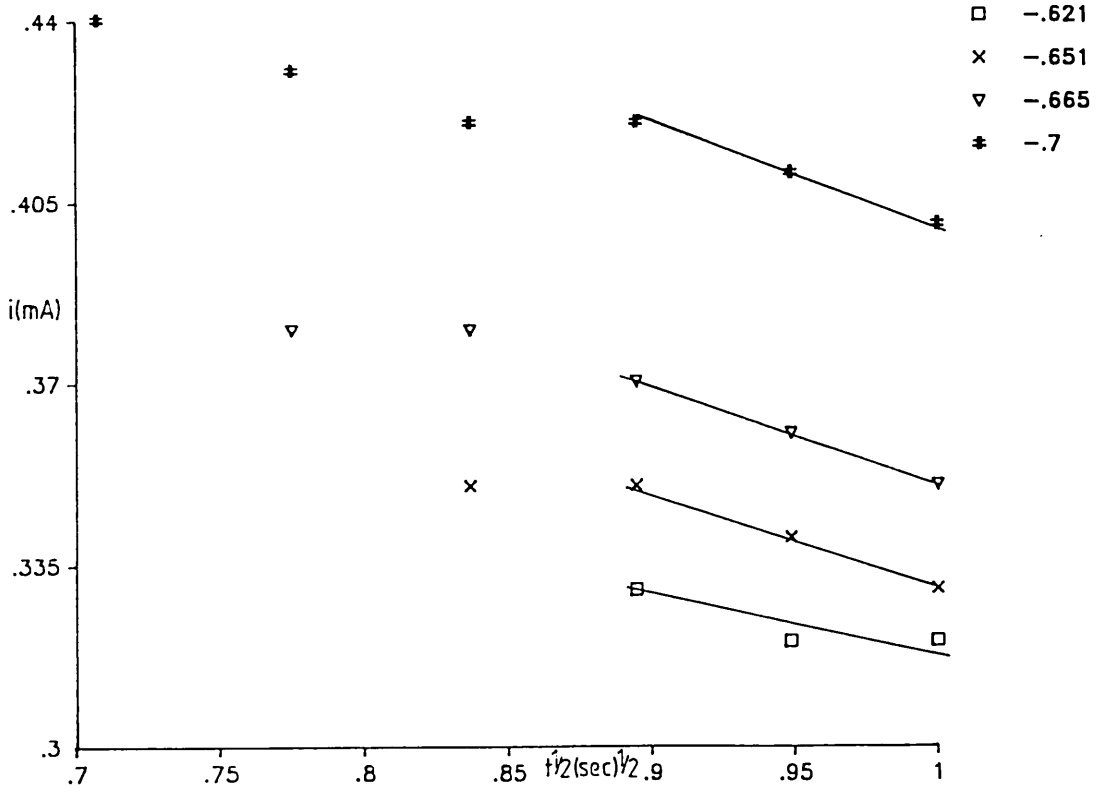

Fig.7.2.1.9. Plots of i vs $t^{1/2}$, for the falling current region corresponding to Mo deposition at W. ($C=28.7x10^{-3}molkg^{-1}$)

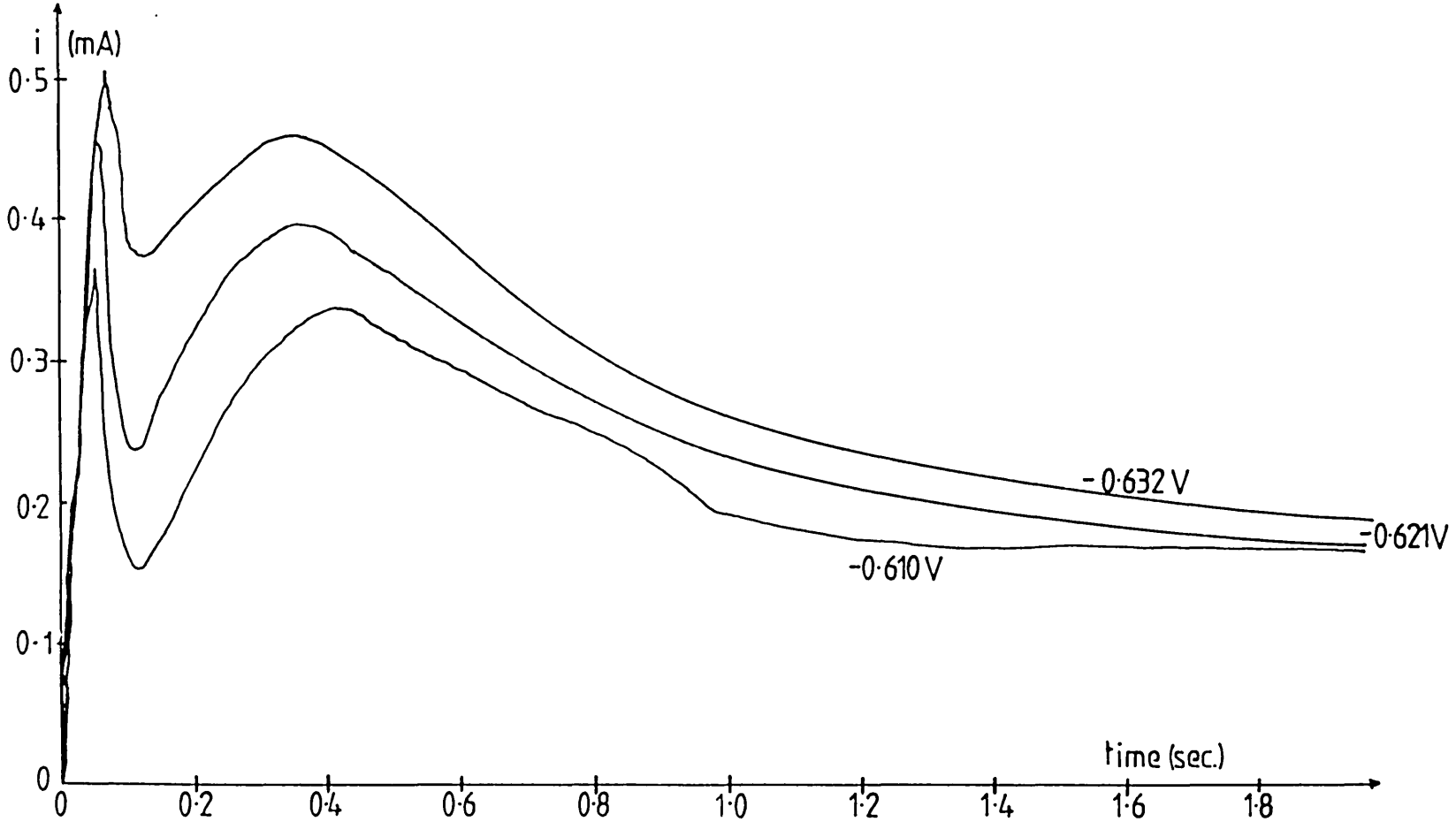

Fig.7.2.1.10. i-t potentiostatic transients for the electrodeposition of Molybdenum at platinum

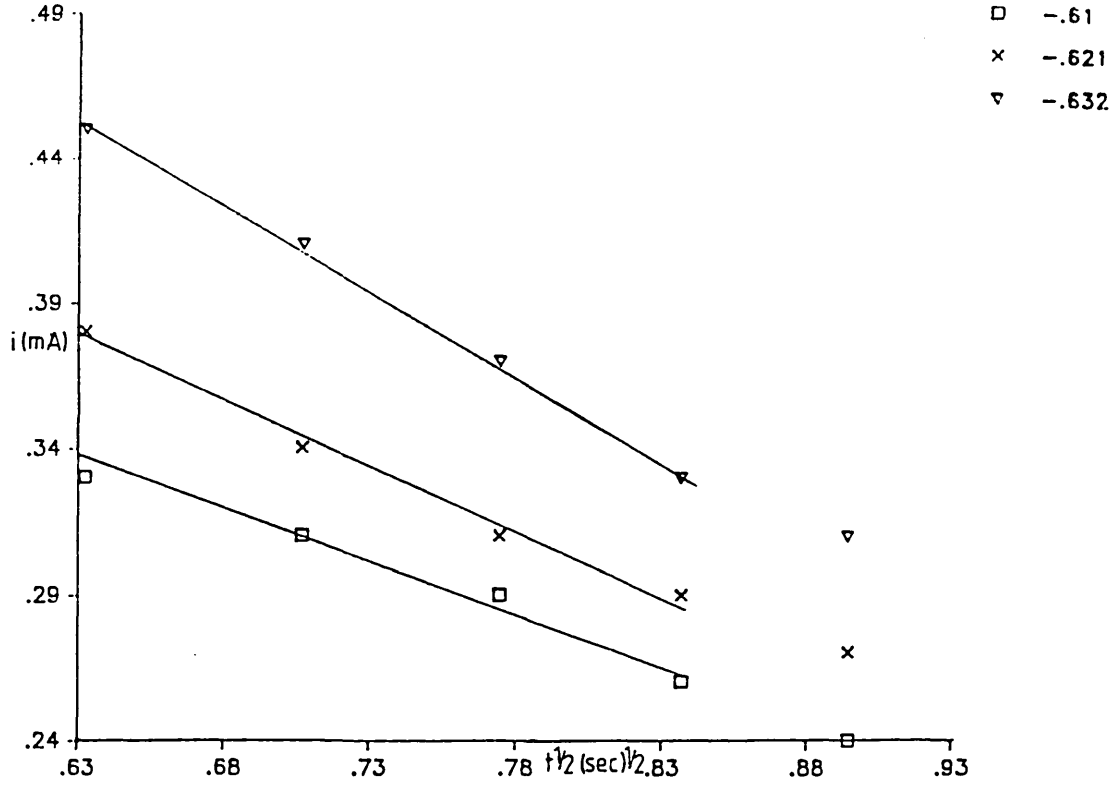

Fig.7.2.1.11.Plots of i vs t^2 for the falling current region corresponding to Mo deposition at Pt.

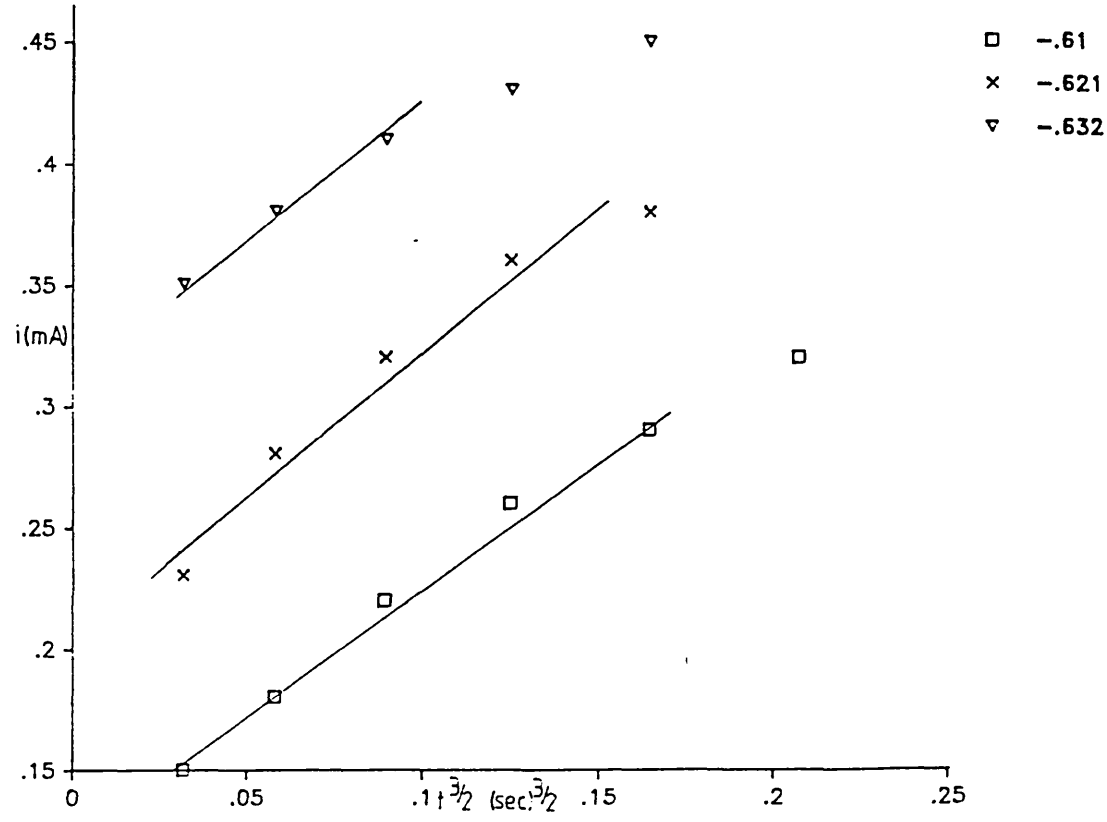

Fig.7.2.1.12.Plots of i vs $t^{3/2}$ for the rising current region corresponding to Mo deposition at Pt.

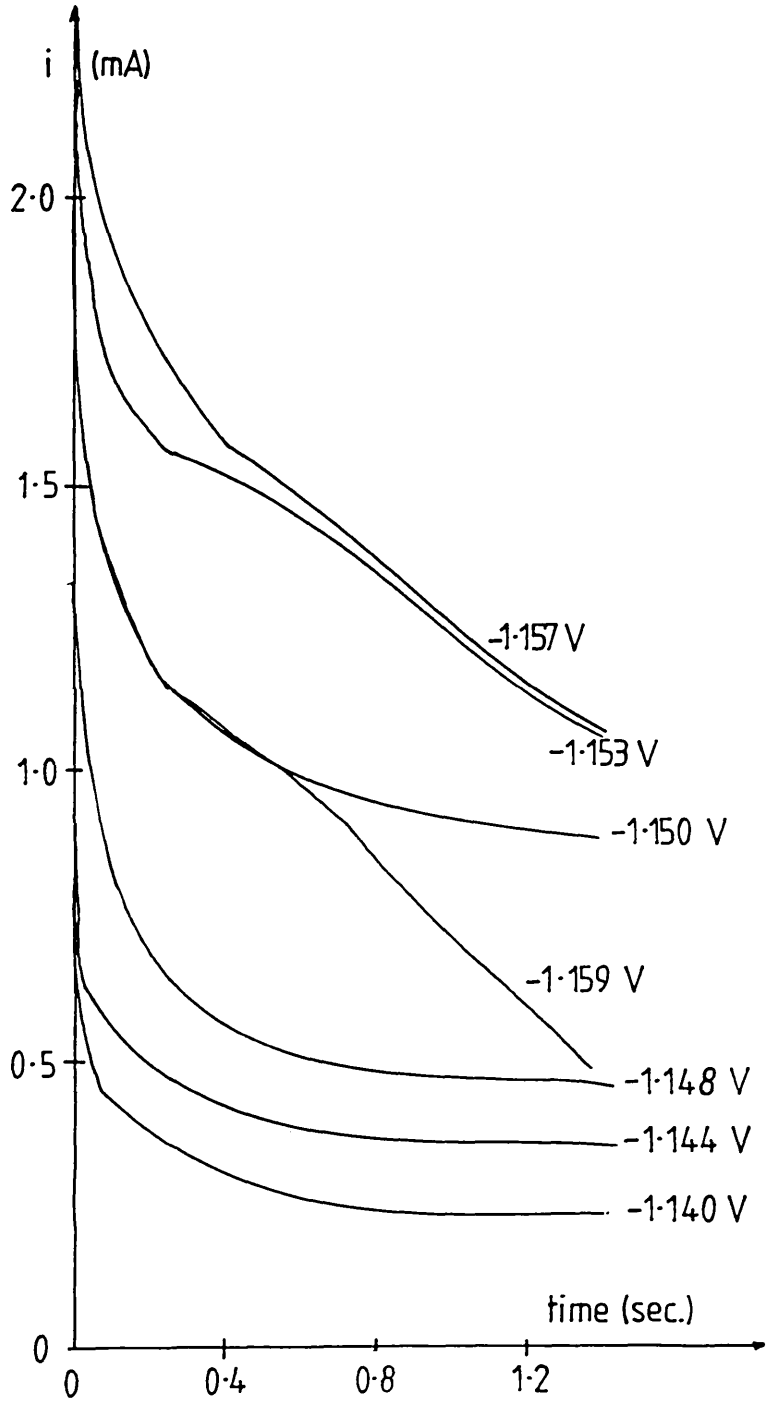

Fig.7.2.21. i-t potentiostatic transients for the electrodeposition of carbon at tungsten.

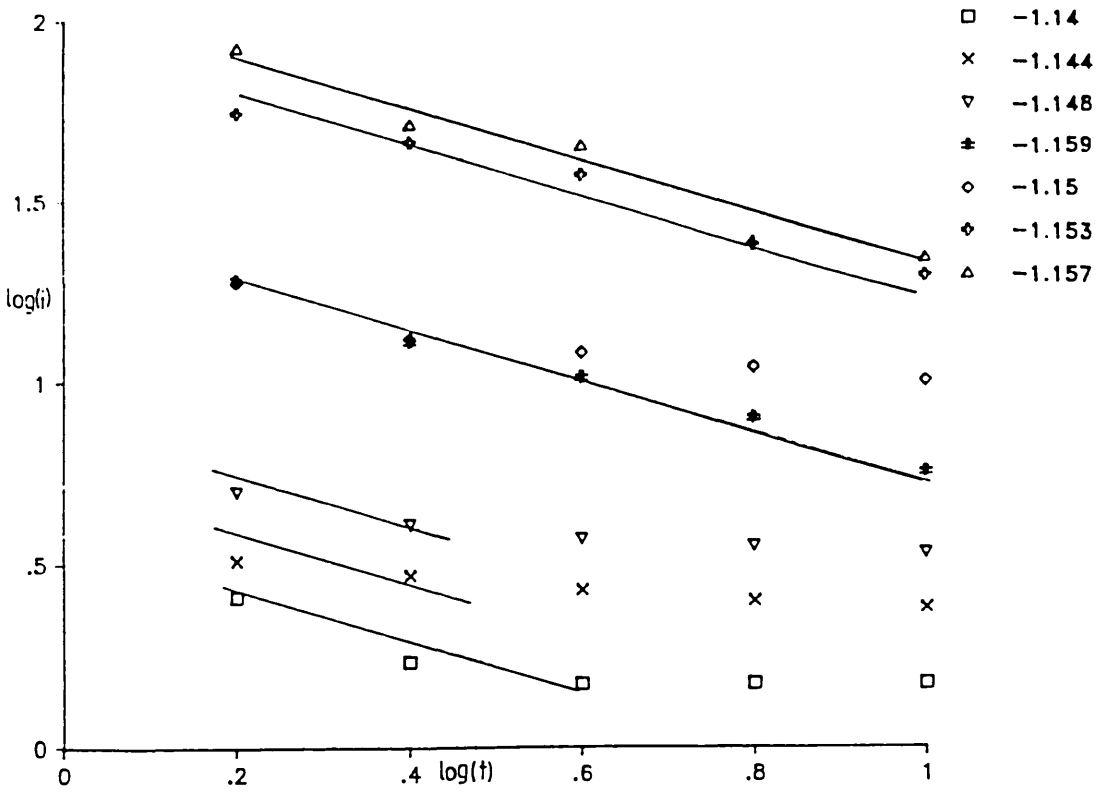

Fig.7.2.2.2.Plots of logi vs logt for the falling current region corresponding to carbon deposition at W.

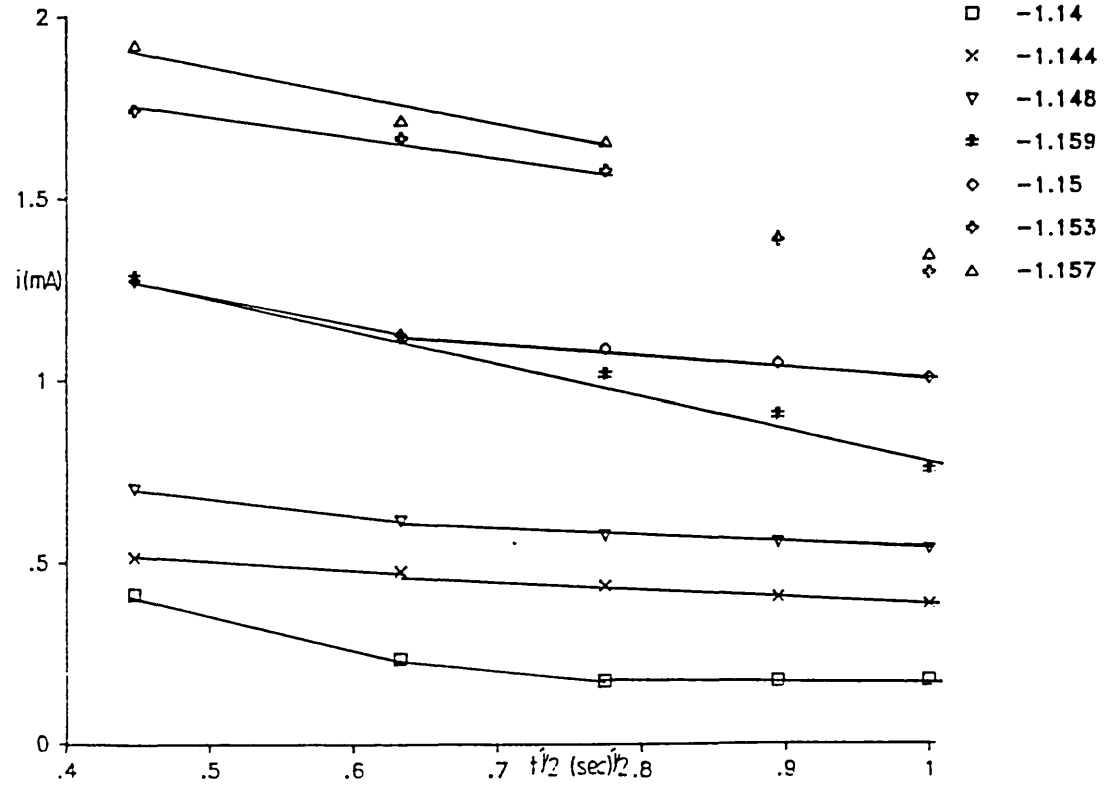

Fig.7.2.2.3.Plots of i vs $t^{1/2}$ for the rising current region corresponding to carbon deposition at W.

and O_2^{2-} and would not have allowed the investigation of these processes. In order to cathodically protect the stainless steel large overpotentials for Mo deposition are required. Unfortunately chronoanperometry at large overpotentials, does not yield information about the formation of nuclei. Deposition of carbon and molybdenum was achieved at stainless steel electrodes by constant potential electrolysis for a range of potentials greater than -1.0 V wrt. Pt ref.

7.3.1.Characteristics of molybdenum deposits on stainless steel substrates.

Molybdenum electrodeposits have been produced at potentials from -1.0 to -1.6 V wrt. Pt ref., for various times by constant potential electrolysis. A typical set of coatings are shown in Fig.7.3.1.1, for potentials -1.6,-1.4,-1.3 and -1.1 V. The $MoCl_6^{3-}$ concentration of the solutions used varied from 20 to 88 $x10^{-3}molkg^{-1}$, but this did not appear to affect the morphology of the coatings or their chemical composition, only the overpotential and deposition time appear to affect these properties. There is a progression in the morphology developed. Large spherical particles are formed at high overpotentials, decreasing in size and forming rippled layers as the overpotential is decreased. The thickness of the coating increases with increasing deposition time.

As was noted in section 7.2.1., at potentials from -0.607 to -0.954 the nucleation of Mo at W and Pt occurs by simultaneous nucleation and growth. As the potential increases, these processes are expected to occur similarly, but the number of nuclei formed and thus beginning to grow at a particular instant will be higher for a higher overpotential. This may account for the change in surface morphology noted when changing the overpotential from -400mV to -1000mV, when the surface becomes progressively less rippled (136). At higher overpotentials more sites are favoured for nucleation and thus more even surfaces are observed. At -400mV the

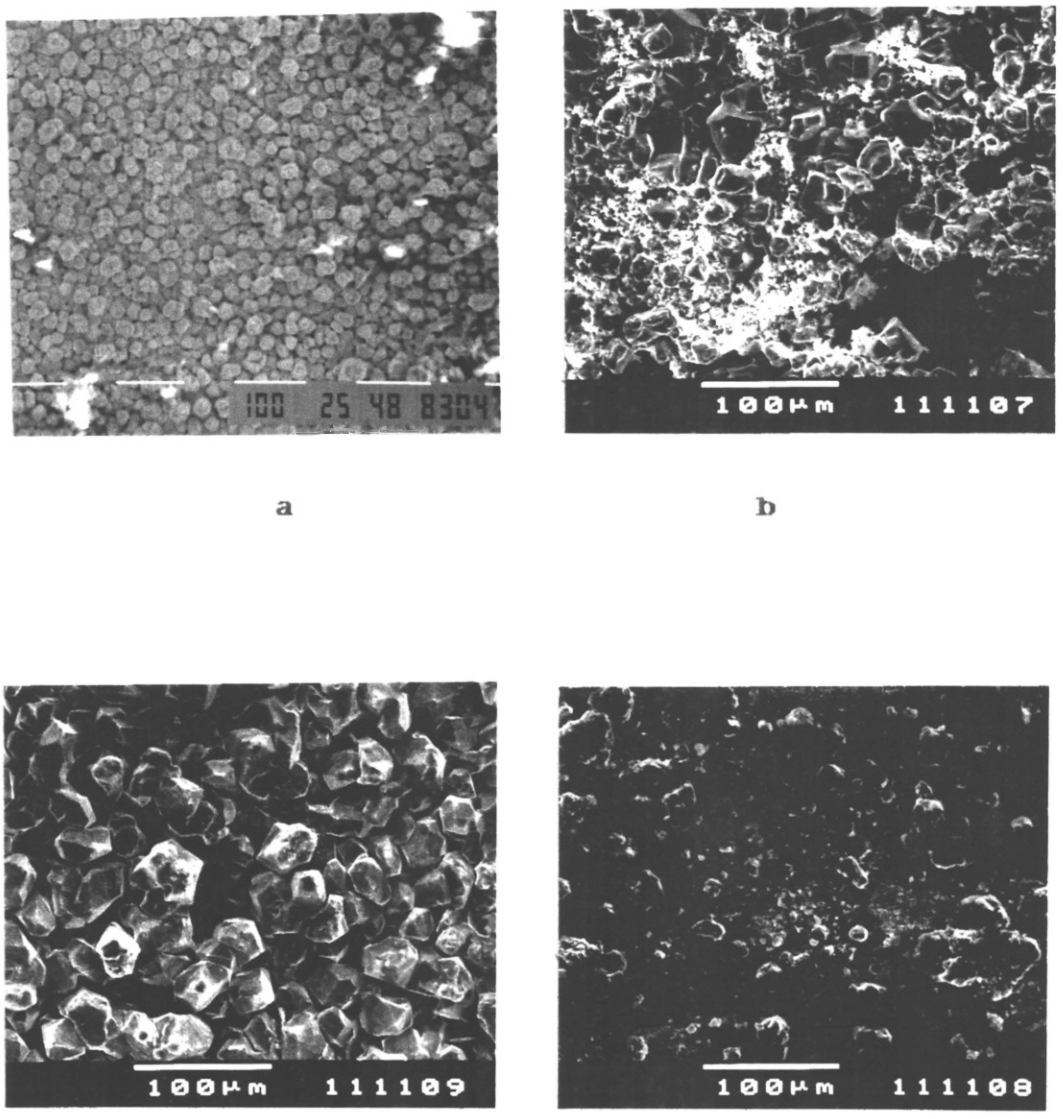

a b

c d

Fig.7.3.1.1. Molybdenum coatings deposited on stainless steel for deposition potentials and times:- a) -1.6 V for 45 mins. b) -1.4 V for 36 mins c) -1.3 V for 1.5 hours. d) -1.1 V for 15 mins.

overpotential is still sufficiently large to give the conditions for mass transfer controlled growth of the coating, this encourages the development of unstable growth.(11) Thus a coherent layer of nuclei is not formed, despite the good coverage caused by many nucleation sites.

X-ray diffraction of the coatings revealed their chemical composition. A general trend was noted, for increasing overpotentials compounds become increasingly rich in Mo. Table 7.3.1.1. summarises the phases found for various potentials and deposition times. For the longer times, the coating is richer in Mo (Fe_2Mo from Fe_3Mo), noting (4) and (5) at the same potential. At these longer times the presence of occluded melt is noted by the presence of $CaCl_2.2H_2O$ as a phase. These time effects are probably due to the increased amount of Mo deposited and also the interdiffusion of Fe and Mo, which occurs rapidly at these temperatures.

	potential (V) wrt Pt	time (mins.)	phases present
1	-1.0	21	Ni-Cr-Fe(substrate) FeMo
2	-1.5	38	Ni-Cr-Fe Cr-Fe-Mo-Ni Fe_2Mo
3	-1.6	45	Ni-Cr-Fe $Mo_5Cr_6Fe_{18}$ FeMo Mo
4	-1.3	10	Ni-Cr-Fe Fe_3Mo
5	-1.3	92	Ni-Cr-Fe Fe_2Mo $CaCl_2.2H_2O$

Table 7.3.1.1. PHASES FOUND BY X.R.D.FOR DIFFERENT Mo DEPOSITION CONDITIONS

Closer scanning electron microscopy of a deposit produced at -1.6 V for 45 mins. revealed the formation of an initial layer on the surface (shown in Fig.7.3.1.2.a) with the unstable growth developing above.(b) Insitu energy dispersive X-ray analysis of this coating revealed Mo,Ca Cl^- and substrate peaks(c). X-ray analysis gave the pattern indicated in Table 7.3.1.2.
These peaks reveal the expected occluded $CaCl_2$ as $CaCl_2.4/6H_2O$ and various Mo compounds and also Mo itself. The development of increasingly rich Mo alloys at the growing interface may be envisaged, when considering the simultaneous deposition of Mo and substrate elements and Mo diffusion.

7.3.2.Characteristics of carbon deposits on stainless steel substrates.

Carbon electrodeposits have been produced at potentials from -1.1 V to -1.9 V wrt. Pt for various deposition times by constant potential electrolysis. A typical set of coatings is shown in Fig.7.3.2.1. The carbonate concentration of the solutions used varied from 12 to 184 $x10^{-3}molkg^{-1}$, but as with Mo, this does not appear to affect the morphology or chemical composition of the coating significantly. The effect of overpotential and deposition time can be seen in Fig.7.3.2.1. Thicker coatings are produced for longer times, but the fine powdery surfaces produced are similar(Figs.7.3.2.1.a,b). At higher overpotentials a much rougher and rippled surface is formed.(Fig.7.3.2.1.c).

The large overpotential used for this deposition(c), is likely to give rise to rapid nucleation and good coverage, but unstable growth from these nuclei. For lower potentials (a) the coverage is poorer but a more coherent deposit is produced as more stable growth can occur at this potential.

X-ray diffraction of these coatings revealed substrate peaks, carbon, iron carbide and hydrated $CaCl_2$.

a

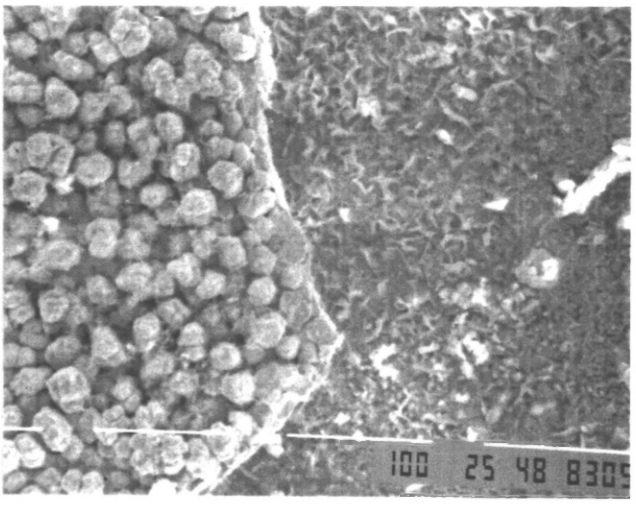

b

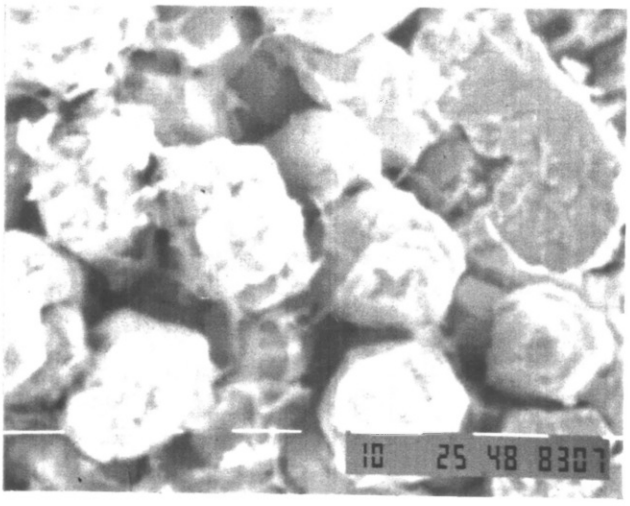

c

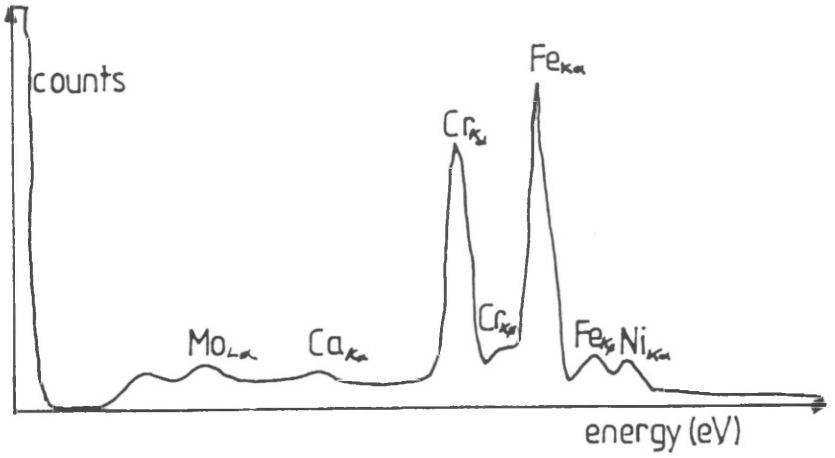

Fig.7.3.1.1. Molybdenum coating deposited on stainless steel at -1.6 V for 45 mins. a) intial coating layer, b) coating detail, c) E.D.A.X. analysis.

d values

sample	Ni-Cr-Fe	Ni-Cr-Fe	Fe_3Mo	Fe_2Mo	FeMo	$Mo_5Cr_6Fe_{18}$	$CaCl_2.6H_2O$	$CaCl_2.4H_2O$
5.51_{30}							5.87_{91}	
4.30_{12}					4.25_2			4.60_{100}
4.00_{20}							3.93_{90}	
3.90_{22}						3.71_8		
3.29_{25}							3.42_{65}	3.29_{38}
3.01_{13}								2.99_{38}
2.86_{14}								2.93_{62}
2.74_{15}							2.79_{75}	
2.57_8					2.55_{10}		2.58_{60}	
2.51_{10}					2.48_{30}			
2.37_{13}			2.37_{90}	2.36_{60}				2.38_{65}
2.29_{13}			2.29_6				2.27_{60}	
2.24_{17}					2.23_{80}			2.21_{62}

Table.7.3.1.2a. X.R.D. PEAKS AND THEIR ASSIGNMENTS,FOR Mo AT STAINLESS STEEL.

sample	Ni-Cr-Fe	Ni-Cr-Fe	Fe_3Mo	Fe_2Mo	FeMo	$Mo_5Cr_6Fe_{18}$	$CaCl_2.6H_2O/CaCl_2.4H_2O$
		d values					
2.17_{33}			2.18_{65}	2.18_{100}			2.16_{100}
2.11_{40}						2.11_{100}	
2.08_{70}	2.05_{80}		2.08_{100}				
2.01_{690}		2.03_{100}		2.02_{100}	2.02_{100}		
1.93_{25}			1.91_{30}			1.90_{65}	
1.83_{10}	1.78_{55}					1.83_{30}	
1.69_{13}							1.70_{25}
1.42_{40}		1.43_{14}				1.45_{18}	
1.30_{10}			1.29_{100}				
1.27_{8}	1.26_{100}						
1.20_{8}						1.21_{65}	
1.19_{10}		1.17_{35}				1.19_{20}	
1.15_{53}						1.17_{50}	
1.01_{28}		1.01_{11}					

Table.7.3.1.2b. X.R.D. PEAKS AND THEIR ASSIGNMENTS,FOR Mo AT STAINLESS STEEL.

a

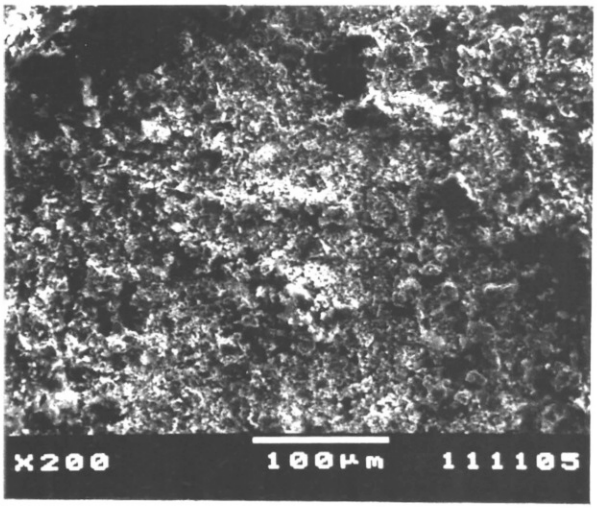

b

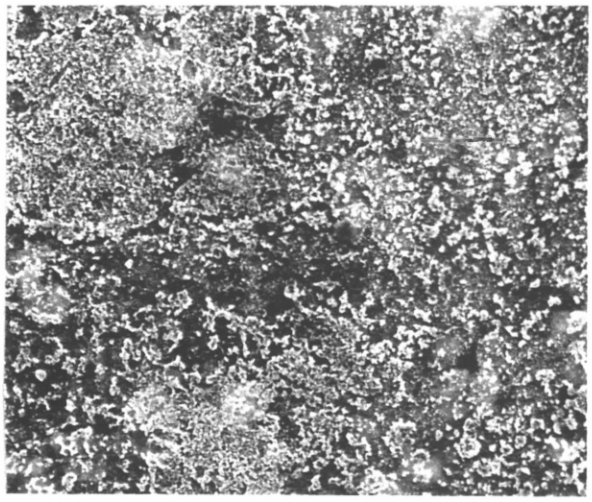

c

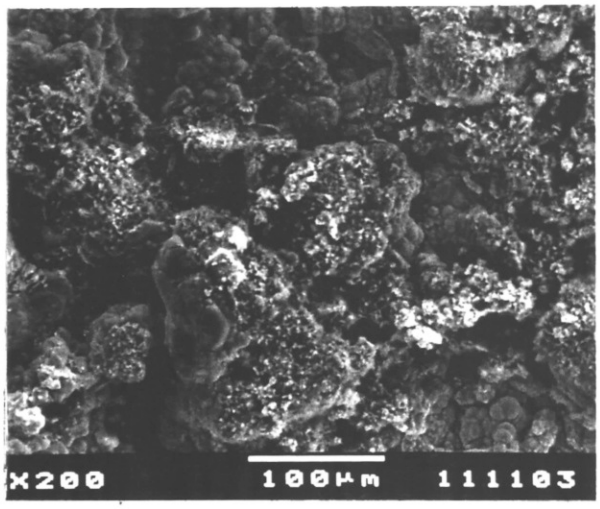

Fig.7.3.2.1.Carbon coating deposited on stainless steel for deposition potentials and times :- a) -1.1 V for 48 mins. b) -1.1 V for 31 mins. c) -1.9 V for 30 mins.

The $CaCl_2$ occluded into the coatings hydrated upon exposure to the atmosphere. At low potentials, hydrated $CaCl_2$ was not found, again indicating the coherency of these coatings. $CaCl_2$ could not be occluded as no dendritic structure was developed and thus no hydrated $CaCl_2$ was noted by X-ray diffraction in these coatings. The diffraction peaks and their assignments are shown for a carbon deposit produced at high overpotential in Table.7.3.2.1.

7.4.DISCUSSION.

The processes of nucleation and growth of electrodeposits of Mo at W and Pt, have been found to be simultaneous nucleation and growth for a range of overpotentials(-7 to 354mV). The same behaviour for Cr at W, stainless steel and copper was reported by Vargas(135). Thus at the higher overpotentials required to cathodically protect stainless steel, this process may be assumed to occur, but more rapidly. However this assumption is based on the continued reduction of the monomer form of Mo(III). This will only occur if sufficient $MoCl_6^{3-}$ is present in solution. If not the reduction of the dimer may occur at more cathodic potentials (large overpotentials for the monomer reduction). The effect of this chemical equilibrium on the nucleation process has not been examined.(This potential range was not considered at W or Pt.) Coatings produced at these constant potentials show unstable growth phenomena, but good initial coverage of the substrate. The unstable growth probably arises due to the rate of charge transfer at the growing coating/melt interface being greater than that of the diffusion of $MoCl_6^{3-}$ (or the rate of dissociation of the dimer). This results in favoured deposition for areas of coating protruding into the melt(locally $MoCl_6^{3-}$ richer regions of the melt). Thus dendritic and columnar growth forms are

favoured. The high temperatures also allow good interdiffusion of substrate and coating elements, such that good coating adherence is likely.

The irreversible nature of the carbon from carbonate deposition nucleation process which involves a slow charge transfer step (110) gives coherent deposits at potentials close to the reduction potential for carbonate. At more cathodic potentials rough coatings which occlude the melt during deposition are observed. A switch from charge transfer to mass transfer control for the growth of the coating may be occuring as the deposition potentials become more cathodic. Iron carbide is also formed, probably by the diffusion of C into the surface of the substrate.

8. CO-DEPOSITION OF MOLYBDENUM AND CARBON

8.1.INTRODUCTION.

In this chapter aspects of the co-deposition of Mo and C are considered. The type of nucleation and growth process for this co-reduction were investigated by chronoamperometry at a tungsten electrode, and the coatings produced at stainless steel electrodes were examined by X.R.D. and scanning electron microscopy to determine the nature of the coatings produced.

8.2.CHRONOAMPEROMETRY.

The i-t potentiostatic transients for the potential range -1.202 to -1.322 V wrt. Pt ref. were examined. From the cyclic voltammetric analysis of $MoCl_6^{3-}$ and carbonate system, the co-reduction to Mo and C occurs in this potential range. (Fig.6.2.2.1) The same type of waveform used for Mo and C separately (section 7.2) was used here.

Fig.8.2.1. shows the i-t transients obtained and the rising current region observed indicates the presence of a discrete nucleation stage in the formation of the deposit. This is followed by the typical $t^{-1/2}$ current decay, due to the "slow" diffusion of reactants to the electrode. The log t vs log i and the i vs $t^{3/2}$ plots show this power relationship for the rising portion. (Figs.8.2.2.,8.2.3.) Fig.8.2.3. shows how this process is affected by increasing overpotential, giving steeper gradients, indicating the relative ease of nucleation with increasing overpotential. (This response is very similar to that noted for Mo nucleation in section 7.2.1. This $t^{3/2}$ current dependence indicates the simultaneous formation and growth of nuclei, the steeper gradients for higher overpotentials indicating the increasing number of nuclei formed. The current decay is shown to be a function of $t^{1/2}$ in Fig.8.2.4., and this is also similar to that noted for Mo deposition.

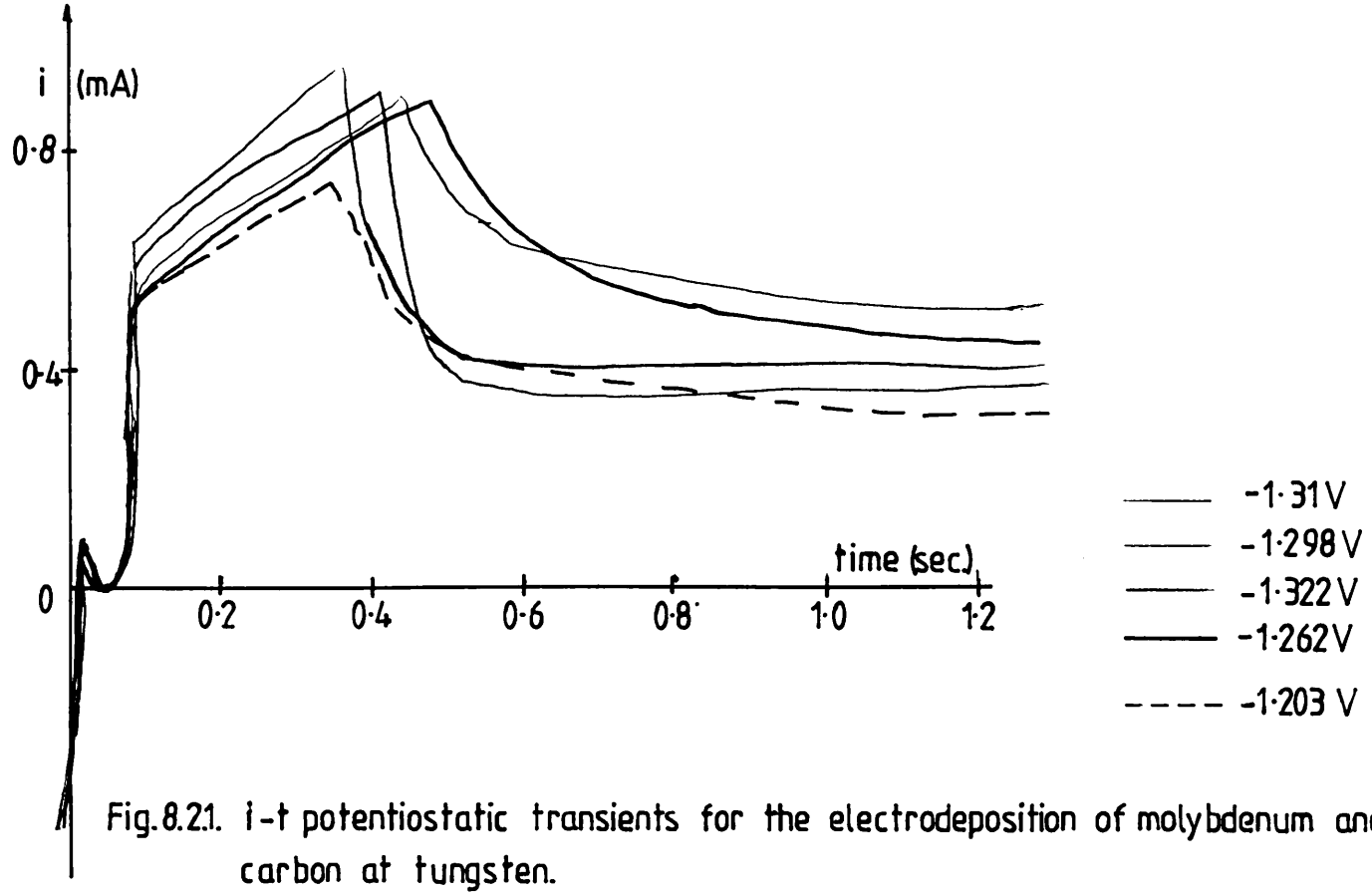

Fig. 8.2.1. i-t potentiostatic transients for the electrodeposition of molybdenum and carbon at tungsten.

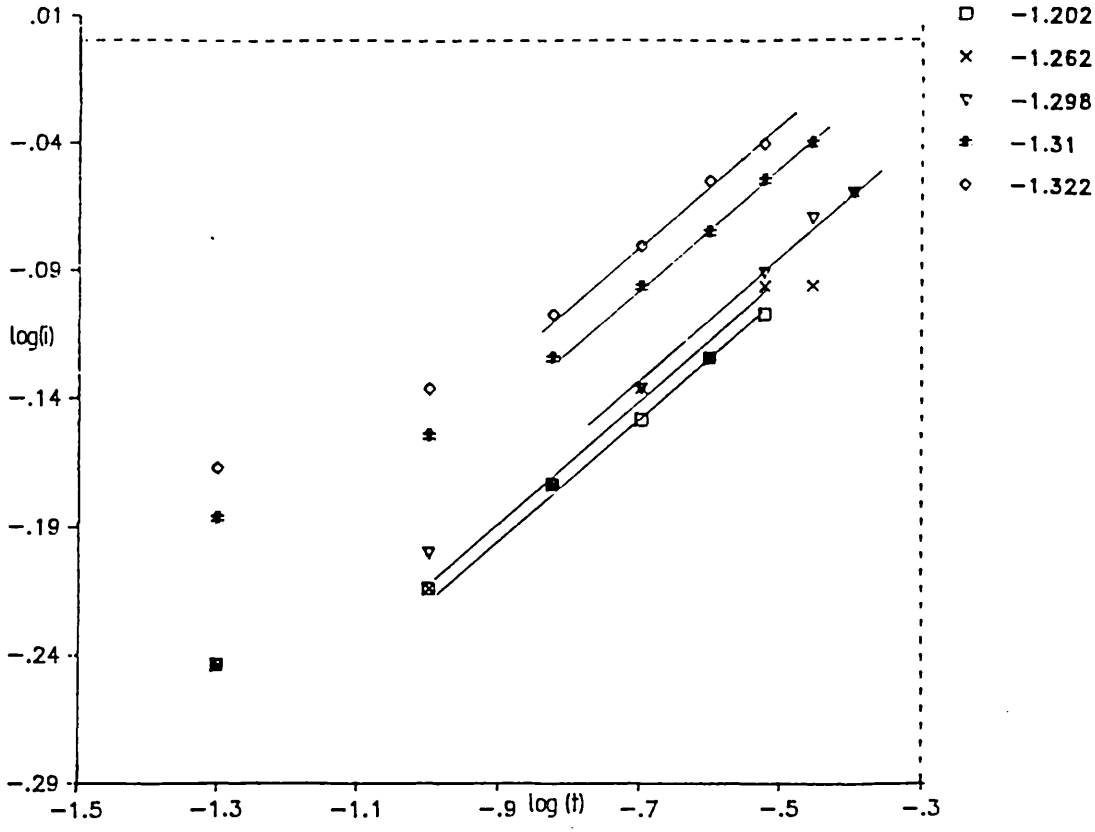

Fig.8.2.2.Plots of logi vs logt for the rising current region corresponding to Mo and C deposition at W.

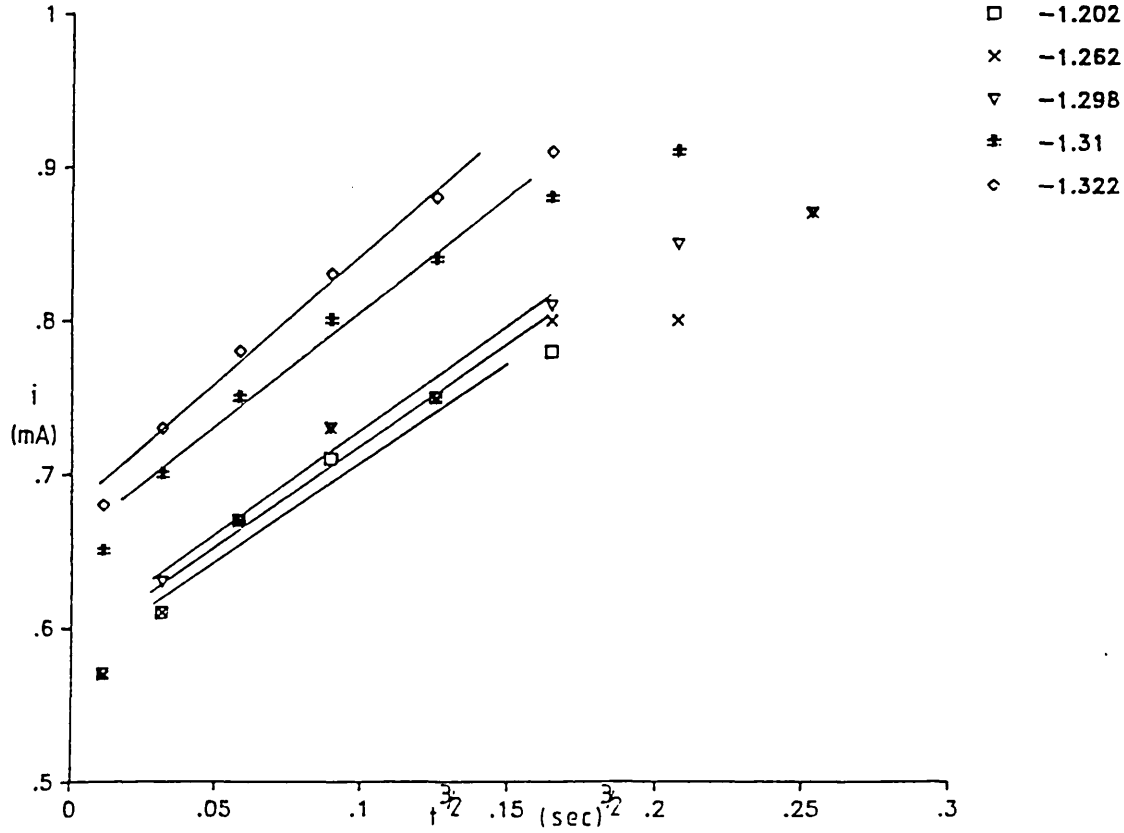

Fig.8.2.3.Plots of i vs $t^{3/2}$ for the rising current region corresponding to Mo and C deposition at W.

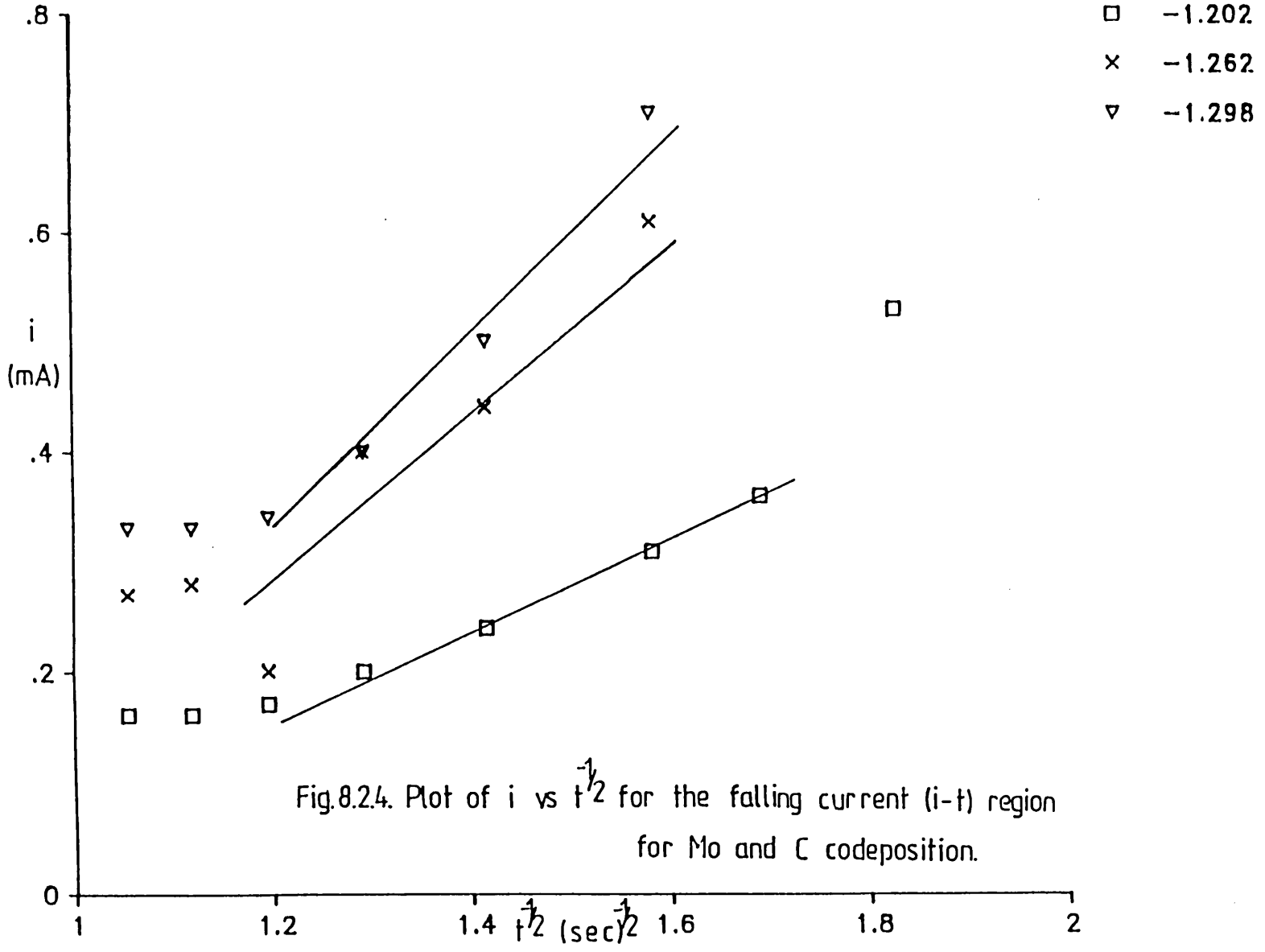

Fig.8.2.4. Plot of i vs $t^{-1/2}$ for the falling current (i-t) region for Mo and C codeposition.

8.3.CHARACTERISATION OF Mo_2C DEPOSITS ON STAINLESS STEEL SUBSTRATES.

Molybdenum carbide deposits have been produced at potentials -1.3 to -1.1 V wrt. Pt quasi ref., for various times by constant potential electrolysis, the concentration of $MoCl_6^{2-}$ varying from 10 to 88 $x10^{-3}$ $molkg^{-1}$ and from 12 to 184 $x10^{-3}$ $molkg^{-1}$ CO_3^{2-}. In constrast with the carbon and molybdenum deposition, both concentration and potential dependence are marked. Mo_2C coatings were only produced for the potential range -1.1 to -1.3 V and for concentrations such that the carbonate concentration was >2X that of $MoCl_6^{3-}$. At higher potentials and higher relative $MoCl_6^{3-}$ concentrations, molybdenum and carbon coatings were produced rather than the carbide. Under these conditions the coatings show unstable growth phenomena, similar to that noted for molybdenum. The dendritic structure developed is shown in Fig.8.3.1. The surface morphology is shown in a, and b shows the backscattered image of the same area as a. A grey pear shaped particle shown in a, becomes white in b, indicating the difference in the topography and the chemical composition of the coating. The constrast is developed by topography and in b by the atomic number distribution. Insitu E.D.A.X. for the substrate, and various parts of the coating are given in c. A very inhomogeneous phase distribution is revealed, with at least three different "effective" atomic number phases present. The E.D.A.X. anaysis indicates that one of these phases is $CaCl_2$, as peaks for Ca and Cl are present. A section through the coating is shown in Fig.8.3.2., the coating thickness being approx. 30m. The secondary and backscattered images a and b show areas corresponding to occluded melt and other areas of varying chemical composition. X.R.D. results of this coating are given in

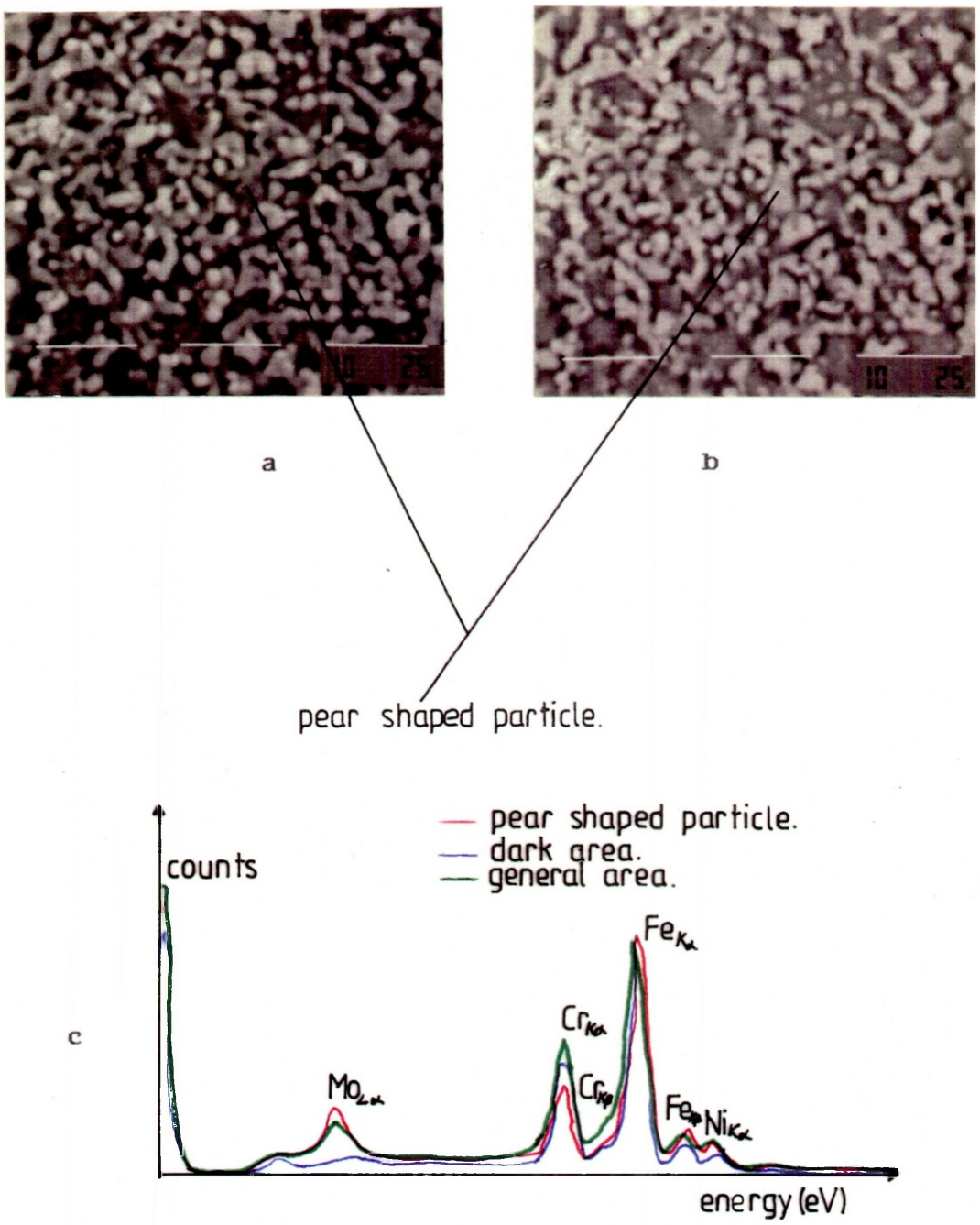

Fig.8.3.1.1. Surface of Mo_2C coating deposited on stainless steel at -1.3 V for 35 mins. a) secondary electron image, b) corresponding backscattered image, c) E.D.A.X. analysis.

a

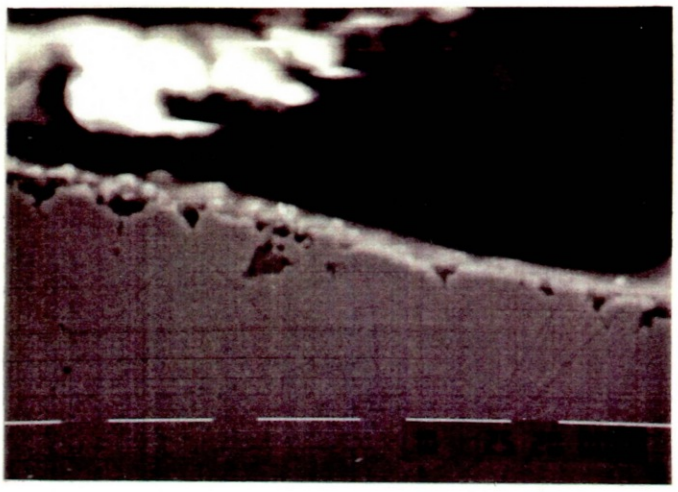

b

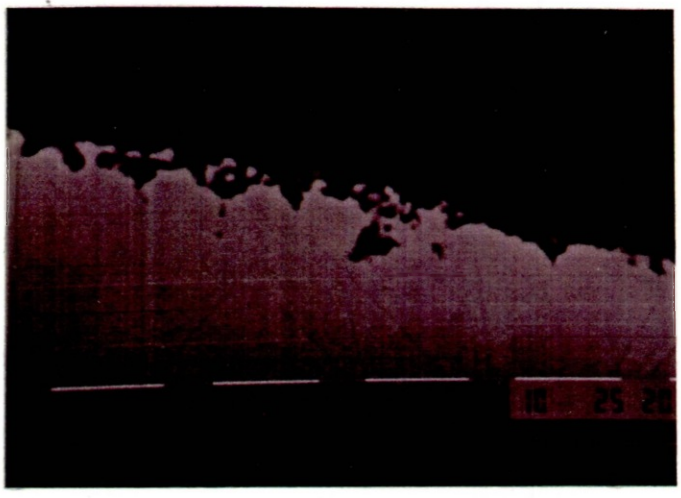

c

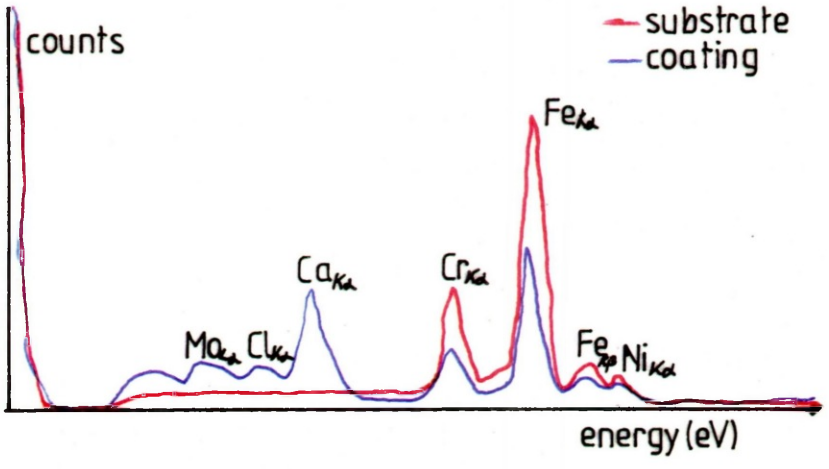

Fig.8.3.2. Section of Mo_2C coating deposited on stainless steel at -1.3 V for 35 mins. a) secondary electron image b) corresponding backscattered image c) E.D.A.X. analysis.

Table.8.3.1., showing the presence of substrate, FeCrMo,Mo_2C and hydrated $CaCl_2$.

8.4.DISCUSSION.

The particular conditions required for Mo_2C formation probably arise from the nature of the interaction between the co-depositing species. The molybdenum deposition directly from $MoCl_6^{3-}$ is highly favoured at these potentials, whereas, comparatively, the deposition of C is not. At more cathodic potentials the carbon deposits are likely to become more open and entrap melt, and Mo deposition from the dimer will also occur. Under these conditions the diffusion of C into neighbouring Mo is difficult, assuming nucleation of Mo and C occurs discretely. The concentration condition of CO_3^{2-} >2X $MoCl_6^{3-}$ could also be due to the favouring of the monomer form of Mo(III) (low $MoCl_6^{3-}$ concs, Chapter 4, and high CO_3^{2-} concs.,Chapter 6.)and thus the favoured deposition of Mo over C to give Mo_2C proportionally. At more cathodic potentials direct reduction of the dimer may occur and in this case the prefered deposition of C over Mo might occur. The extra CO_3^{2-} concentration may also be required due to the thermal decomposition of the CO_3^{2-} and thus the effective CO_3^{2-} concentration available for reduction may be far less than that added.

The open structure of the deposit and the observation of occluded melt would not favour the formation of Mo_2C by diffusion between discrete growing C and Mo nuclei. The inhomogeneity of the coatings and the presence of Mo alloys without C does not readily support this method of formation. The large overpotential for Mo deposition from monomer Mo(III) encourage the formation of dendrites, whilst at these potentials more coherent C coatings are produced. The dendritic structure of these

d values

sample	Mo_2C	FeCrMo	Cr-Ni-Fe	Ni-Cr-Fe	$CaCl_2.6H_2O$/$CaCl_2.4H_2O$	
4.77_{33}						4.60_{100}
3.90_{4}					3.93_{90}	
3.09_{4}					3.42_{65}	
2.93_{19}					2.94_{62}	2.99_{38}
2.78_{18}					2.79_{75}	2.71_{71}
2.59_{54}	2.60_{20}				2.58_{60}	
2.50_{59}		2.46_{50}				
2.36_{73}	2.37_{30}	2.37_{50}				2.38_{65}
2.28_{234}	2.28_{100}				2.27_{60}	
2.13_{100}		2.13_{100}				
2.08_{79}		2.10_{50}	2.08_{100}			
2.03_{79}		2.01_{100}	2.05_{80}	2.03_{100}		
1.96_{34}		1.96_{50}				
1.87_{5}					1.89_{12}	
1.79_{39}			1.80_{45}	1.77_{55}		
1.75_{28}	1.75_{16}					
1.59_{13}					1.57_{12}	
1.55_{5}					1.56_{12}	
1.50_{18}	1.50_{12}					
1.44_{27}		1.45_{50}	1.43_{14}			
1.35_{20}	1.35_{18}				1.37_{5}	
1.27_{106}	1.27_{16}	1.29_{50}	1.27_{26}	1.26_{100}		
1.25_{13}	1.26_{8}	1.26_{50}				
1.17_{40}				1.17_{35}		
1.09_{42}			1.08_{11}	1.07_{40}		

Table.8.3.1. X.R.D. PEAKS AND THEIR ASSIGNMENTS, FOR Mo AND C DEPOSITION AT STAINLESS STEEL.

coatings may be due to the nucleation and growth of Mo, with the nucleation of C on to the advancing Mo dendrite/melt interface, followed by the diffusion of carbon to form Mo_2C at suitable sites. This method could give rise to the inhomogenous Mo distributions, especially as the charge transfer reaction to give C controls the deposition and dendritic tips sites are not favoured for this process. It can be envisaged that the dendrites develop by the nucleation and growth of Mo but at less favoured Mo nucleation sites C is deposited and local diffusion gives Mo_2C.

A complex mixture of the effects of the charge transfer processes and mass transfer to and from the electrode and the chemistry and interaction of melt species seems the most likely means of Mo_2C formation. Further study and quantification of these processes is required to indicate the real nature of this deposition and carbide formation.

9.OTHER INVESTIGATIONS

9.1.INTRODUCTION

This chapter indicates some of the other "lines" of investigation for the electrodeposition of refractory metal carbides which have been examined. In particular the electrodeposition of titanium carbide has been considered.

9.2.THE ELECTRODEPOSITION OF TITANIUM AND CARBON FROM CHLORIDE MELTS.

Initially the co-deposition of titanium and carbon from the molten LiCl-KCl eutectic was considered, especially as the deposition of Ti and C from this solvent has already been investigated.(82,103). However the carbonate and titanium species reacted readily in this solvent and produced insoluble lithium titanates. In order to avoid this problem the use of an oxide free source of C was considered. C_2^{2-} provides a suitable alternative although the deposition of carbon occurs by the oxidation of the carbide ion rather than its reduction.(117) The carbide ion is also very unstable and reacts readily with any impurities, generating Ca metal. This was found to be an easy method for increasing the final melt purity, but the generation of Ca metal gave rise to problems with the melt, due to the solubility of this metal in the melt. This was a particular problem as both carbide oxidation and titanium chloride reduction occur close to the cathodic limit of the melt. To extend this range and to avoid confusion of pre cathodic limit reduction of calcium, due to the presence of the Ca, with the Ti and C_2^{2-} waves, pure $CaCl_2$ was used rather than the eutectic. This required the use of higher temperatures and thus increased experimental difficulties. The cyclic voltametric responses for $TiCl_3$ containing and C_2^{2-} containing melts at a tungsten electrode are shown in Figs 9.2.1.and 9.2.2. The combined solutes however did not

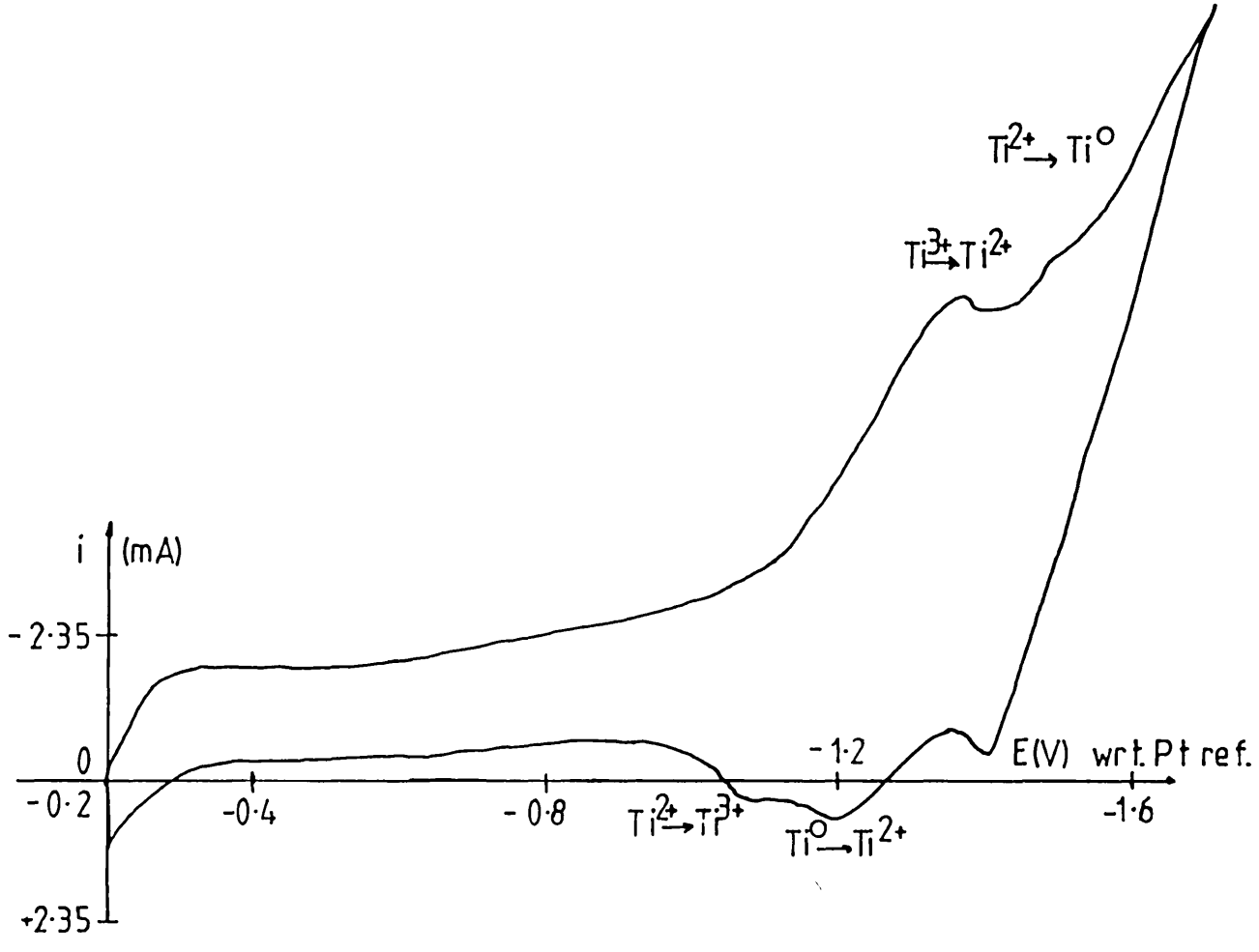

Fig.9.2.1. A typical voltammetric response for anodically dissolved Ti in $CaCl_2$.

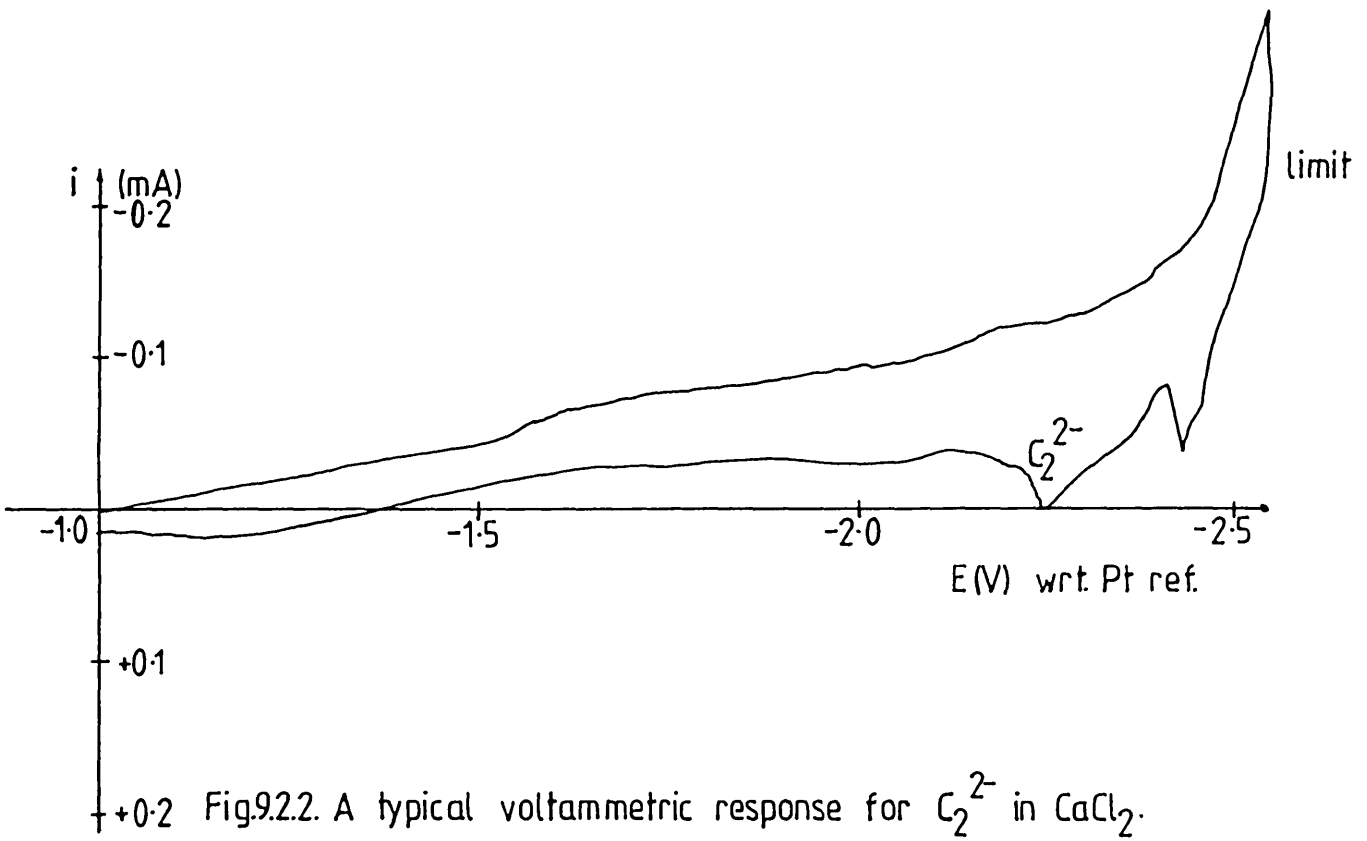

Fig.9.2.2. A typical voltammetric response for C_2^{2-} in $CaCl_2$.

yield a combined response, but the cathodic limit was shifted anodically obscuring the response. Also electrodeposition of both Ti and C did not yield TiC.

9.3.DISCUSSION

The acidity of $TiCl_3$ is largely responsible for the reaction with carbonates, especially as the ability of chloride ions to complex titanium species is limited. This effect has been noted in fluoride melts, where the complexing power of F^- is much greater, but the titanium ion is much more strongly attracted to oxide ions. (revealed by the insolubility of K_2TiO_3 in FLiNaK(137)) In order to avoid the oxide ions generated by carbonates, carbide appeared to be a suitable alternative, however the generation of calcium metal by the thermal decomposition of CaC_2 led to the loss of melt range.(114) This is because the activity of calcium becomes less than unity, due to the presence of dissolved calcium, this shifts the Ca^{2+} ion reduction potential to more anodic potentials. The generation of explosive acetylene also occurs. This Ca metal may interfere with the deposition of Ti and C and stop TiC formation by chemical oxidations and reductions.

10.CONCLUSIONS AND SUGGESTIONS FOR FURTHER WORK.

The main findings of this study and possible areas for extention are :-

a) The complex chemical and electrochemical behaviour of anodically dissolved molybdenum, investigated by cyclic voltammetry, was found to be consistant with a disproportionation reaction forming volatile $MoCl_5$ and Mo metal :-

$$5\ MoCl_6^{3-} \longrightarrow 2\ Mo + 3\ MoCl_5 + 15\ Cl^-$$

and the electrochemical/chemical reactions: -

$$Mo^{5+} + 2\ e \rightleftharpoons Mo^{3+}$$

$$2\ MoCl_6^{3-} \rightleftharpoons Mo_2Cl_6^{3-} + 3\ Cl^-$$

$$MoCl_6^{3-} + 3\ e \rightleftharpoons Mo + 6\ Cl^-$$

The anodically dissolved Mo forming an anionic complex ($MoCl_6^{3-}$) with the melt Cl^- ions before oxidation to Mo^{5+} at -0.45 V wrt. Pt quasi ref. when sweeping anodically. Reduction to Mo occurs at -1.0 V, but the dimer dissociation and reduction process occurs at more cathodic potentials. (-1.4 V)

b) The monomer/dimer equilibrium affects the process leading to the reduction to Mo. Increasing the temperature and concentration of $MoCl_6^{3-}$ shifts this equilibrium in favour of the monomer and dimer respectively.

c) In order to predict the conditions required for molybdenum deposition, these chemical and electrochemical reactions, require quantification. Determination of the equilibrium constants for the chemical reactions, would indicate the relationship between the rate of loss of $MoCl_6^{3-}$ as $MoCl_5$ and Mo and the rate of dimer formation for a particular set of conditions.

d) The study of the cyclic voltammetric behaviour of carbonate ions revealed an ill defined reduction wave indicating that a complex reduction process was occurring at -1.1 V. This oxyanion appeared to be irreversibly reduced :-

$$CO_3^{2-} + 4\ e \longrightarrow C + 3\ O^{2-}$$

Also the thermal decomposition of $CaCO_3$ at 820 - 865°C is favoured: -

$$CaCO_3 \rightleftharpoons Ca^{2+} + CO_2 + O^{2-}$$

e) To suppress this dissociation reaction a CO_2 protective atmosphere only resulted in the co-reduction of CO_2. At these temperatures CO_2 is reduced to CO rather than carbon. However sufficient carbonate ions remain in the melt, despite their thermal decomposition, to allow successful deposition of carbon.

f) The electrochemistry of both Mo species and cabonate ions in $CaCl_2$ revealed that the presence of carbonate/oxide ions in the melt, shifs the dimer/monomer equilibrium in favour of the monomer, especially when the carbonate ion concentration exceeds that of $MoCl_6^{3-}$.

g) The interaction of Mo^{5+} with O^{2-},O_2^{2-} and CO_3^{2-} generates volatile oxychlorides, which are rapidly lost from the melt.

h) Chronoamperometry at low overpotentials showed that molybdenum deposition begins with a well defined nucleation stage at tungsten and platinum, involving the simultaneous formation and growth of nuclei. The growth of these nuclei is controlled by the diffusion of Mo(III) to the electrode.

i) The nucleation of carbon at tungsten, did not appear to reveal any clear nucleation stage, and gowth was found to be controlled by the charge transfer process.

j) The nucleation of both Mo and C together revealed features consitent with the combined nucleation features of Mo and C.

k) Further investigations of the nucleation process, for larger potential and concentration ranges is required to give more information about the nature of the two nucleation processes occurring together. Also the study of nucleation at stainless steel is desirable as the effect of interaction with the substrate in the nucleation

process could then be considered.

l) Electrodeposition of Mo at stainless steel substrates, under potentiostatic conditions indicated the development of dendritic type growth, due to the large overpotentials used for deposition to cathodically protect the steel. Good coverage of the electrode was achieved and alloying with the substrate elements occurred. This was probably due to the ease of diffusion at these temperatures. Melt was occluded in the dendritic structures developed.

m) Electrodeposition of carbon at stainless steel substrates, under potentiostatic conditions, revealed that coherent deposits could be produced at potentials -1.1 to -1.3 V, but at more cathodic potentials dendritic structures were generated. Melt was again occluded in the dendrites.

n) The conditions required for the potentiostatic formation of Mo_2C by the co-deposition of Mo and C at stainless steel were found to be:-

i) deposition potentials in the range -1.1 to -1.3 V

ii) concentrations of carbonate ions >2X the concentration of molybdenum ions.

Dendritic coating structures were developed with occluded melt and an irregular phase distribution. The coatings were not coherent.

o) The conditions of potentiostatic deposition studied do not lead to the generation of electrodeposits suitable for protective coatings. The use of more complex potential pulse plating could be considered, especially if an initial layer could be formed at high overpotentials, so protecting the substate. This would allow the use of low growth overpotentials, possibly moving the growth process from a mass transport controlled region to a charge transfer controlled region, allowing the formation of coherent deposits.

p) Investigations into the co-deposition of Ti from $TiCl_2$ and C from C_2^{2-} did not yield TiC.

ACKNOWLEDGEMENTS

I would like to express my thanks to my supervisor, Prof.D.Inman, for his guidance and support during this study.

I would also like to thank my colleagues in the "Nuffield Group" for their helpful discussions and suggestions.

Thanks are also due to Mr.G.Hicks for his expert glass blowing and Mr.J.Wright for his technical advice.

I would like to express my appreciation to Miss.J.Sawistowska for her help with the production of this thesis.

I would also like to thank Dr.M.P.Hill and the C.E.G.B. for financial support for this project.

BIBLIOGRAPHY

(1) L.E.Toth "Transition Metal Carbides and Nitrides", Academic Press, (1971), 6

(2) J.L. Murray, "Binary Alloy Phase Diagrams, Vol.1 ", (ed.T.B.Massalski) A.S.M. (1986), 595

(3) H.C.Gaur and R.S.Sethi, *Ind.J.Chem.*, 5(1967), 485

(4) A.D.Graves et al."Advances in Electrochemistry and Electrochemical Engineering" Vol 4, (P.Delahay ed.), Interscience Publ., (1965), 473

(5) G.W.Mellors and S.Senderoff, *J. Electrochem.Soc.*, **112**, (1965), 266

(6) D.Inman and S.H.White. *J.Appl.Electrochem.*, **8**, (1978), 375

(7) J.Wurm, *Met.Finish.*, **78**, (1980), 37

(8) G.J.Janz, "Molten Salts Handbook", Academic Press, (1967), 287

(9) G.J.Hills et al., *J.Electrochem.Soc.*, **120**, (1973), 157.

(10) H.A.Laitinen et al., *ibid*, **104**, (1957), 516

(11) J.L.Barton and J.O'M.Bockris, *Proc.Roy.Soc*, **A268**, (1962), 485

(12) S.Senderoff, *Metallurgical Reviews*, **11**, (1966), 97

(13) D.Inman, Proc.Int.Symp."Molten Salts", Electrochem.Soc. (1986)

(14) J.Heyrovsky and D.Ilkovic, *Coll.Czech.Chem.Commun.*, **7**, (1935), 198

(15) R.Kaishew and B.Mutaftschien, *Electrochim.Acta.* **10** (1965), 643

(16) S.Toshev and B.Mutaftschien, *ibid.*, **9**, (1964), 1203

(17) A.Damjanovic and J.O'M.Bockris, *J.Electrochem.Soc.*, **110**, (1963), 1035

(18) D.J.Astley et al., *J.Electroanal.Chem.*, **19**, (1968), 325

(19) P.Delahay, "New Instrumental Methods in Electrochemistry." New York, Interscience, 1954

(20) R.S.Nicholson and I.Shain, *Anal.Chem*, **36**, (1964), 706

(21) G.Mamantov et al. *J.Electroanal.Chem.*., **9**, (1965), 253

(22) R.S.Nicholson, *Anal.Chem.*, **38**, (1966), 1406

(23) R.S.Nicholson and I.Shain, *Anal.Chem*, **37**, (1965), 178

(24) W.H.Reinmuth, *Anal.Chem.*, **32**, (1960), 1891

(25, 26) D.Inman et al. "Electrochemistry"**1** and **2** ed.G.J.Hills Electrochem. Soc. (1970, 1972), 166, 61

(27) G.J.Hills et al., *Electrochim.Acta*, **19**, 657, (1974)

(28) C.G.Fink, U.S.Patent **1,581,188** (1926)

(29) A.H.Sully, "Metallurgy of the Rarer Metals-1:Chromium", Butterworths, London, (1954)

(30) J.T.Vargas and D.Inman, *J.Appl.Electrochem.*, **17**, (1987), 270

(31) G.W.Mellors and S.Senderoff, Canadian Patent **688,546** (1964)

(32) S.Senderoff and A.Brenner, *J.Electrochem.Soc.*, **101**, (1954) 16, 28, 31

(33) G.L.Davis and C.H.R.Gentry, *Metallurgica*, **53**, (1956), 3

(34) F.X.McCawley et al., *U.S.Bur.Mines* **Rep.Invest.No.6454**, (1964)

(35) D.Zuckerbrod and R.A.Bailey, *Proc.Int.Symp.Molten Salts* ed.Saboungi, Electrochem.Soc.(1985)

(36) J.A. Plambeck, "Encyclopedia of Electrochemicistry of the Elements", Vol X, Ed. A.J. Bard, Dekker, New York, (1976), 50

(37) G.D.Cordner and H.W.Worner, *Aust.J.Appl.Sci.*, **2**, (1951) 358

(38) A. Brenner, and S. Senderoff, *J. Electrochem. Soc.* **99**, (1958), 223C

(39) B.J.Fortin et al., *ibid.*, **106**, (1959), 428

(40) I.A.Menzies et al. *J.Electroanal.Chem.*, **1**, (1959/60), 161

(41) M.J.Rand and L.J.Reiment, *J.Electrochem.Soc.*, **111**, (1964), 429

(42) J.De Lepinay et al., *J.Appl.Electrochem.*, **17**, (1987), 294

(43) A.W.Schlechten et al, *J.Electrochem.Soc.*, **102**, (1955), 81

(44) M.E.Straumanis et al, *ibid.*, **104**, (1957), 17

(45) J-L.Andrieux and G.Weiss, *Compt.Rend.*, **219**, (1944), 550

(46) G.Wiess, *ann.Chim.*, **1 ser12**, (1946), 446

(47) H.J.Heinen et al.**Rep.Invest U.S.Bur.Mines** No.6590 (1965)

(48) A.K. Suri et. al. *ibid.*, **120**, (1973), 622

(49) V.I.Shapoval et. al. *Poroshk. Metall(Kiev)*, **7**, (1986), 43

(50) J.M.Gomes and M.M.Wong, **Rep.Invest U.S.Bur.Mines** No.7247, (1969)

(51) A.J.Hockman and R.S.Feigelson, *J.Electrochem.Soc*, **130**, (1983), 221

(52) K.H.Stern and S.T.Godomski, *ibid.*, **130**, (1983), 300

(53) K.H.Stern and M.L.Deanhardt, *ibid.*, **132**, (1985), 189

(54) K.H.Stern and C.E.Williams, *ibid.* **133**, (1986), 2157

(55) K.H.Stern et al. *Thin Solid Films*, **108**, (1983), 9

(56) Hideki Yabe et al. Unpublished results

(57) D.C.Topor and J.R. Selman, *J.Electrochem.Soc.*, **135** (1988), 384

(58) Kh.B.Kushkhov et. al. *Elecktrokhimiya*, **24**, (1988), 1496

(59) G.W.Mellors and S.Senderoff, *J.Electrochem.Soc.*, **113**, (1966), 60

(60) M. Makyta et al., Unpublished Report, (1988)

(61) J-L.Andrieux. *Rev.Met*, **XLV**, (1948), (1+2)

(62) D.Schalain et al., *J.Electrochem.Soc*, **116**, (1969), 12

(63) S.E.Bresler, *Acta Physicochim.URSS*, **10**, (1939), 491

(64) Y.I.Frenkel, *ibid.*, **3**, (1935), 637, 913

(65) K.Sakai, *J.Phys.Chem.*, **61**. (1957), 1131

(66) H.Lux, *Z.Elektrochem*, **45**, (1939), 303

(67) H.Flood and J.Forland, *Acta Chem.Scand.*, **1**, (1947), 592

(68) "Handbook of Chemistry and Physics", 55th Edition, R.C. Weast, editor CRC Press, Cleveland, 1974-1975

(69) K. Komarek and P. Herasymenko, *J. Electrochem.Soc.*, **105**, (1958), 217

(70) P. Ehrlich and H. Kuhnl, *Z. Anorg. Allg.Chem.*, **292**, (1957), 148

(71) E.Chassaing et al., *J.Appl.Electrochem.*, **11**, (1981), 187

(72) R.Baboian et al. , *Canad.J.Chem.*, **43**, (1965), 197

(73) Yu. V. Baimakov and M.M. Vetyukov, *Elektroliz rasplavlennnykh solei*, Metallurgiya, Moscow (1966)

(74) J. O'M. Bockris et al., *Nature*, **178**, (1956), 654

(75) M.B. Alpert et al., *J. Electrochem. Soc.*, **104**, (1957), 555

(76) J. Burgess et al., *J. Appl. Chem.*, **8**, (1958), 6

(77) M.B. Alpert et al., *J. Electrochem.Soc.*, **106**, (1959), 142

(78) V.P. Elyutin et al., *Elektrokhimiya*, **3**, (1967), 356, 432, 549

(79) S. Tokumoto et al., *Jap. Kokai*, **77**, (1976), 120, 925

(80) S. Tokumoto et al., *J. Met.*, **27**, (1975), 18

(81) E. Tanaka et al., *Jap. Kokai*, **78**, (1976), 22, 111

(82) A. Brenner and S. Senderoff, *J. Electrochem. Soc.*, **99**, (1952), 223C

(83) M.A.Steinberg et al., *J.Electrochem.Soc.*, **102**, (1955), 332C

(84) M.E.Sibert and M.A.Steinberg, *ibid.*, **102**, (1955), 641

(85) C. Guang-Sen et al., *J.Appl. Electrochem.*, **18**, (1988), 80

(86) V.S Balikhin and S.B. Makarov, *Zashch.Metal*, **17**, (1981), 125, 22

(87) M.E. Sibert et al., *J. Electrochem.Soc.*, **102**, (1955), 252

(88) T.P. Madhawan et al., *Chem. Zvesti*, **25**, (1971), 253

(89) Y. Hashimoto et al., *Denki Kagaku*, **39**, (1971), 516

(90) Y. Hashimoto, *Denki Kagaku*, **39**, (1971), 938, **40**, (1972).39

(91) R.Littlewood, *J.Electrochem.Soc.*, **109**, (1962), 525

(92) D.M. Ferry et al., *Trans. Inst. Min. Metal.*, Sect. C, (1988), 97

(93) J.Phillips and R.A.Osteryoung, *J.Electrochem.Soc.*, **124**, (1977), 1465

(94) S.H.White and U.M.Twardoch, *J.Appl.Electrochem.*, **17**, (1987), 225

(95) S.Senderoff and B.W.Mellors, *J.Electrochem.Soc.*, **114**, (1967), 556

(96) S.Senderoff and A.Brenner, *Ibid*, **101**, (1954), 16, 38

(97) D. Inman et. al. *J. Electroanal. Chem.*, **29**, (1971), 137

(98) V. I. Shapoval et al. *Ukrainskii, Khimicheskii Zh.*, **53**, (1987), 1286

(99) B.N. Popov and H.A. Laitien, *J. Electrochem. Soc.*, **120**, (1973), 1346

(100) V. I. Shapoval and V.F. Makogon, *Elektrokhimiya*, **12**, (1976), 1723

(101) K. Koyama et al., *J. Less Common Metals*, **134**, (1987), 141

(102) J. Hladik ang G. Morand, *J. Chim. Phys.*, **63**, (1966), 24

(103) J.R. Selman, Proc. Int. Symp. "Molten Salts" -Electrochem. Soc. 1981

(104) S.H. White and D.R. Morris, Proc. Richardson Conf. (IMM. London 1974), 195

(105) M.D. Ingram and G.J. Janz, *Electrochim. Acta*, **10**, (1965), 783

(106) H.E. Bartlett and C.E. Johnson, *J. Electrochem. Soc.*, **114** (1967), 457

(107) M.L. Deanhardt et al., *J. Electrochem. Soc.* **133**, (1986), 133

(108) K.H. Stern and S.T. Gadmorski, *ibid.*, **130**, (1983), 300

(109) K.V. Young, "Electrodeposition of amorphous carbon from dilute carbonate solns. at 450°C" unpublished report

(110) W.J. Mo, D.I.C. thesis 1985

(111) Yu.K. Delmarski etal. *ElektroKhimiya*, **7**, (1971), 1301

(112) M.V. Smirnov et al. *ibid.*, **7**, (1971), 566

(113) W.A. Barber and C.L. Sloan, *J. Phys. Chem.*, **65**, (1961) 2026

(114) C. Aksaranan et al., *Can. J. Chem.*, **49**, (1971), 2014

(115) J.F. Maillot and D.R. Morris, *Can. J. Chem.*, **50**, (1972), 839

(116) A. Bonomi et al., *J. Electrochem. Soc.*, **124**, (1977), 982

(117) S.H. White, Unpublished report.

(118) R. Odgord et al., *Proc. Int. Symp. "Molten Salts"*, Electrochem. soc. 1985, 361

(119) P.V. Shigolev, "Electrolytic and Chemical Polishing of Metals" 2nd. Ed. Freund (1974), 140.

(120) E.D.Black and T.De Vries, *Anal.Chem.*, **27**, (1955), 906

(121) H.A.Laitinen et al., *J.Electrochem.Soc.*, **104**, (1957), 516

(122) C.R.Boston and G.P.Smith, *J.Amer.Chem.Soc.*, **62** (1958), 409

(123) D.L.Maricle and D.N.Hume, *J.Electrochem.Soc.*, **107** (1960), 354

(124) D.Inman and J.O'M.Bockris, *J.Electroanal.Chem.*, **3** (1962), 126

(125) S.H.White, "Ionic Liquids" Ed. D.Inman and D.G.Lovering, Plenum Press, (1980), 185

(126) S.Selis, *J.Electrochem.Soc.*, **113**, (1966), 37

(127) R.S.Nicholson and T.Shain, *Anal.Chem.*, **36**, (1964), 706

(128) R.S.Nicholson, *ibid.*, **37**, (1965), 667

(129) M.L.Omstead, et al., *ibid.*, **41**, (1969), 260

(130) J.M.Saveant and E.Vianello, *Electrochim.Acta*, **12**, (1967), 1545

(131) J.M.Saveant and E.Vianello, *ibid.*, **10**, (1965), 905

(132) H.Matsuda and Y.Ayabe, *Z.ElektroKhim*, **59**, (1955), 494

(133) R.S.Nicholson, *Anal.Chem.*, **37**, (1965), 1351

(134) H.C.Brookes and D.Inman, Unpublished work, (1985)

(135) J.T.Vargas, ph.D. thesis 1984

(136) A.Damjanovic et al. *Electrochim. Acta*, **10**, (1965), 111

(137) K.H.Stern, *J.Electrochem.Soc.*, **136**, (1989), 439